

AD-760 175

**THEORETICAL INVESTIGATION OF THE EFFECT
OF PARTICLE CONTAMINANTS ON LASER-IN-
DUCED AIR BREAKDOWN**

Frank D. Felock, et al

KMS Technology Center

Prepared for:

**Air Force Weapons Laboratory
Advanced Research Projects Agency**

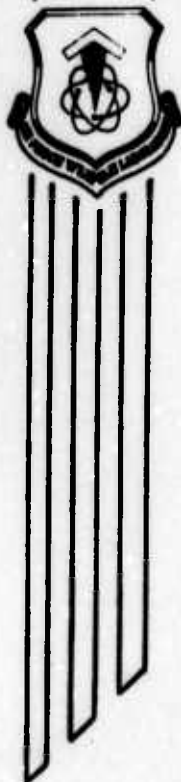
April 1973

DISTRIBUTED BY:

NTIS

**National Technical Information Service
U. S. DEPARTMENT OF COMMERCE
5285 Port Royal Road, Springfield Va. 22151**

AD 760175



THEORETICAL INVESTIGATION OF THE EFFECT OF PARTICLE CONTAMINANTS ON LASER-INDUCED AIR BREAKDOWN

Frank D. Feiock

Lester K. Goodwin

KMS Technology Center

TECHNICAL REPORT NO. AFWL-TR-72-172

April 1973



AIR FORCE WEAPONS LABORATORY

Air Force Systems Command

Kirtland Air Force Base

New Mexico

Reproduced by
**NATIONAL TECHNICAL
INFORMATION SERVICE**
U S Department of Commerce
Springfield VA 22151

Approved for public release; distribution unlimited.

AIR FORCE WEAPONS LABORATORY
Air Force Systems Command
Kirtland Air Force Base
New Mexico 87117

When US Government drawings, specifications, or other data are used for any purpose other than a definitely related Government procurement operation, the Government thereby incurs no responsibility nor any obligation whatsoever, and the fact that the Government may have formulated, furnished, or in any way supplied the said drawings, specifications, or other data, is not to be regarded by implication or otherwise, as in any manner licensing the holder or any other person or corporation, or conveying any rights or permission to manufacture, use, or sell any patented invention that may in any way be related thereto.

DO NOT RETURN THIS COPY. RETAIN OR DESTROY.

ACCESSION FOR	
NTIS	Write Section <input checked="" type="checkbox"/>
PIC	Entire Section <input type="checkbox"/>
UNCLASSIFIED	<input type="checkbox"/>
DISSEMINATION	
BY	
USE BY SECTION/AVAILABILITY CODES	
DATE	
FACILITY AND/OR SPECIAL	
1A	

UNCLASSIFIED

Security Classification

DOCUMENT CONTROL DATA - R & D

(Security classification of title, body of abstract and indexing annotation must be entered when the overall report is classified)

1. ORIGINATING ACTIVITY (Corporate author) KMS Technology Center Irvine, California 92664		2a. REPORT SECURITY CLASSIFICATION UNCLASSIFIED	
		2b. GROUP	
3. REPORT TITLE THEORETICAL INVESTIGATION OF THE EFFECT OF PARTICLE CONTAMINANTS ON LASER-INDUCED AIR BREAKDOWN			
4. DESCRIPTIVE NOTES (Type of report and inclusive dates) 22 June 1971-30 August 1972			
5. AUTHOR(S) (First name, middle initial, last name) Frank D. Felock; Lester K. Goodwin			
6. REPORT DATE April 1973		7a. TOTAL NO. OF PAGES 194 196	7b. NO. OF REFS 45
8a. CONTRACT OR GRANT NO. F29601-71-C-0118		8b. ORIGINATOR'S REPORT NUMBER(S) AFWL-TR-72-172	
b. PROJECT NO. 1256			
c. Task No. 09		9b. OTHER REPORT NO(S) (Any other numbers that may be assigned this report)	
d.			
10. DISTRIBUTION STATEMENT Approved for public release; distribution unlimited.			
11. SUPPLEMENTARY NOTES		12. SPONSORING MILITARY ACTIVITY AFWL (DYT) Kirtland AFB, NM 87117	
13. ABSTRACT (Distribution Limitation Statement A) The effect of atmospheric contaminants on the laser-induced breakdown of air is investigated. Calculations were performed using a one-dimensional, Lagrangian, hydrodynamic code developed for this study. The results of this study indicate that the interaction of a laser beam with atmospheric contaminants such as SiO_2 and Al_2O_3 can supply a primary electron density that will lead to a significant decrease in the laser-induced breakdown threshold for air.			

14.

KEY WORDS

LINK A		LINK B		LINK C	
ROLE	WT	ROLE	WT	ROLE	WT

Laser-induced gas breakdown
Atmospheric particles
Two-temperature hydrodynamics
CO₂ laser
Thermionic emission

ia

AFWL-TR-72-172

THEORETICAL INVESTIGATION OF THE EFFECT OF PARTICLE
CONTAMINANTS ON LASER-INDUCED AIR BREAKDOWN

Frank D. Feiock
Lester K. Goodwin
KMS Technology Center

TECHNICAL REPORT NO. AFWL-TR-72-172

Approved for public release; distribution unlimited.

ih

FOREWORD

This report was prepared by KMS Technology Center, Irvine, California, under Contract F29601-71-C-0118. The research was performed under Program Element 62301D, Project 1256, Task 09, and was funded by the Advanced Research Projects Agency (ARPA) under ARPA Order 1256.

Inclusive dates of research were 22 June 1971 through 30 August 1972. This report was submitted 1 March 1972 by the Air Force Weapons Laboratory Project Officer, Captain Philip E. Nielsen (DYT).

Publication of this report does not constitute Air Force approval of the report's findings or conclusions. It is published only for the exchange and stimulation of ideas.

Philip E. Nielsen

PHILIP E. NIELSEN
Captain, USAF
Project Officer

Jay R. Roland

JAY R. ROLAND
Major, USAF
Chief, Theoretical Physics Branch

John K. Lerohl

JOHN K. LEROHL
Colonel, USAF
Chief, Technology Division

CONTENTS

<u>Section</u>		<u>Page</u>
I	INTRODUCTION	1
II	AIR BREAKDOWN ANALYSIS	3
	1. Cross Sections	6
	a. Vibrational Excitation	6
	b. Electronic Excitation	6
	(1) Nitrogen Cross Section for $A^3\Sigma_u^+$ State	9
	(2) Nitrogen Cross Section for $B^3\Pi_g$ State	10
	(3) Nitrogen Cross Section for $C^3\Pi_u$ State	12
	(4) Nitrogen Cross Sections for the $a^1\Pi_g$ State	12
	c. Ionization	16
	d. Total Scattering	16
	2. Breakdown Analysis	20
III	THE HYDRODYNAMIC EQUATIONS	34
	1. Collision Frequencies	36
	a. Electric Excitation	36
	b. Vibrational Excitation	37
	c. Ionization Frequencies	38
	d. Electron-Ion Elastic Collision Frequency	38
	2. Ambipolar Diffusion Coefficient	39
	3. Free-Free Absorption Coefficient	40
IV	PARTICLE DESCRIPTION AND INTERACTIONS	43
	1. Energy Absorption from the Laser Beam	43
	a. Mass Absorption	43

CONTENTS (Cont.)

<u>Section</u>	<u>Page</u>
(1) SiO_2	44
(2) Al_2O_3	46
(3) NaCl	48
(4) Carbon	48
b. Absorption by Electrons	52
2. Equation of State	52
3. Thermal Conductivity	55
4. Thermionic Emission	59
5. Macromolecular Complexes	60
V RESULTS	61
VI CONCLUSIONS	71
Appendix I - Description of CELAB Code	73
Appendix II - Air Breakdown Reduction by Transparent Particles	143
Appendix III - Monte Carlo Computer Program	161
References	182

ILLUSTRATIONS

<u>Figure</u>		<u>Page</u>
1	Sum of N_2 Vibrational Cross Sections	5
2	Excitation Functions for the $A^3\Sigma_u^+$ State for N_2	11
3	Excitation Functions for the $B^3\Pi_g$ State for N_2	13
4	Excitation Functions for the $C^3\Pi_u$ State for N_2	14
5	Excitation Functions for the $a^1\Pi_g$ State for N_2	15
6	Total N_2 Ionization Cross Section	17
7	Total O_2 Ionization Cross Section	18
8	Total N_2 Electron Scattering Cross Section	19
9	Comparison of Air Breakdown Calculations	31
10	Absorption Coefficient for Al_2O_3 as a Function of Wavelength	47
11	Absorption Coefficient for SiO_2 and SiO as a Function of Wavelength	45
12	Absorption Coefficient for $NaCl$ as a Function of Wavelength	49
13	Mass Absorption Coefficient for Carbon (soot) as a Function of Wavelength	51
14	Thermal Conductivity of Various Material from Equation (120)	57
15	Air Conductivity, K , and Diffusivity, D , at One Atmosphere Pressure	58
16	Electron Density vs Time for Different Size Al_2O_3 Particles in the Beam CO_2 Laser at an Intensity of 3×10^8 watts/cm ² .	62
17	Electron Density vs Time for Different Size SiO_2 Particles in the Beam CO_2 Laser at an Intensity of 3×10^8 watts/cm ² .	63
18	Electron Density vs Time for Different Size SiO_2 Particles in the Beam CO_2 Laser in an Intensity of 1×10^8 watts/cm ² .	65
19	Electron Density vs Time for a 48μ Al_2O_3 Particlie in the Beam of a CO_2 Laser at Two Different Intensities	66

Illustrations (Cont.)

<u>Figure</u>		<u>Page</u>
20	Electron Density vs Time for a 48μ Al_2O_3 Particle in the Beam of a CO_2 Laser at Two Different Intensities	67
21	Electron Density vs Time for a 48μ Al_2O_3 Particle in the Field of a CO_2 Laser at an Intensity of 3×10^8 watts/cm ² at Different Ambient Pressures	69
22	Electron Density vs Time for a 48μ SiO_2 Particle in the Field of a CO_2 Laser at an Intensity of 3×10^8 watts/cm ² for Different Values of the SiO_2 Absorption Coefficient	70
23	Comparison of electron energy distributions for laser power of 8×10^9 watts/cm ²	157
24	Comparison of electron energy distributions for laser power of 2×10^{11} watts/cm ²	158
25	Electron energy distribution functions ($f/E^{\frac{1}{2}}$) from Monte Carlo calculations for various CO_2 laser powers.	159

SECTION I

INTRODUCTION

The optical properties of a medium can be altered by a laser beam of sufficient intensity. This alteration can range from relatively small changes in the index of refraction leading to diffraction effects to complete breakdown of the propagating medium. Thus, the interaction between a laser beam and the surrounding environment can impose limitations on the size and intensity of the beam that is to be used for a given purpose.

In the case of air, laboratory experiments with the $10.6\ \mu$ radiation from a CO_2 laser have shown that atmospheric breakdown occurs at an intensity of approximately 2×10^9 watts/cm² for sea level density (Ref. 1). It is shown in Section II that this is about the same intensity predicted by theoretical considerations if it is assumed that initially there is one free electron per cm³.

Further experiments indicated that the breakdown threshold for air could be as low as 10^8 watts/cm² (Ref. 2). Since the later experiments were carried out with air under normal conditions while the earlier experiments used cleaner air meeting laboratory standards, it was postulated that the lowering of the breakdown threshold was due to the presence of an increased amount of contaminants in the dirty air.

Contaminants such as quartz (SiO_2) and sapphire (Al_2O_3) are assumed to be present in the form of solid particles ranging in size from $1\ \mu$ to $100\ \mu$ radius. These particles absorb energy, finally reaching the vaporization temperature and moving out into the air. Because of the higher absorption of energy the contaminants can provide the initial source of electrons leading to atmospheric breakdown.

The purpose of the present study is to develop a model suitable for

investigation of the effects of contaminants on atmospheric breakdown. This model utilizes where possible, the known material properties of the contaminant particle to determine the absorption of the laser energy and the subsequent heating. A one dimensional Lagrangian hydrodynamic code, CELAB (Contaminant Effects on Laser Air Breakdown), has been developed to compute the motion of the vaporized material.

Semi-empirical expressions for the relevant molecular cross sections are developed to describe the interactions between the free electrons from the contaminant particle and the atmosphere. The calculated values for the cross sections are compared with the latest data available and found to give reasonable results over a wide range of electron energy.

The results of preliminary calculations on quartz (SiO_2) and sapphire (Al_2O_3) particles of varying sizes indicate that atmospheric contaminants are an important factor in the laser induced breakdown of air. First, they supply a substantial density of free electrons for the coupling of laser energy. Secondly, because of the relatively high density of the solid contaminant, the local degree of ionization in the neighborhood of the evaporated particle will be high making the electron-ion interaction the dominant elastic collision process. This, in turn, increases the rate at which an electron gains energy from the laser and decreases the breakdown threshold intensity.

SECTION II

AIR BREAKDOWN ANALYSIS

The intensity of high-power laser beams propagating through the atmosphere is limited by atmospheric breakdown. For the 10.6-micron radiation of the CO₂ laser, experiments on ordinary laboratory air show that breakdown is initiated at laser powers of about 2×10^9 watts/cm². If it is assumed that there is an initial density of free electrons in the focal volume of the laser beam then the breakdown process can be described by electron cascade theory (Ref. 3). In this theory, the free electrons in the focal volume of the beam absorb energy by inverse bremsstrahlung. When the rate of energy absorption is large enough for an electron to reach the ionization energy during the laser pulse duration, there follows a net rate of growth for the free electron population. If this growth rate exceeds the rate of loss of electrons to attachment, diffusion, etc., then the electron density increases with increasing time and breakdown of the gas is taking place. The breakdown of the gas is complete when the growth rate is large enough that complete ionization takes place within the time of the pulse duration. The process can be described by the rate equation,

$$N_e(t) = N_e(0)e^{\int_0^t (\bar{\gamma} - \alpha_L) dt} \quad (1)$$

where $N_e(t)$ is the time dependent electron density, $\bar{\gamma}$ is the growth rate, and α_L is the loss rate. Assuming that the rates are constant over the duration of the laser pulse, the criterion for breakdown requires that the growth rate satisfies the condition

$$\bar{\gamma} > \alpha_L \quad (2)$$

At standard temperature and pressure conditions (STP) in air, complete breakdown requires

$$\bar{\gamma} = \alpha_L + \frac{45}{t_P} \quad (3)$$

where it has been assumed that a nominal value of $N_e(0) = 1 \text{ cm}^{-3}$ exists and $N_e(t_P) = 3 \times 10^{19} \text{ cm}^{-3}$. In the remainder of the report, the term "breakdown" will always refer to complete breakdown unless otherwise specified.

The dominant loss mechanism in air is 3-body attachment to molecular oxygen,



where M is a third body. The rate for this process is (Ref. 4)

$$\alpha_L \sim 7.5 \times 10^7 (\rho/\rho_0)^2 \text{ sec}^{-1} \quad (5)$$

where ρ_0 is the sea level density. At STP conditions,

$$\bar{\gamma} \approx 7.5 \times 10^7 + \frac{45}{t_P} \text{ sec}^{-1} \quad (6)$$

Thus, for very long pulses, the threshold growth rate for breakdown is

$$\bar{\gamma} = 7.5 \times 10^7 \text{ sec}^{-1} \quad (7)$$

while for pulses in the nanosecond range

$$\bar{\gamma} \approx \frac{45}{t_P} \text{ sec}^{-1} \quad (8)$$

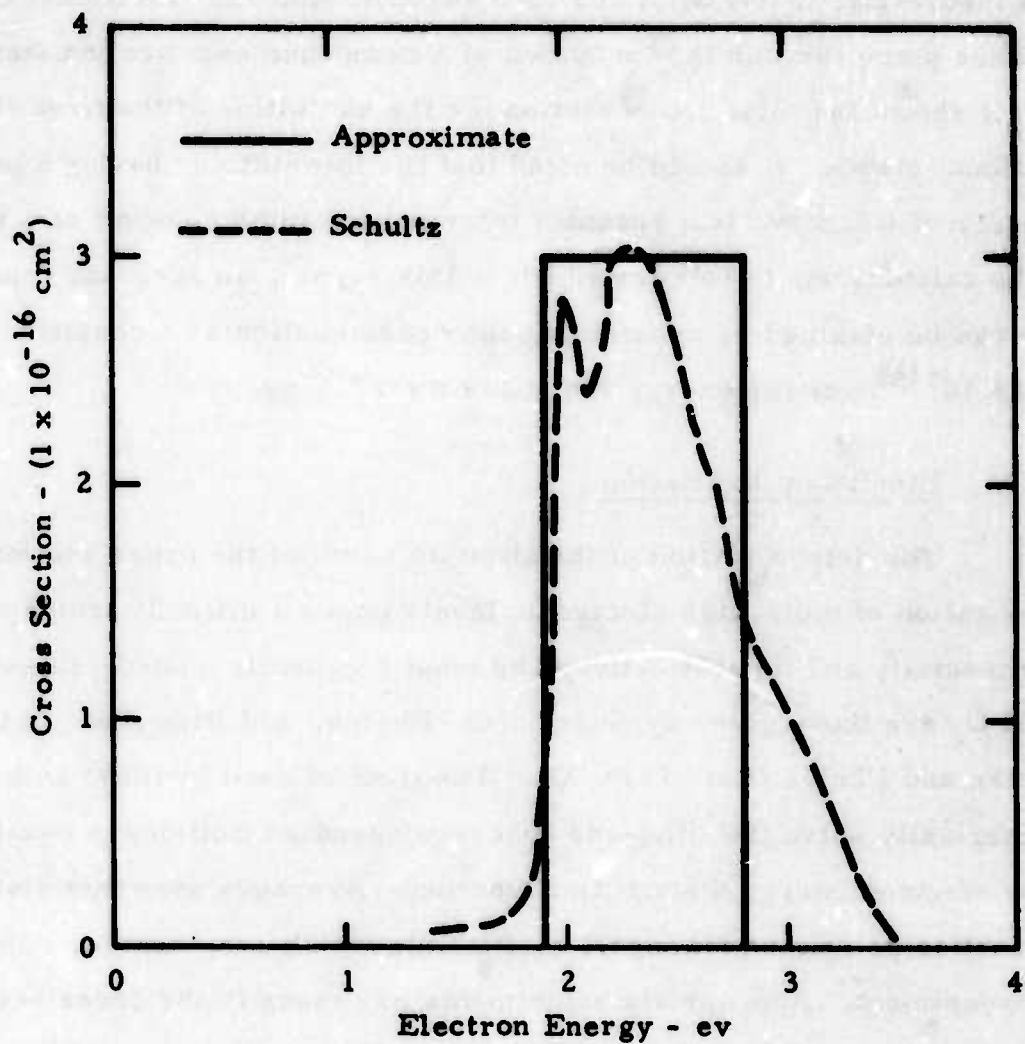


Figure 1. Sum of N_2 Vibrational Cross Sections

1. CROSS SECTIONS

a. Vibrational Excitation

The vibrational excitation of N_2 by electron impact has been studied quite extensively both experimentally and theoretically (Ref. 5). In the theoretical analysis, it has been assumed that the vibrational excitation takes place through the formation of a compound negative ion state. Figure 1 shows the total cross section for the excitation of the first eight vibrational states. It should be noted that the interaction, having a peak at an energy of ~ 2.3 ev, is a resonant interaction having a cut off at ~ 3.5 ev. For the calculations to be carried out in this report, an adequate representation can be obtained by considering the cross section as a constant $\sigma_v \sim 3 \times 10^{-16}$ over the energy range $1.9 \leq \epsilon \leq 2.8$ ev.

b. Electronic Excitation

The determination of the absolute value of the cross sections for the excitation of molecular electronic levels poses a difficult problem both experimentally and theoretically. The most frequently quoted values for N_2 and O_2 are those given by Engelhardt, Phelps, and Risk (Ref. 6) for N_2 and Hake and Phelps (Ref. 7) for O_2 . The method used by these authors is to numerically solve the time-and space-independent Boltzmann equation for the electron energy distribution function. Averages over this distribution function determine transport coefficients which are, in turn, compared with experiment. Appropriate adjustments are made to the cross sections until a satisfactory fit with the experimental data for the transport coefficients are obtained. The thresholds for the various cross sections are obtained from other experimental data. The cross sections giving the best fit to the experimental transport coefficients over a wide energy range are then plotted.

More recently, Borst (Ref. 8) has made an experimental determination of the absolute cross sections for the excitation of the $A^3\Sigma_u^+$.

$a^1\Pi_g$ and $E^3\Sigma_g^+$ states of N_2 . Ajello (Ref. 9) has also made measurements of the cross section for the excitation of the $a^1\Pi_g$ state of N_2 . There appears to be substantial disagreement between the two measurements. The experimental data will be shown in appropriate portions of this section where comparisons are to be made with calculated values of the cross sections.

An approximate method for the calculation of the relevant cross sections can be obtained from classical mechanics. The transfer of energy between two electrons is

$$\Delta\epsilon = \epsilon \sin^2 \theta/2 \quad (9)$$

where ϵ is the kinetic energy of the incident electron and θ is the scattering angle. The relation between the impact parameter, energy, and scattering angle is (Ref. 10)

$$b = \frac{e^2}{2\epsilon} \cot \theta/2 \quad (10)$$

hence,

$$\Delta\epsilon = \frac{\epsilon}{1 + \frac{4b^2\epsilon^2}{e^4}} \quad (11)$$

where b is the impact parameter and e is the electronic charge.

According to classical mechanics, the cross section is defined by the integral

$$\sigma(\epsilon) = 2\pi \int_0^{b_M} b db = \pi b_M^2 \quad (12)$$

where b_M is the maximum value of the impact parameter for the particular interaction process under consideration. For electronic excitation, the

required value of the impact parameter can be determined from equation (11) by setting $\Delta\epsilon = \epsilon_x$.

$$b_M^2 = \frac{e^4}{4\epsilon^2 \epsilon_x} (\epsilon - \epsilon_x) \quad (13)$$

and

$$\sigma_x(\epsilon) = \frac{\pi e^4}{4\epsilon^2 \epsilon_x} (\epsilon - \epsilon_x) \quad (14)$$

where ϵ_x is the excitation energy. Equation (14) has a peak value at $\epsilon = 2\epsilon_x$ giving a peak value of the cross section

$$\sigma_x(2\epsilon_x) = \frac{\pi e^4}{16\epsilon_x^2} \quad (15)$$

Equation (14) seems to give reasonable behavior for singlet-singlet transitions such as $1\Sigma^+ \rightarrow a^1\Pi_g$. However, for the singlet-triplet transitions such as $1\Sigma_g^+ \rightarrow A^3\Sigma_u^+$, equation (14) does not fall off rapidly enough with increasing energy. The functional form for the triplet excitation cross section is

$$\sigma_x(\epsilon) = \sigma_1 [a(\epsilon - \epsilon_x)] e^{-a\epsilon} \quad (16)$$

where σ_1 and a are constants to be determined.

The maximum value for the cross section given by equation (16) occurs at the energy

$$\epsilon_M = \frac{1}{a} + \epsilon_x$$

Setting $\epsilon_M = 2\epsilon_x$ so that the peak cross section occurs at the same energy as predicted by equation (14) gives the result $a = \epsilon_x^{-1}$, and

$$\sigma_x(\epsilon) = \sigma_1 \left(\frac{\epsilon - \epsilon_x}{\epsilon_x} \right) e^{-\epsilon/\epsilon_x} \quad (17)$$

Setting $\epsilon = 2\epsilon_x$ in equation (17) and equating the resulting cross section to the peak cross section given by equation (14) leads to an expression for σ_1 ,

$$\sigma_1 = 0.461 \frac{\pi e^4}{\epsilon_x^2} \quad (18)$$

and

$$\sigma_x(\epsilon) = 0.461 \frac{\pi e^4}{\epsilon_x^3} (\epsilon - \epsilon_x) e^{-\epsilon/\epsilon_x} \quad (19)$$

Equations (14) and (19) will be used to calculate the various electronic excitation processes of interest in this report and the results compared with existing experimental data and the results of other calculations.

(1) Nitrogen Cross Section for $A^3\Sigma_u^+$ State

The excitation energy for this state is about $\epsilon_x = 6.7$ ev (Ref. 11); hence, the calculated peak value of the cross section will occur at $\epsilon = 13.4$ ev and the peak value of the cross section calculated from equation (19) is $\sigma_x(2\epsilon_x) = 9.1 \times 10^{-17} \text{ cm}^2$.

The experimental data of Borst (Ref. 3) place the peak at $\epsilon \sim 11$ ev, which is in reasonable agreement with calculated value. The measured value of the peak cross section is $\sigma_x = \left(5.3^{+4.0}_{-3.0} \right) \times 10^{-17} \text{ cm}^2$. The upper limit is very close to the calculated value.

The calculated peak value of Engelhardt, et al. (Ref. 6) is $\sigma_x \approx 0.6 \times 10^{-16} \text{ cm}^2$, but their peak occurs at about 7.5 ev, which is about 4 ev lower than the experimental value. The calculated value of Chung and Lin (Ref. 12) has a peak value at about 11 ev, but their calculated peak cross section is $\sigma_x \approx 1.21 \times 10^{-16} \text{ cm}^2$.

The cross section used by Kroli and Watson (Ref. 11) for excitation of the $N_2(A^3\Sigma_u^+)$ level is

$$\sigma_x(\epsilon) = 3.45 \times 10^{-16} (\epsilon - 6.7) e^{-\epsilon/6.7} \text{ cm}^2 \quad (20)$$

where ϵ is in units of ev. This is to be compared with the equation used in this report,

$$\sigma_x(\epsilon) = 1.01 \times 10^{-16} (\epsilon - 6.7) e^{-\epsilon/6.7} \text{ cm}^2 \quad (21)$$

Thus, Kroll and Watson obtain a peak cross section about a factor of 3 higher than obtained in the present calculation. This is attributed to the fact that Kroll and Watson multiplied by a scale factor to give the measured low-frequency breakdown threshold in air.

Various excitation functions for the $A^3\Sigma_u^+$ state of N_2 are compared in figure 2. The peak value error bar given by Borst is shown to indicate the magnitude of the experimental uncertainties involved. The values of Kroll and Watson equation (20) are not plotted since they are similar to those for equation (21) except off scale a factor of about 3 higher.

(2) Nitrogen Cross Section for $B^3\Pi_g$ State

The excitation energy for this state is about 7.4 ev, giving a peak value of the cross section at 14.8 ev of $7.5 \times 10^{-17} \text{ cm}^2$ calculated from equation (19). Chung and Lin (Ref. 12) report both a corrected experimental excitation function for N_2 and a theoretical one. These are

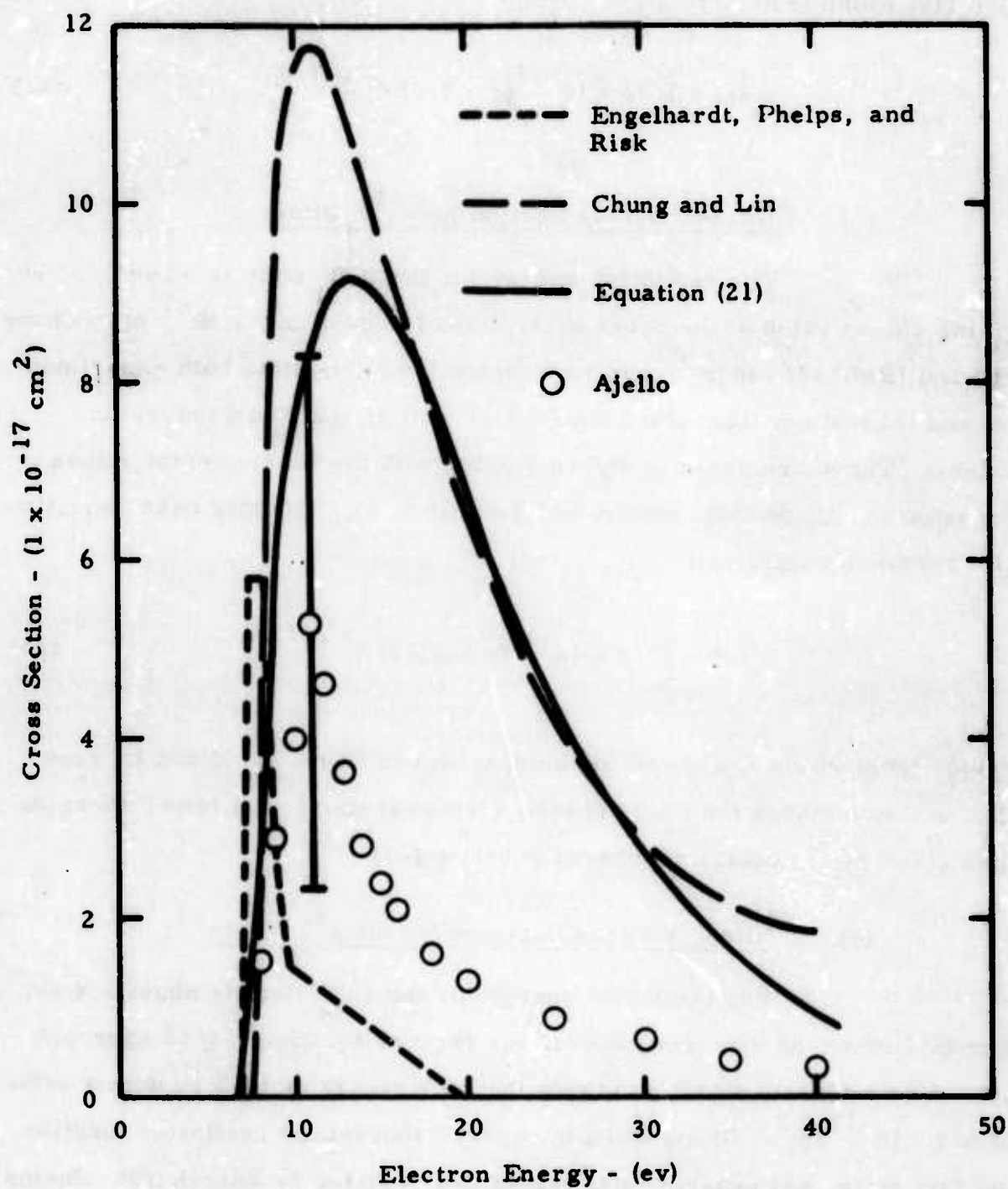


Figure 2. Excitation Functions for the $A^3\Sigma_u^+$ State For N_2

shown in figure 3. Also shown is the theoretical curve obtained from equation (19) which is numerically

$$\sigma_x(\epsilon) = 7.16 \times 10^{-17} (\epsilon - 7.4) e^{-\epsilon/7.4} \quad (22)$$

(3) Nitrogen Cross Section for $C^3\Pi_u$ State

The excitation energy for the $C^3\Pi_u$ state is about 11.2 ev giving a peak value of the cross section at 22.4 ev of 3.3×10^{-17} ev. Chung and Lin (Ref. 12) report excitation functions for this state both experimental and theoretical from other sources as well as their own theoretical values. These are shown in figure 4 along with the experimental values reported by Engelhardt, Phelps and Risk (Ref. 6). For this case, equation (19) becomes numerically

$$\sigma_x(\epsilon) = 2.15 \times 10^{-17} (\epsilon - 11.2) e^{-\epsilon/11.2} \quad (23)$$

values from which are shown for comparison in figure 4. It can be seen that in this instance the peak appears somewhat sharper at lower energies than given by the classical form of equation (23).

(4) Nitrogen Cross Sections for the $a^1\Pi_g$ State

The excitation energy for the $a^1\Pi_g$ state is about 8.4 ev. For this state, as discussed above, the form of equation (14) is appropriate. The peak cross section in this instance occurs at 16.8 ev with a value of $5.8 \times 10^{-17} \text{ cm}^2$. Chung and Lin report a theoretical excitation function for this state, and experimental values are reported by Engelhardt, Phelps and Risk (Ref. 6), by Ajello (Ref. 9) and by Borst (Ref. 8), all of which are shown in figure 5. The numerical form of equation (14) for this case is

$$\sigma_x(\epsilon) = 1.94 \times 10^{-15} (\epsilon - 8.4)/\epsilon^2 \quad (24)$$

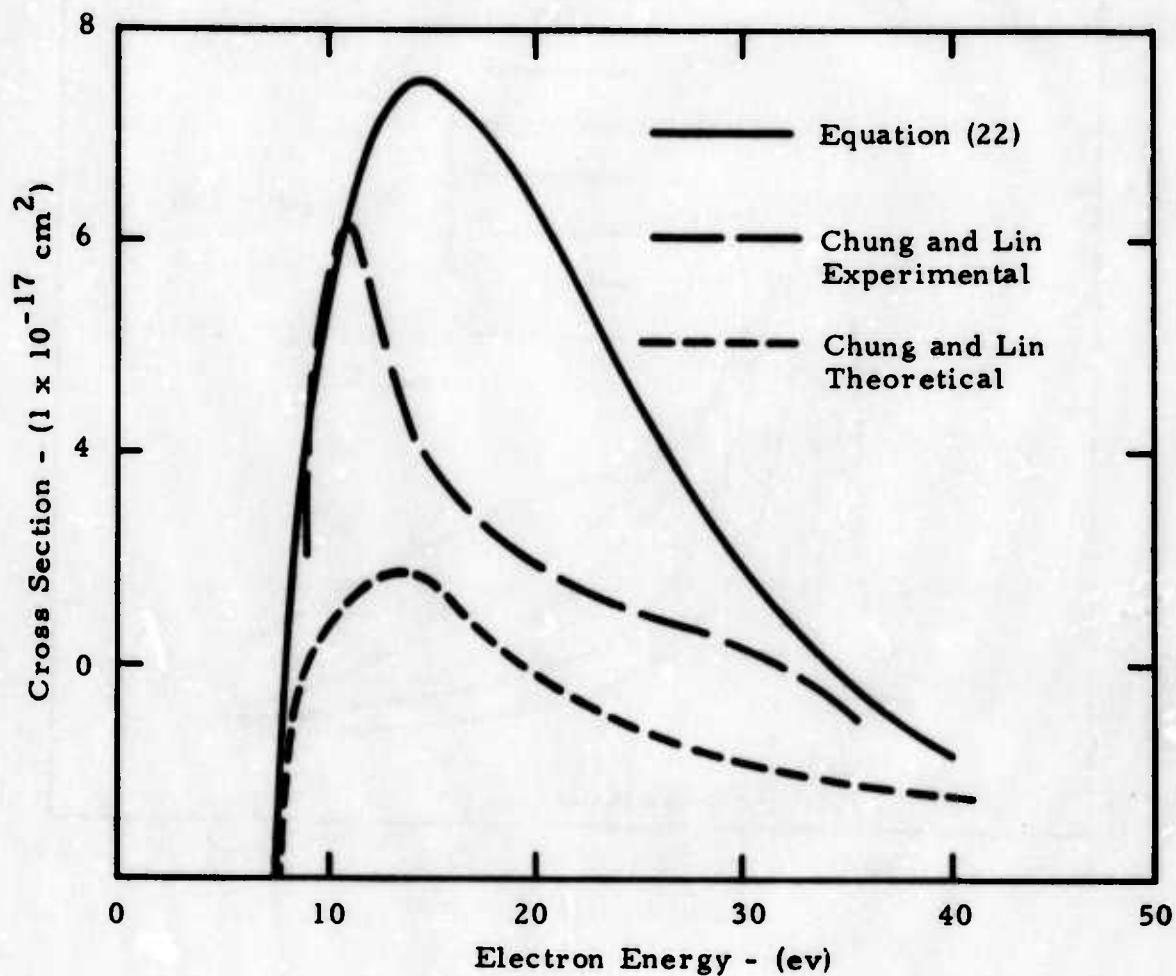


Figure 3. Excitation Functions for the $B^3\Pi_g$ State For N_2

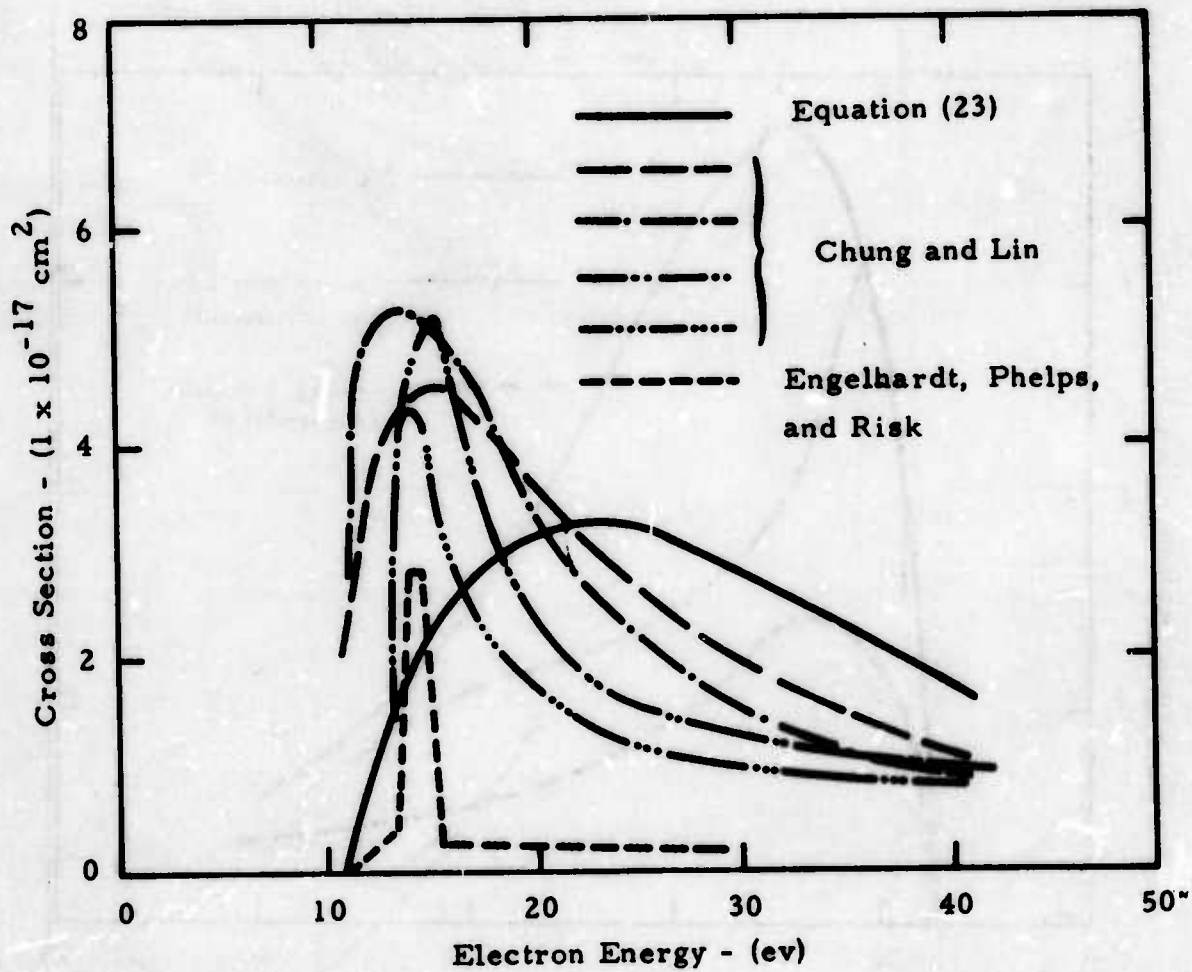


Figure 4. Excitation Functions for the $C^3\Pi_u$ State For N_2

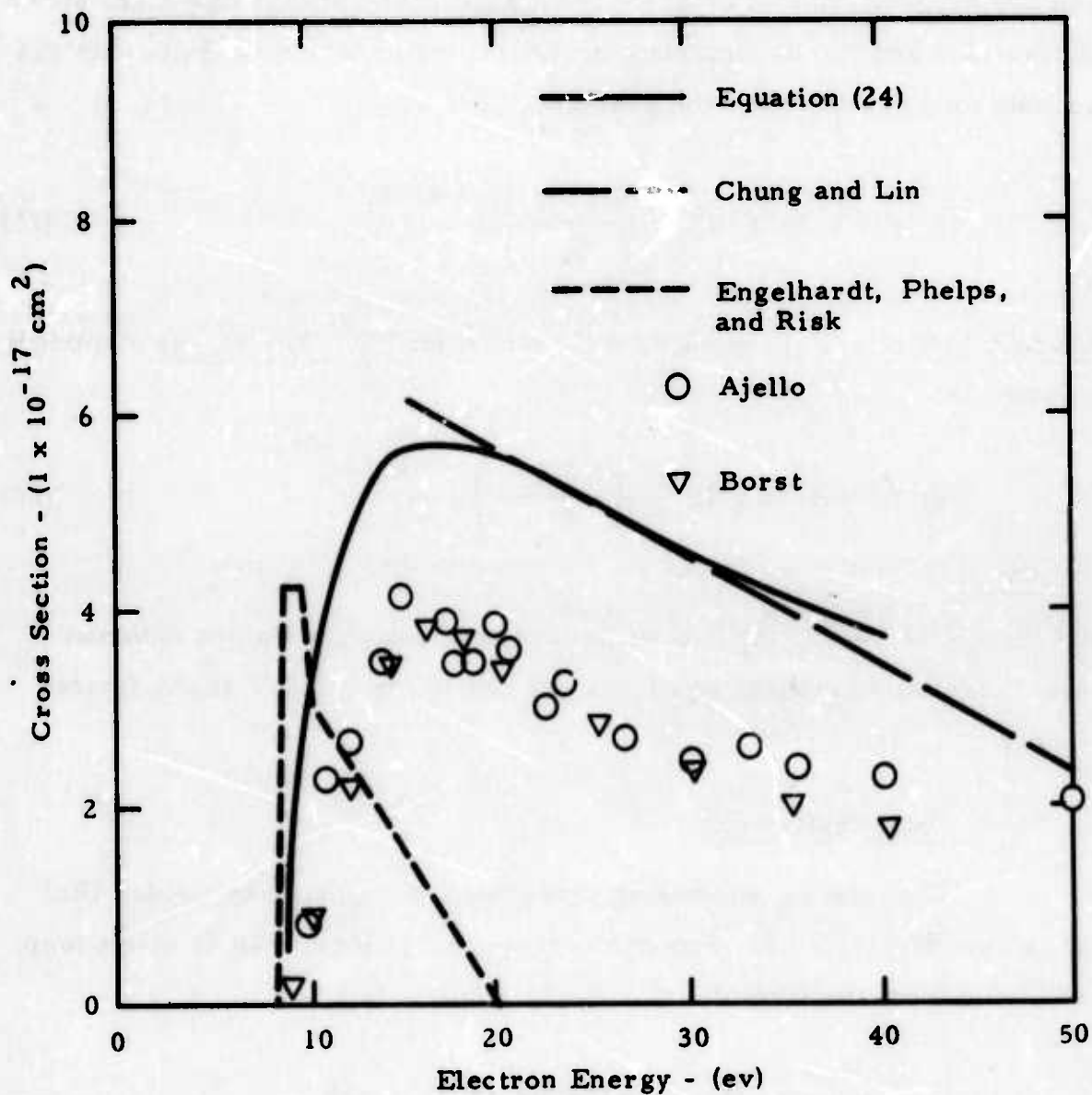


Figure 5. Excitation Functions for the $a^1\Pi_g$ State For N_2

Values obtained from this equation are also shown in figure 5 for comparisons.

c. Ionization

Extensive data exists for ionization cross sections in both nitrogen and oxygen. Values obtained from a summary of these data are shown in figures 6 and 7. Approximate empirical forms which fit these data reasonably well at least over the peak are for N_2 :

$$\sigma_i(\epsilon) = 1.76 \times 10^{-15} \left(\frac{\epsilon - \epsilon_i}{\epsilon_i} \right) e^{-\epsilon/5\epsilon_i} \quad (25)$$

where $\epsilon_i = 15.58$ ev, the ionization threshold for N_2 . For O_2 the empirical equation is:

$$\sigma_i(\epsilon) = 5.10 \times 10^{-16} \left(\frac{\epsilon - \epsilon_i}{\epsilon_i} \right) e^{-\epsilon/15\epsilon_i} \quad (26)$$

where $\epsilon_i = 12.06$ ev, the ionization threshold for O_2 . Values obtained from these two empirical equations are shown for comparison in figures 6 and 7.

d. Total Scattering

The total N_2 scattering cross section reported by Golden (Ref. 13) is shown in figure 8. For comparison, an empirical fit is also shown calculated from the formula.

$$\sigma_T(\epsilon) = \left[1 + 2e^{-2(\epsilon - 2.5)^2} \right] \times 10^{-15} \quad (27)$$

All of the empirical formulae described above are approximate, but considering the large uncertainties present in much of the experimental

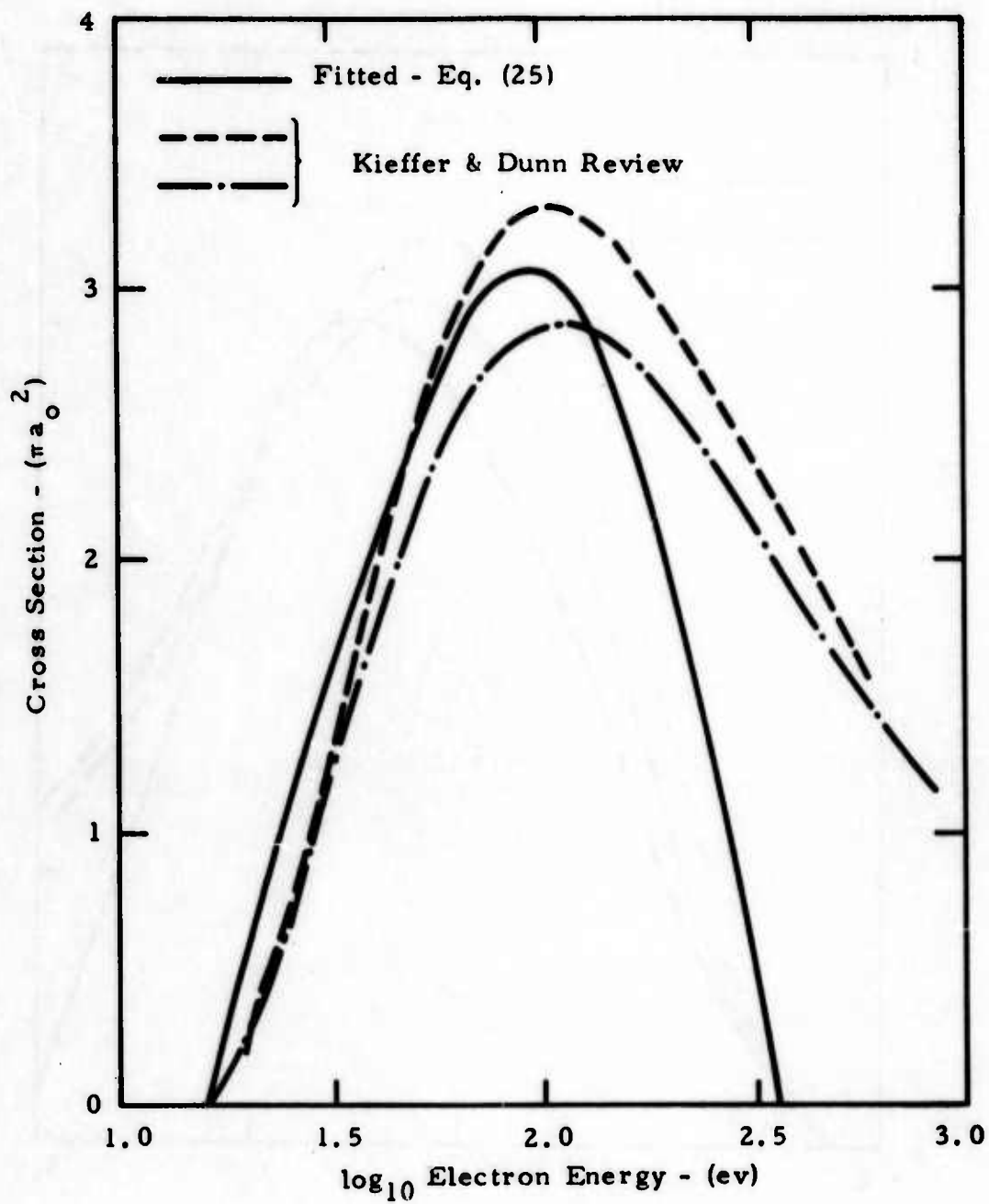


Figure 6. Total N_2 Ionization Cross Section

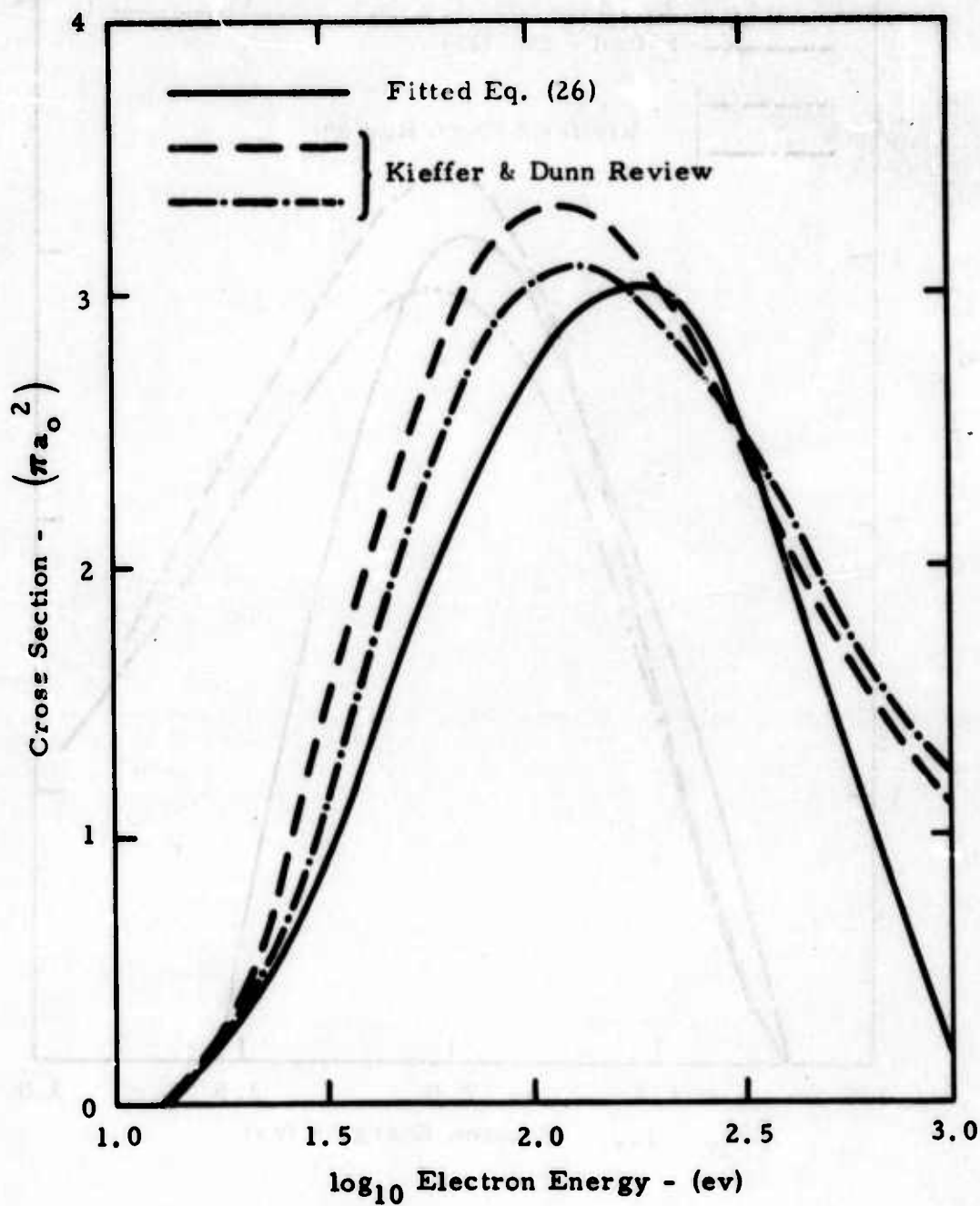


Figure 7. Total O₂ Ionization Cross Section

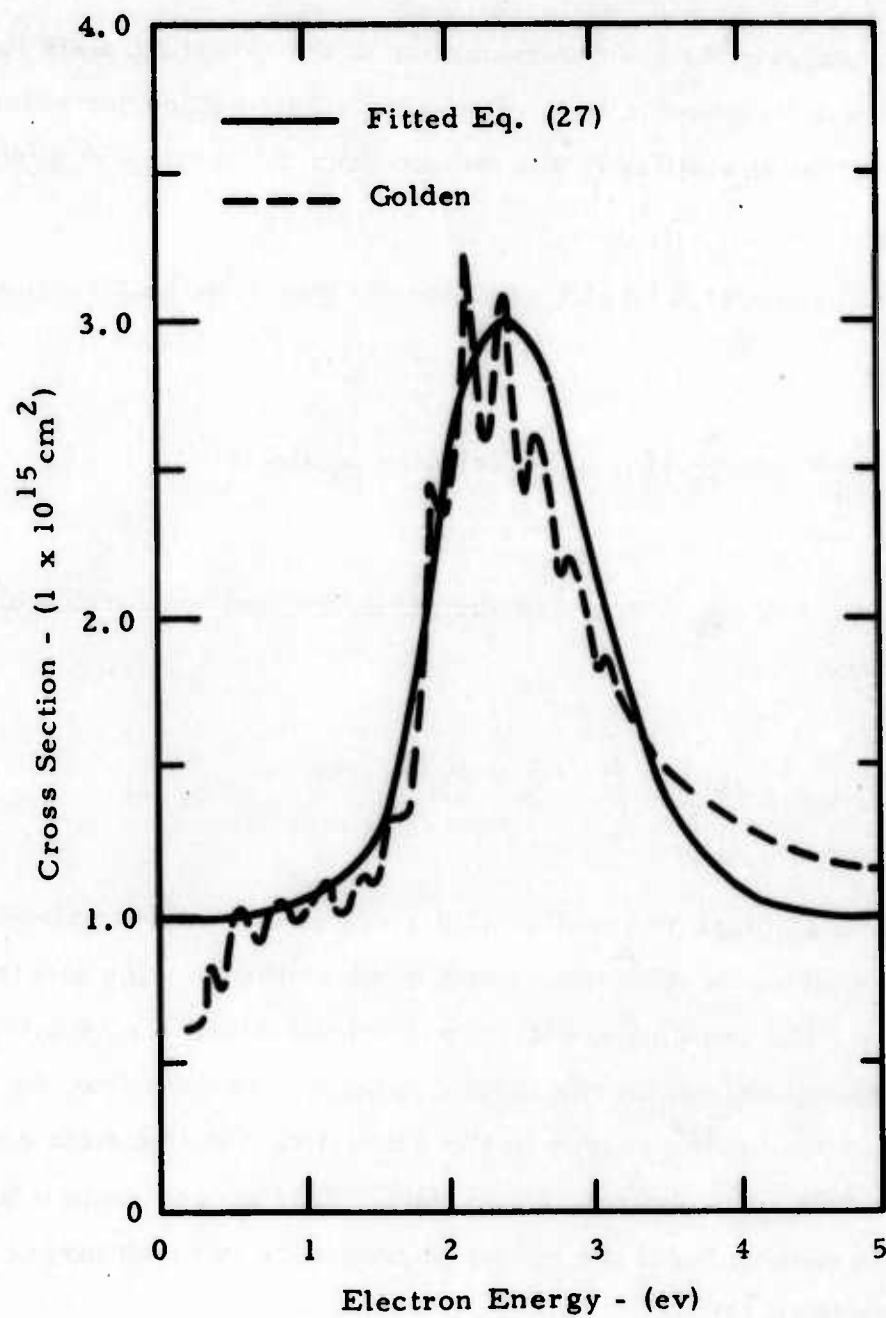


Figure 8. Total N₂ Electron Scattering Cross Section.

data available, these formulae are useful for purposes of estimation.

2. BREAKDOWN ANALYSIS

An analysis for the determination of the threshold field leading to breakdown will be given in this subsection. The method for solving the kinetic equation is similar to the method used by Baraff and Buchsbaum (Ref. 14).

An approximate kinetic equation for electrons gaining energy at a rate k is

$$\left(\frac{\partial}{\partial t} + k \frac{\partial}{\partial \epsilon} \right) f(\epsilon, t) = \delta(\epsilon) g(t) - \nu_{xi} f(\epsilon, t) \quad (28)$$

where $\nu_{xi} = \nu_x + \nu_i$, ν_x and ν_i are the excitation and ionization collision frequencies, and

$$g(t) = \int_0^{\infty} (\nu_x + 2\nu_i) f(\epsilon, t) d\epsilon \quad (29)$$

The factor of 2 enters in equation (29) since electrons are gained in the distribution following an ionization event in which the ionizing electron is left with energy ϵ and ionizing events in which the ionized electron has an energy ϵ . The approximation for the kinetic equation assumes that the rate at which an electron gains energy in the oscillating electric field can be represented in terms of an "effective" dc field. This approximation has been shown to be reasonable if the radiation frequency is much larger than electron growth rate (Ref. 14).

Defining the Laplace transforms of the distribution function $f(\epsilon, t)$ and the function $g(t)$,

$$\tilde{f}(\epsilon, p) = \int_0^{\infty} f(\epsilon, t) e^{-pt} dt \quad (30)$$

$$\tilde{g}(p) = \int_0^{\infty} g(t) e^{-pt} dt \quad (31)$$

$$= \int_0^{\infty} v(\epsilon) \tilde{f}(\epsilon, p) d\epsilon$$

where $v(\epsilon) = 2v_1(\epsilon) + v_x(\epsilon)$. Equation (28) becomes

$$\left(k \frac{\partial}{\partial \epsilon} + p + v_{xi} \right) \tilde{f}(\epsilon, p) = \delta(\epsilon) [1 + \tilde{g}(p)] \quad (32)$$

where the assumption

$$f(\epsilon, 0) = \delta(\epsilon) \quad (33)$$

has been used. Dividing equation (32) by $[1 + \tilde{g}(p)]$,

$$\left(k \frac{\partial}{\partial \epsilon} + p + v_{xi} \right) \tilde{G}(\epsilon, p) = \delta(\epsilon) \quad (34)$$

where

$$\tilde{G}(\epsilon, p) = \frac{\tilde{f}(\epsilon, p)}{1 + \tilde{g}(p)} \quad (35)$$

Multiplying equation (35) by $v(\epsilon)$ and integrating over all ϵ

$$\int_0^{\infty} v(\epsilon) \tilde{G}(\epsilon, p) d\epsilon = \frac{1}{1 + \tilde{g}(p)} \int_0^{\infty} v(\epsilon) \tilde{f}(\epsilon, p) d\epsilon \quad (36)$$

Using equation (31), equation (36) can be rewritten as

$$\tilde{g}(p) = \frac{\tilde{N}(p)}{1 - \tilde{N}(p)} \quad (37)$$

where

$$\tilde{N}(p) = \int_0^{\infty} v(\epsilon) \tilde{G}(\epsilon, p) d\epsilon \quad (38)$$

Taking the Laplace inversion of equation (37),

$$g(t) = \frac{1}{2\pi i} \int_{\beta - i\infty}^{\beta + i\infty} \frac{\tilde{N}(p)}{1 - \tilde{N}(p)} e^{pt} dp \quad (39)$$

Equation (39) can be integrated by closing the contour in the left half of the complex p-plane giving

$$g(t) = - \frac{\tilde{N}(\gamma)}{\left(\frac{d\tilde{N}}{dp}\right)_{p=\gamma}} e^{\gamma t} \quad (40)$$

where γ is the value of p for which $\tilde{N}(p = \gamma) = 1$. Thus, γ is the growth rate for electron production and is determined by the condition $\tilde{N}(\gamma) = 1$.

Solving equation (34) for $\tilde{G}(\epsilon, \gamma)$,

$$\tilde{G}(\epsilon, \gamma) = \frac{1}{k} e^{-\frac{1}{k} \int_0^\epsilon (\gamma + v_{xi}) d\epsilon'} \quad (41)$$

Substituting equation (41) into equation (38) and using the relation $\tilde{N}(\gamma) = 1$,

$$\frac{1}{k} \int_0^\infty v(\epsilon) \exp \left[-\frac{1}{k} \left(\gamma \epsilon + \int_0^\epsilon v_{xi}(\epsilon') d\epsilon' \right) \right] d\epsilon = 1 \quad (42)$$

Equation (42) can be written in the equivalent form

$$\begin{aligned} & \int_0^\infty \left(\frac{v_{xi} + \gamma}{k} \right) \exp \left[-\int_0^\epsilon \left(\frac{v_{xi} + \gamma}{k} \right) \right] d\epsilon' d\epsilon \\ & + \frac{1}{k} \int_0^\infty v_i(\epsilon) \exp \left[-\frac{1}{k} \left(\gamma \epsilon + \int_0^\epsilon v_{xi}(\epsilon') d\epsilon' \right) \right] d\epsilon \\ & - \frac{\gamma}{k} \int_0^\infty \exp \left[-\frac{1}{k} \left(\gamma \epsilon + \int_0^\epsilon v_{xi}(\epsilon') d\epsilon' \right) \right] d\epsilon = 1 \end{aligned} \quad (43)$$

The first integral of equation (43) integrates to unity, hence,

$$\gamma = \frac{\int_0^\infty v_i(\epsilon) e^{-\frac{\gamma \epsilon}{k} - \frac{1}{k} \int_0^\epsilon v_{xi}(\epsilon') d\epsilon'} d\epsilon}{\int_0^\infty e^{-\frac{\gamma \epsilon}{k} - \frac{1}{k} \int_0^\epsilon v_{xi}(\epsilon') d\epsilon'} d\epsilon} \quad (44)$$

When the energy is less than the ionization energy, the numerator of equation (44) is zero, therefore equation (44) can be rewritten as

$$\gamma = \frac{e^{-\bar{\nu}_x \Delta \epsilon / k} \int_{\epsilon_i}^{\infty} \nu_i(\epsilon) e^{-\frac{\gamma \epsilon}{k} - \frac{1}{k} \int_{\epsilon_i}^{\epsilon} \nu_{xi}(\epsilon') d\epsilon'} d\epsilon}{\int_0^{\infty} e^{-\frac{\gamma \epsilon}{k} - \frac{1}{k} \int_0^{\epsilon} \nu_{xi}(\epsilon') d\epsilon'} d\epsilon} \quad (45)$$

where

$$\bar{\nu}_x \Delta \epsilon = \int_{\epsilon_x}^{\epsilon_i} \nu_x(\epsilon') d\epsilon' \quad (46)$$

and ϵ_i , ϵ_x are the ionization and excitation energies, respectively.

Equation (45) can be written in terms of a mean value of the ionization frequency,

$$\gamma = \langle \nu_i \rangle e^{-\bar{\nu}_x \Delta \epsilon / k} \left[1 - \frac{B}{1+B} \right] \quad (47)$$

where B is a correction factor describing the deviation of the ionization frequency from its mean value. The value of B can range from B = 0, corresponding to no excitation levels, to B = ∞, corresponding to an infinite excitation frequency. In the case B = 0, the ionization frequency will be just the inverse of the time required for the electron to gain an amount of energy equal to the ionization energy.

$$\langle \nu_i \rangle \approx \frac{k}{\epsilon_i} \quad (48)$$

hence,

$$\gamma = \frac{k}{\epsilon_i} e^{-\bar{v}_x \Delta \epsilon / k} \left(1 - \frac{B}{1+B} \right) \quad (49)$$

As a first approximation it will be assumed that B is small and that the growth rate is adequately described by

$$\gamma = \frac{k}{\epsilon_i} e^{-\bar{v}_x \Delta \epsilon / k} \quad (50)$$

The electrons in the laser field will gain energy at some distribution varying about the mean rate of energy gain. A general distribution function of the form

$$j(k) dk = \left(\frac{\eta}{k_0} \right)^\eta \frac{1}{\Gamma(\eta)} k^{\eta-1} e^{-\eta k/k_0} dk \quad (51)$$

where η is a numerical factor and k_0 is the mean rate of energy gain will be considered. It should be noted that equation (51) satisfies the conditions

$$\begin{aligned} \int_0^\infty j(k) dk &= 1 \\ \int_0^\infty k j(k) dk &= k_0 \end{aligned} \quad (52)$$

If a value $\eta = \frac{3}{2}$ is used equation (51) has a Maxwellian shape about the mean energy gain.

The mean growth rate is

$$\bar{\gamma} = \frac{\eta^{\eta} k_o}{\Gamma(\eta) \epsilon_i} \int_0^{\infty} y^{\eta} e^{-\left(\eta y + \frac{\bar{v}_x \Delta \epsilon}{k_o y}\right)} dy \quad (53)$$

where

$$y = k/k_o \quad (54)$$

Making the transformation

$$y = \left(\frac{\bar{v}_x \Delta \epsilon}{\eta k_o} \right)^{\frac{1}{2}} e^{\zeta} \quad (55)$$

in equation (53) gives

$$\bar{\gamma} = \frac{\eta^{\eta} k_o}{\Gamma(\eta) \epsilon_i} \left(\frac{\bar{v}_x \Delta \epsilon}{\eta k_o} \right)^{(\eta+1)/2} \int_{-\infty}^{\infty} e^{(\eta+1)\zeta} e^{-2 \left(\frac{\eta \bar{v}_x \Delta \epsilon}{k_o} \right)^{\frac{1}{2}} \cosh \zeta} d\zeta$$

or

$$\bar{\gamma} = 2 \frac{\eta^{\eta} k_o}{\Gamma(\eta) \epsilon_i} \left(\frac{\bar{v}_x \Delta \epsilon}{\eta k_o} \right)^{(\eta+1)/2} \int_0^{\infty} \cosh[(\eta+1)\zeta] e^{-2 \left(\frac{\eta \bar{v}_x \Delta \epsilon}{k_o} \right)^{\frac{1}{2}} \cosh \zeta} d\zeta \quad (56)$$

The integral in equation (56) is a well known integral representation for a modified Bessel function of the second kind (Ref. 15)

$$\bar{\gamma} = 2 \frac{\eta^{\eta} k_o}{\Gamma(\eta) \epsilon_i} \left(\frac{z}{2\eta} \right)^{\eta+1} K_{\eta+1}(z) \quad (57)$$

where

$$z = 2 \left(\frac{\eta \bar{v}_x \Delta \epsilon}{k_0} \right)^{\frac{1}{2}} \quad (58)$$

Thus, one can utilize equation (57) to study the average electron growth rate for a very generalized distribution in the rate of energy gain.

For the present study a Maxwellian type of distribution function will be assumed, thus,

$$\bar{\gamma} = \frac{4}{\pi} \left(\frac{\bar{v}_x \Delta \epsilon}{\epsilon_i} \right) [z k_2(z)] \quad (59)$$

where

$$z k_2(z) = \sqrt{\frac{\pi z}{2}} K_{5/2}(z) = \frac{\pi}{2} e^{-z} (1 + 3z^{-1} + 3z^{-2}) \quad (60)$$

and

$$z = \left(\frac{6 \bar{v}_x \Delta \epsilon}{k_0} \right)^{\frac{1}{2}} \quad (61)$$

It should be noted that when z is large enough so that $3z^{-1}$ and $3z^{-2}$ can be neglected in comparison to unity then equation (59) has the particularly simple form

$$\bar{\gamma} \approx 2 \left(\frac{\bar{v}_x \Delta \epsilon}{\epsilon_i} \right) e^{-z} \quad (62)$$

The only parameter in equations (59) and (62) which involves the laser properties is z , hence, the relation of the threshold field to the state of the propagating medium can be seen quite clearly.

The rate at which an electron gains energy in the field of a laser beam is given by the relation

$$k_o = \frac{e^2 E^2}{2m\omega^2} \quad \nu_c = 3 \times 10^{-17} \lambda^2 \nu_c P \text{ (watts/cm}^2\text{)} \frac{\text{ergs}}{\text{sec.}} \quad (63)$$

where λ is the radiation wavelength and P , as indicated, is in units of watts/cm². Thus, in the definition of z , there is a ratio of excitation frequency to total collision frequency. In a first approximation it will be assumed that

$$\frac{\bar{\nu}_x}{\nu_c} = \frac{\bar{\sigma}_x}{\sigma_c} \quad (64)$$

and, in analogy to equation (46),

$$\bar{c}_x \Delta \epsilon = \int_{\epsilon_x}^{\epsilon_i} \sigma_x(\epsilon) d\epsilon \quad (65)$$

The electronic excitation processes to be considered are shown in Table I along with other relevant information. The excitation of the N_2

Species	State	Ex. Energy(ev)	Ion. Energy(ev)
N_2	$A^3\Sigma_u^+$	6.7	15.8
	$a^1\Pi_g$	8.4	
	$C^3\Pi_u$	11.2	
O_2	$B^3\Sigma_u^-$	6.1	12.2

Table I
Electronic Excitation Processes

vibrational levels is assumed to have a constant cross section of $3 \times 10^{-16} \text{ cm}^2$, over the energy interval 1.9 to 2.8 ev.

For the singlet transitions, the cross section is given by equation (14). Integrating over the energy interval,

$$\begin{aligned} \bar{\sigma}_x \Delta \epsilon &= \frac{\pi e^4}{4\epsilon_x} \int_{\epsilon_x}^{\epsilon_i} \left(\frac{\epsilon - \epsilon_x}{\epsilon^2} \right) d\epsilon \\ &= \frac{\pi e^4}{4\epsilon_x} \left[\ln \left(\frac{\epsilon_i}{\epsilon_x} \right) - \left(\frac{\epsilon_i - \epsilon_x}{\epsilon_i} \right) \right] \end{aligned} \quad (66)$$

(singlet transition)

The integral for the triplet transitions, using the cross section given by equation (19),

$$\begin{aligned} \bar{\sigma}_x \Delta \epsilon &= 0.461 \frac{\pi e^4}{\epsilon_x} \int_{\epsilon_x}^{\epsilon_i} (\epsilon - \epsilon_x) e^{-\epsilon/\epsilon_x} d\epsilon \\ &= 0.17 \frac{\pi e^4}{\epsilon_x} \left(1 - 2.72 \frac{\epsilon_i}{\epsilon_x} e^{-\epsilon_i/\epsilon_x} \right) \end{aligned} \quad (67)$$

(triplet transitions)

The contributions from each of the levels is given in Table II.

Species	State	$\bar{\sigma}_x \Delta G$ (cm-ev)
N ₂	A ³ Σ_u^+	6.38×10^{-16}
	C ³ Π_u	5.89×10^{-17}
	a ¹ Π_g	3.12×10^{-16}
	VIB.	2.70×10^{-16}
O ₂	B ³ Σ_u^-	3.42×10^{-16}

Table II
Contributions From Each Level

Assuming a composition of 78% N₂ and 21% O₂, the total integral of the excitation cross section over the energy range from threshold to ionization is,

$$\bar{\sigma}_x \Delta \epsilon = 1.07 \times 10^{-15} \text{ cm}^2 \cdot \text{ev} \quad (68)$$

The contribution from the N₂(C³ Π_u) and O₂(B³ Σ_u^-) (Schumann-Runge band) bands is negligible in comparison to the other states.

The calculated results for the complete breakdown of air, assuming an initial electron density of one electron per cm³, are shown in figure 9. The results of calculations by Canavan et al. (Ref. 16) are shown for purposes of comparison. The agreement is relatively good but is somewhat higher than the quoted experimental value of $\rho \sim 2 \times 10^9$ watts/cm².

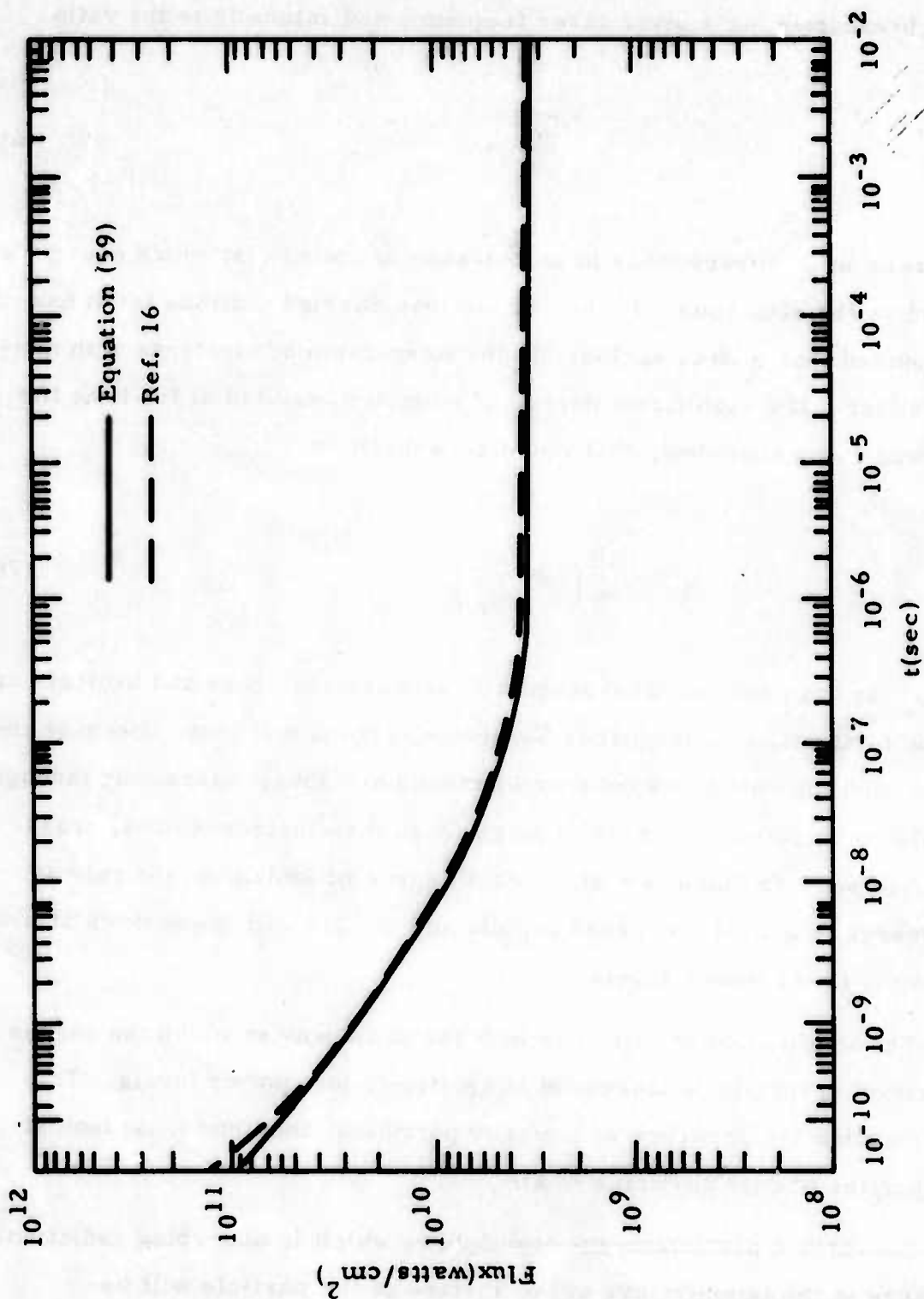


Figure 9. Comparison of Air Breakdown Calculations

Nevertheless, it is clear that the critical parameter in the determination of breakdown for a given laser frequency and intensity is the ratio

$$\frac{\bar{\nu}_x \Delta \epsilon}{\nu_c} \quad (69)$$

An increase in ν_c corresponds to an increase in the rate at which energy is absorbed by the electrons. In the calculations carried out thus far it has been assumed that ν_c was exclusively the interaction of electrons with neutral particles. If a significant degree of ionization existed at the time the energy was being absorbed, this would be written

$$\nu_c = \nu_{en} \left(1 + \frac{\nu_{ei}}{\nu_{en}} \right) \quad (70)$$

where ν_{en} is the total collision frequency between electrons and neutrals and ν_{ei} is the total collision frequency between electrons and ions. Because the cross section for collisions between electrons and ions, interacting through the Coulomb potential, is so much larger than the electron-neutral cross section, as soon as there is a significant degree of ionization the rate at which energy is gained increases rapidly and the air will break down at proportionately lower power levels.

The implication of this is to look for some way in which the degree of ionization in the air is increased at relatively low power levels. This usually implies the presence of impurity particles, thus one must look at the properties of dust particles in air.

Consider a particle in the atmosphere which is absorbing radiation. The change in the temperature at the surface of the particle will be

$$\Delta T \sim \frac{K\phi}{c_v \rho} \Delta t \quad (71)$$

where K is the absorption coefficient, ϕ is the radiation flux, c_v is the specific heat capacity of the absorbing particle, and ρ is the particle density. As a typical example, one can consider quartz (SiO_2) which has an absorption coefficient of $K \sim 10^4 \text{ cm}^{-1}$ at $\lambda \sim 10.6 \mu$, density $\rho \sim 2.7 \text{ gm/cm}^3$, and specific heat capacity $c_v \sim 1.3 \times 10^7 \text{ ergs/gm}^\circ\text{K}$. The vaporization temperature for SiO_2 is $T = 2.5 \times 10^3^\circ\text{K}$, thus, in order to raise the temperature of the surface of the particle to the vaporization level in a time $t \sim 10^{-8} \text{ sec}$. requires a flux $\phi \sim 9 \times 10^7 \text{ watts/cm}^2$. The equilibrium electron density for SiO_2 , which exists as SiO in the vapor state, can be obtained from the Saha equation,

$$\frac{N_e^2}{N_n} = 2 \left(\frac{2\pi m k T}{h^2} \right)^{3/2} \frac{g_+}{g_a} e^{-\epsilon_i/kT} \quad (72)$$

where h is the Planck constant and g is the degeneracy. Solving for N_e ,

$$N_e = \frac{S(T)}{2} \left[-1 + \sqrt{1 + \frac{4N_0}{S(T)}} \right] \quad (73)$$

where $S(T)$ is just the right hand side of equation (72). Taking a particle density of $N_0 \sim 4 \times 10^{22} \text{ cm}^{-3}$ and an ionization energy of $\epsilon_i \sim 10.8 \text{ ev}$, the equilibrium electron density at vaporization temperature will be $N_e \sim 10^{11} \text{ cm}^{-3}$. While this is a significant increase in electron density, it is probably not enough to lead to a major change in the breakdown power levels. Thus, one must do a somewhat more careful study of the heating and subsequent vaporization of dust particles with particular attention to various mechanisms for electron enhancement.

SECTION III

THE HYDRODYNAMIC EQUATIONS

Two separate models, one utilizing a single temperature for both ions and electrons and the other model treating the temperatures separately, have been developed for the description of dirty air breakdown. For this report, however, only the more realistic two-temperature model has been used for calculations. In both models a symmetry is assumed so that the problem can be treated in one dimension. The Lagrangean form of the one-dimensional hydrodynamic equations is used. The first three equations are essentially the same in both models (Ref. 17),

$$\frac{\partial R}{\partial t} = U \quad (74)$$

$$\frac{\partial U}{\partial t} = -R^{\alpha-1} \frac{\partial}{\partial M} (P + Q) \quad (75)$$

$$V = \frac{1}{\rho} = \frac{1}{\alpha} \frac{\partial R^{\alpha}}{\partial M} \quad (76)$$

expressing the definition of velocity U , the conservation of momentum and the conservation of mass. The artificial viscosity Q is necessary for numerical stability of the difference equations discussed in Appendix I. The geometry of the single dimension is plane, cylindrical or spherical for $\alpha = 1, 2$ or 3 , respectively, and M is the Lagrangean mass coordinate.

The one-temperature model is based on the assumption that the free electrons are in thermal equilibrium with the neutral molecules and ions of the shock heated air and blow off vapor. The electron density is determined by the Saha equation. The energy equation of hydrodynamics is

$$\frac{\partial E}{\partial t} = -\bar{P} \frac{\partial V}{\partial t} + \phi \bar{K} + \frac{\partial}{\partial M} \left[\chi R^{\alpha-1} \frac{\partial T}{\partial R} \right] \quad (77)$$

where χ is the thermal conductivity, ϕ is the laser flux and \bar{K} is the effective mass absorption coefficient for the material and free electrons. The hydrodynamic description is completed by air equation of state giving the pressure P as a function of the density ρ and specific internal energy E .

In the two-temperature model, it is assumed that the electrons are in a Boltzmann distribution at temperature T_e . The electrons interact with the neutral molecules and ions which are in a second Boltzmann distribution with temperature T_i . The total pressure in the momentum equation is the sum of the partial pressures of the electrons and ions.

$$P = P_e + P_i \quad (78)$$

For notation, the neutral molecules and ions are referred to collectively as "ions."

The energy equation now has separate components for the ions and electrons,

$$\frac{\partial E_i}{\partial t} = -\bar{P}_i \frac{\partial V}{\partial t} + \frac{\partial}{\partial M} \left[\chi_i R^{\alpha-1} \frac{\partial T_i}{\partial R} \right] + \phi \bar{K}_i + \bar{\nu}_c 2 \left(\frac{m_e}{m_i} \right) (E_e - E_i) \quad (79)$$

$$\frac{\partial E_e}{\partial t} = -\bar{P}_e \frac{\partial V}{\partial t} + \frac{\partial}{\partial M} \left[\chi_e R^{\alpha-1} \frac{\partial T_e}{\partial R} \right] + \phi \bar{K}_e - \bar{\nu}_c 2 \left(\frac{m_e}{m_i} \right) (E_e - E_i) \quad (80)$$

$$- \frac{\bar{\nu}_x N_e \epsilon_x}{\rho} - \frac{\bar{\nu}_i N_e \epsilon_i}{\rho} - \bar{\nu}_a E_e$$

where $\bar{P}_i + \bar{P}_e = P + Q$, $\bar{\nu}$ represents a collision frequency, ϵ is an energy, and E is a specific energy. The subscripts c , x , a and i represent elastic

collisions, excitation collisions, attachment, and ionization, respectively.

The change in the electron density is given by

$$\frac{\partial N_e}{\partial t} = \rho \frac{\partial}{\partial M} \left[D_e R^{\alpha=1} \frac{\partial N_e}{\partial R} \right] + \bar{v}_i N_e - \bar{v}_\alpha N_e \quad (81)$$

where D_e is the electron diffusion coefficient. Functional forms for these parameters are discussed in the next section.

1. COLLISION FREQUENCIES

The energy losses within the electron and ion gases are expressed in terms of the various collision frequencies averaged over some suitable distribution of energies. For the calculations to be carried out in this report, it will be assumed that the components of the gas have a Maxwellian velocity distribution about some temperature representative of the component under consideration, thus

$$\bar{v} = N \frac{\left(\frac{2}{\pi m} \right)^{\frac{1}{2}}}{(kT)^{3/2}} \int \epsilon \sigma(\epsilon) e^{-\epsilon/kT} d\epsilon \quad (82)$$

where N is the density of target particles, m is the mass of the colliding particle (in some cases the reduced mass), and σ is the cross section for the interaction under consideration. The integration is carried out over the appropriate energy range.

a. Electronic Excitation

Utilizing equation (14) of Section II for the cross section for singlet transitions,

$$\bar{v}_x = \frac{N_m e^4}{\epsilon_x (kT_e)^{3/2}} \left(\frac{\pi}{2m} \right)^{\frac{1}{2}} \int_{\epsilon_x}^{\infty} \left(\frac{\epsilon - \epsilon_x}{\epsilon} \right) e^{-\epsilon/kT} d\epsilon \quad (83)$$

where m is the electron mass, e is the electron charge, and T_e is the electron temperature. The integration is straightforward,

$$\bar{\nu}_x = \frac{N_m e^4}{\epsilon_x} \left(\frac{\pi}{2mkT_e} \right)^{\frac{1}{2}} e^{-\epsilon_x/kT_e} \left[1 - \frac{\epsilon_x}{kT_e} E_1 \left(\frac{\epsilon_x}{kT_e} \right) e^{\epsilon_x/kT_e} \right] \quad (84)$$

(singlet transition)

where $E_1(z)$ is an exponential integral of the first kind. In the special case $\epsilon_x \gg kT_e$,

$$\bar{\nu}_x = \frac{N_m e^4}{2\epsilon_x} \left(\frac{\pi kT_e}{2m} \right)^{\frac{1}{2}} e^{-\epsilon_x/kT_e} \quad (85)$$

(singlet transition)

A similar calculation for the triplet transitions gives

$$\bar{\nu}_x = \frac{0.340 e^4 N_m}{(kT_e + \epsilon_x)} \left(\frac{\pi}{2mkT_e} \right)^{\frac{1}{2}} e^{-\epsilon_x/kT_e} \left[1 + \frac{(1 - \epsilon_x/kT_e)(2 + \frac{\epsilon_x}{kT_e})}{(1 + \epsilon_x/kT_e)} \right] \quad (86)$$

(triplet transition)

b. Vibrational Excitation

The cross section for the resonant excitation of N_2 vibrational levels has been assumed to be constant over the energy range of interest, hence,

$$\bar{\nu}_x = N_m \sigma_v \left(\frac{8kT_e}{\pi m} \right)^{\frac{1}{2}} \left[\left(1 + \frac{\epsilon_1}{kT_e} \right) e^{-\epsilon_1/kT_e} - \left(1 + \frac{\epsilon_2}{kT_e} \right) e^{-\epsilon_2/kT_e} \right] \quad (87)$$

where $\sigma_v \approx 3 \times 10^{-16} \text{ cm}^2$, $\epsilon_1 \approx 1.8 \text{ eV}$ and $\epsilon_2 \approx 2.8 \text{ eV}$.

c. Ionization Frequencies

For N_2 , using equation (25) for the cross section,

$$\bar{\nu}_i(N_2) = \frac{1.64 \times 10^{-15} \epsilon_i^2}{(kT_e)^{3/2}} \left(\frac{2}{\pi m} \right)^{1/2} \frac{e^{-\epsilon_i/kT_e}}{\left(1 + 5 \frac{\epsilon_i}{kT_e} \right)} N_M \times \left[1 + \frac{54 \left(1 - \frac{5}{9} \frac{\epsilon_i}{kT_e} \right) \left(1 + \frac{5}{6} \frac{\epsilon_i}{kT_e} \right)}{\left(1 + \frac{5\epsilon_i}{kT_e} \right)^2} \right] \quad (88)$$

and for O_2 , using equation (26),

$$\bar{\nu}_i(O_2) = \frac{1.74 \times 10^{-15} \epsilon_i^2}{(kT_e)^{3/2}} \left(\frac{2}{\pi m} \right)^{1/2} \frac{e^{-\epsilon_i/kT_e}}{\left(1 + 15 \frac{\epsilon_i}{kT_e} \right)} N_m \times \left[1 + \frac{464 \left(1 - \frac{15}{29} \frac{\epsilon_i}{kT_e} \right) \left(1 + \frac{15}{16} \frac{\epsilon_i}{kT_e} \right)}{\left(1 + \frac{15\epsilon_i}{kT_e} \right)^2} \right] \quad (89)$$

d. Electron-Ion Elastic Collision Frequency

The elastic collision frequency for two particles interacting through a Coulomb potential can be evaluated from classical considerations (Ref. 18). The result, after averaging over the relative velocities is,

$$\bar{v} = \frac{4\pi N e^4}{m_o^{1/2} (2kT)^{3/2}} \ln \Lambda \quad (90)$$

where m_o is the reduced mass and

$$\Lambda = \frac{3kT}{e^2} r_D \quad (91)$$

$$r_D = \left[\frac{kT}{4\pi e^2 (N_i + N_e)} \right]^{\frac{1}{2}} \quad (92)$$

The length, r_D , is the well known Debye length and N_i , N_e are the ion and electron number densities, respectively. For the case of electron-ion collisions, the reduced mass in equation (90) is replaced by the electron mass.

2. AMBIPOLAR DIFFUSION COEFFICIENT

When the Debye length in a plasma is small in comparison to the characteristic diffusion length, the free electron diffusion coefficient must be replaced by the ambipolar diffusion coefficient. The Debye length is defined by

$$r_D = \left(\frac{kT}{8\pi N_e e^2} \right)^{\frac{1}{2}} \quad (93)$$

For typical conditions of interest, $T \sim 3 \times 10^3$ °K, $N_e > 10^{15} \text{ cm}^{-3}$, the Debye length is $r_D \sim 10^{-5} \text{ cm}$. The free electron diffusion coefficient under the same conditions will be $D_e \sim 10^2 \text{ cm}^2/\text{sec}$. The characteristic relaxation time of interest will be $\tau \sim 10^{-8} \text{ sec}$, hence,

$$L_D \sim \sqrt{D_e \tau} \sim 10^{-3} \text{ cm.} \quad (94)$$

Thus, one must consider the space charge effects on the diffusion of the electrons.

To do so one notes that the effect of the space charge will be to cause the electron to pull an ion along with it. This can be viewed as increasing the mass of the electron in the electron diffusion coefficient by the mass of the ion. The ion collision cross section with heavy particles will be about twice that of the electron cross section, hence,

$$\frac{\left(\frac{8kT_e}{\pi M_i}\right)^{\frac{1}{2}}}{N_a \sigma_i} = 2D_i \quad (95)$$

This is correct only when the ion and electron temperatures are equal. However, for purposes of the present report the temperatures will be close enough over times of interest so that equation (95) can be used.

3. FREE-FREE ABSORPTION COEFFICIENT

The interaction between a current and an electric field is described by the Maxwell's equations,

$$c \nabla \times \vec{E} = - \frac{\partial \vec{B}}{\partial t} \quad (96)$$

$$\nabla \times \vec{B} = \frac{4\pi \vec{j}}{c} + \frac{1}{c} \frac{\partial \vec{E}}{\partial t} \quad (97)$$

Reducing equations (96) and (97) to a single wave equation

$$\nabla^2 \vec{E} = \frac{1}{c^2} \frac{\partial^2 \vec{E}}{\partial t^2} = \frac{4\pi}{c^2} \frac{\partial \vec{j}}{\partial t} \quad (98)$$

where \vec{j} is the current density,

$$\vec{j} = -Ne\vec{v} \quad (99)$$

where N is the electron density and \vec{v} is the electron velocity.

The motion of an electron in an electric field is described by the equation of motion

$$\frac{d\vec{v}}{dt} + \nu_c \vec{v} = -\frac{e\vec{E}}{m} \quad (100)$$

where ν_c is the collision frequency. Assuming that the vector quantities all have the time behavior $e^{-i\omega t}$ where ω is the oscillation frequency, reduces equations (98) and (100)

$$\vec{v} = -\frac{e\vec{E}(\nu_c + i\omega)}{m(\omega^2 + \nu_c^2)} \quad (101)$$

$$\nabla^2 \vec{E} + \frac{\omega^2}{c^2} \vec{E} = i\frac{4\pi}{c^2} \omega N_e \vec{v} \quad (102)$$

Substitution of equation (101) into equation (102)

$$\nabla^2 \vec{E} + k^2 \vec{E} = 0$$

where

$$k = \frac{\omega}{c} \left[1 + i \frac{4\pi e^2 N(\nu_c + i\omega)}{m\omega(\omega^2 + \nu^2)} \right]^{\frac{1}{2}} \quad (103)$$

Assuming that the second term in the square brackets is small in comparison to unity, one can use the usual approximation.

$$k \approx \frac{\omega}{c} \left[1 + i \frac{2\pi e^2 N(\nu_c + i\omega)}{m\omega(\omega^2 + \nu^2)} \right] \quad (104)$$

The absorption coefficient will be just the imaginary portion of equation (104)

$$K_{ff} = \frac{2\pi N_e^2}{mc(\omega^2 + \nu^2)} \nu_c \quad (105)$$

This is the usual form for the free-free absorption coefficient. The mass absorption coefficient of equation (105) is just

$$\bar{K}_e = \frac{K_{ff}}{\rho} \quad (106)$$

SECTION IV

PARTICLE DESCRIPTION AND INTERACTIONS

The size of particles in dry atmospheric aerosols range from about 0.005μ to 20μ . Smaller particles are quickly attached to larger particles and are found only in a region of constant production. Particles larger than about 20μ are lost by sedimentation and are found only in the vicinity of a source. The density of particles versus radius shows a maximum near 10μ (Ref. 19).

Air breakdown experiments have been performed on particles in the range 40 - 100μ (Ref. 2). In order to compare our results with these experiments, computer runs were made for particles ranging in diameter from 12μ to 96μ .

1. ENERGY ABSORPTION FROM THE LASER BEAM

Energy is absorbed from the laser beam by two processes: mass absorption by the particle material, and inverse bremsstrahlung absorption by free electrons. As the particles are heated and ionized, the mechanism for absorption of energy from the laser beam shifts from the first to the second kind.

a. Mass Absorption

In general, it is necessary to know the mass absorption coefficients of the various types of dust particles which may be encountered in the atmosphere. Specifically under consideration are the materials Al_2O_3 , SiO_2 , C. and NaCl as representative of the common types of particles found in the atmosphere. The absorption coefficient is needed as a function of wavelength (at least for specific laser wavelengths of interest), as a function of particle material temperature, and as a function of material density as the particle melts and vaporizes.

Data of the kind needed are scarce. Data are available for normal density solids in the wavelength range of particular interest in optical (Ref. 20) and infrared (Ref. 21) applications at room temperatures. Good data for solids at elevated temperatures are known only for sapphire (Ref. 22) in the 0.5 to 6 μm wavelength range. An analysis of the absorption coefficient of quartz vapor (SiO) in air has been given for 10.6 μm wavelength as a function of temperature and density (Ref. 23). The reflection coefficient for neodymium laser light on a carbon target and targets of other materials has been reported as a function of laser pulse power (Ref. 24) level. Common salt is quite transparent at most wavelengths of interest. In all, the available empirical data are far from complete, and further experimental measurements in this area would be highly desirable. The known information is summarized below.

(1) SiO_2

Extensive data exist (Refs. 20 and 25) on the values of the absorption coefficient of SiO_2 in its various forms at room temperature for wavelengths in the range from 0.2 to 4.8 μm . The temperature dependence is not known to have been measured, however, as it has for sapphire. When SiO_2 is heated in air, it forms SiO vapor as a result of oxidation. The extinction coefficient of SiO has been measured (Ref. 26) as a function of wavelength from 0.24 to 14 μm . A plot of the absorption coefficient from these data is shown in figure 11 for SiO. Also shown in the figure is the room temperature absorption coefficient for silica, and one point measured at AFWL for fused silica at 2.8 μm . A value of the absorption coefficient between 2000° and about 4000°K for normal density ($\rho = 2.13 \text{ gm/cc}$) SiO derived from the work of Chang, Drummond, and Hall is also shown for comparison. It falls below that for the room temperature material despite being for elevated temperatures. Both values were used in the computer runs made.

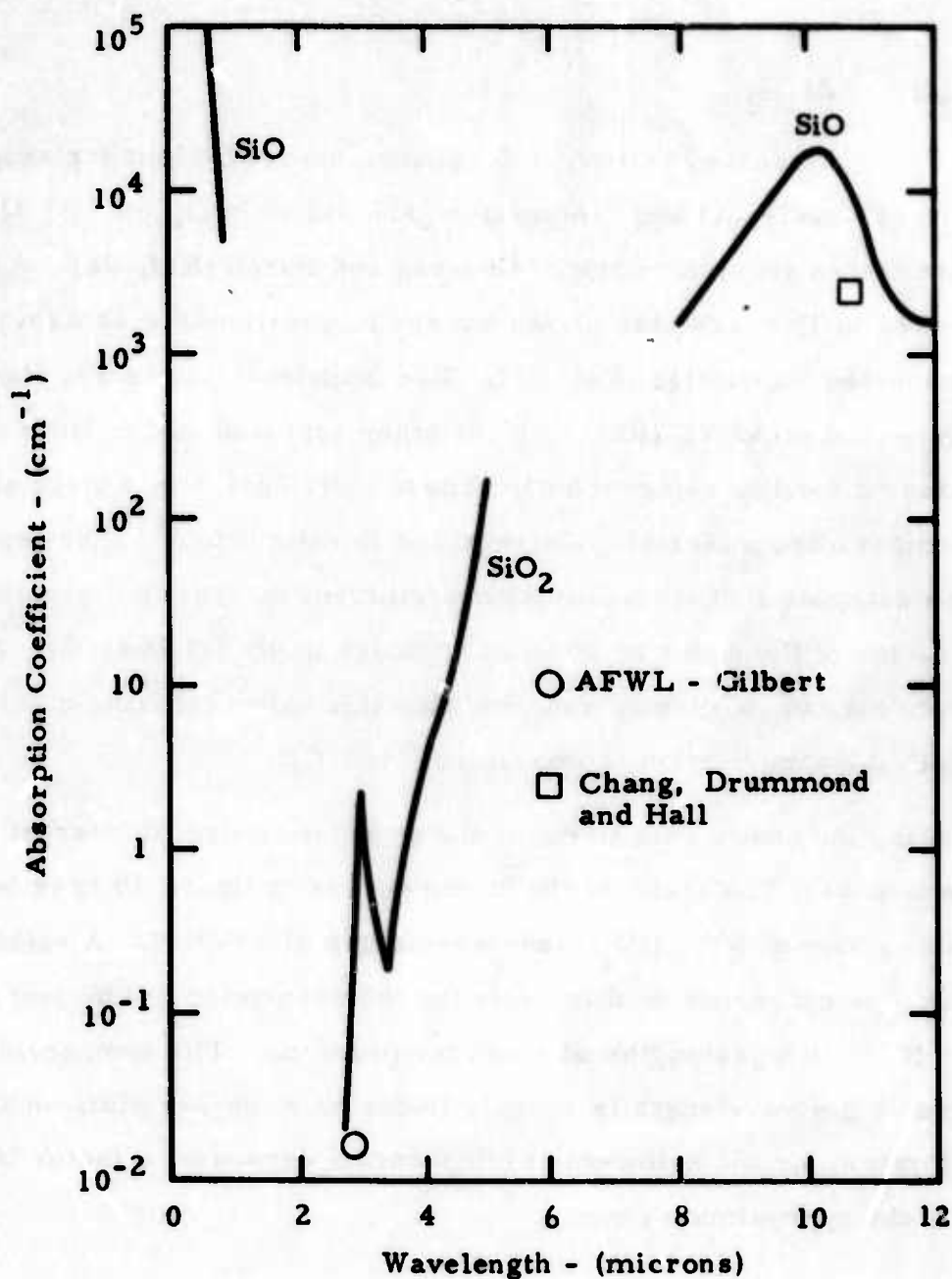


Figure 11. Absorption Coefficient for SiO_2 and SiO as a Function of Wavelength

The density dependence of the absorption coefficient employed was of the form $(\rho/\rho_0)^n$, where n was chosen to equal two for SiO in conformance with the value given for diatomic molecules by Chang, Drummond, and Hall.



Measured values of the absorption coefficient for sapphire as a function of wavelength and temperature are shown in figure 10. Most of these data comes from the work of Gryvnak and Burch (Ref. 22). A few points reported in 1936 are also shown but are of questionable accuracy because of suspected impurities (Ref. 27). Two additional points are shown. One was measured at AFWL (Ref. 28); the other reported as the limit of the transmission band in reference 21. These individual points were all for room temperature material. Gryvnak and Burch (Ref. 22) also report a qualitative estimate that the absorption coefficient increases discontinuously by a factor of the order of 30 when sapphire melts (at 2045°C). As a first approximation, it may be assumed that this value remains about constant up to the vaporization temperature (2980°C).

Extending the known data to cover the complete range of interest is largely speculative. The trend of the known curves in figure 10 have been extrapolated as shown to the CO_2 laser wavelength of interest. A value of about $1.0\mu\text{m}^{-1}$ is estimated on this basis for the absorption coefficient of sapphire at $10.6\mu\text{m}$ wavelengths at room temperature. The temperature dependence at $5\mu\text{m}$ wavelength is roughly linear on a log-log plot, so an empirical formula for the below-melt temperature dependence factor is suggested of the approximate form.

$$f(T) = \exp\left[\frac{T - 300}{790}\right] \text{ for } T < 2318^\circ\text{K} \quad (107)$$

where T is the temperature in degrees Kelvin and $f(T)$ is a multiplying factor for the room temperature absorption coefficient. Above 2318°K a

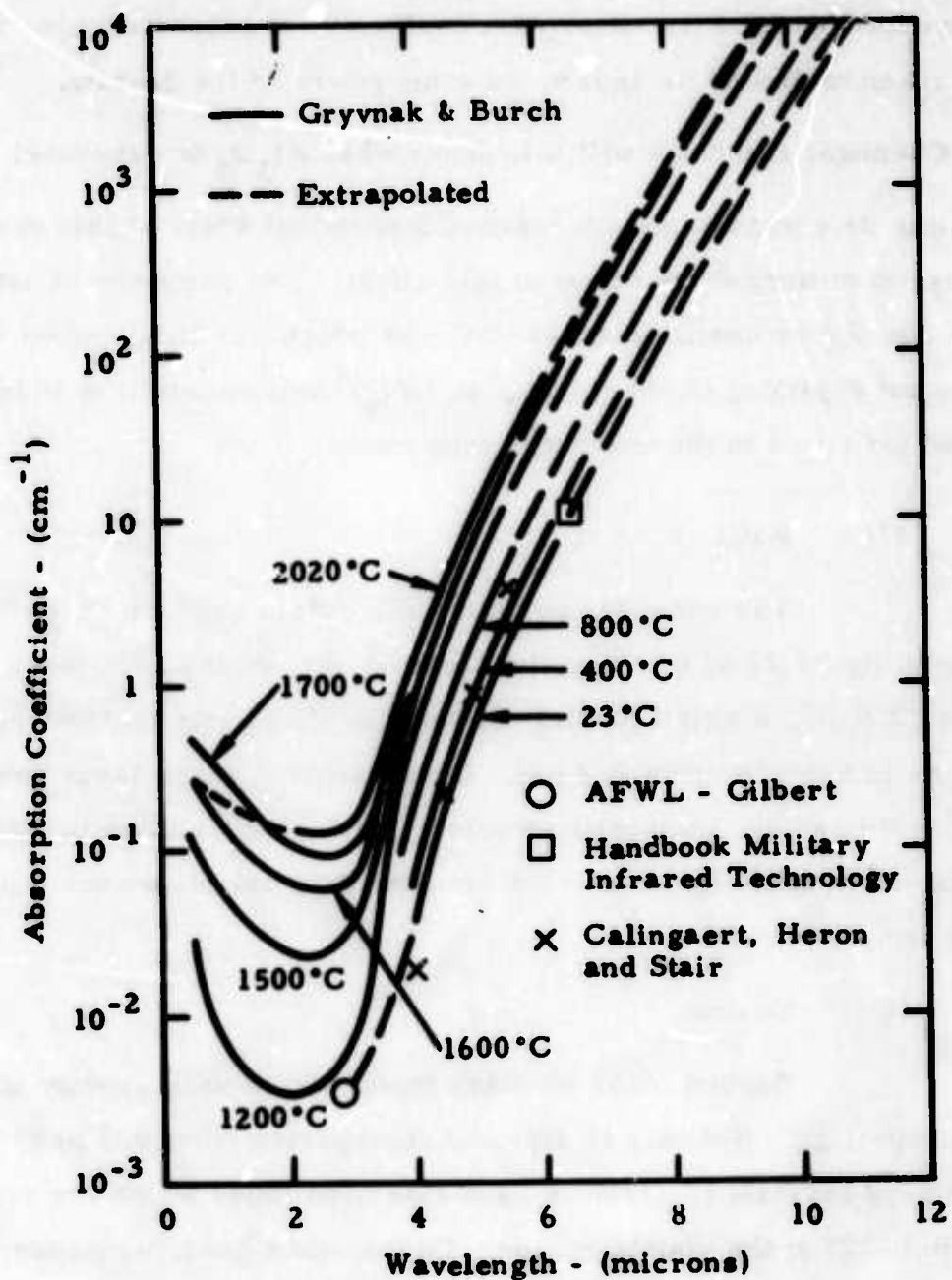


Figure 10. Absorption Coefficient for Al₂O₃ as a Function of Wavelength

constant factor of the order of 400 can be assumed to multiply the room temperature value of the absorption coefficient.

In conformity with the findings of Chang, Drummond and Hall (Ref. 23), the dependence of the absorption coefficient of sapphire vapor can be further taken to depend on density as some power of the density, $\left(\frac{\rho}{\rho_0}\right)^n$. Chemical reactions will take place when Al_2O_3 is vaporized in air which alter its composition. A detailed theoretical study of this problem was considered beyond the scope of this effort. For purposes of estimation, an absorption coefficient was assumed which was independent of temperature but depended on the density as $(\rho/\rho_c)^2$ in conformity with the one employed for silica in the computer runs made.

(3) NaCl

The room temperature absorption coefficient for NaCl is shown in figure 12 at wavelengths above $10\text{ }\mu\text{m}$. At the CO_2 laser wavelength of $10.6\text{ }\mu\text{m}$, a small particle of NaCl is effectively transparent, and it remains so down to about $0.2\text{ }\mu\text{m}$. Consequently, at the laser powers of interest in this study, the heating would be very slow relative to that of the other materials investigated at $10.6\text{ }\mu\text{m}$. No data are known for NaCl at elevated temperatures.

(4) Carbon

Carbon takes on many forms which vary greatly in their optical properties. Not only is diamond transparent from 0.3 to $80\text{ }\mu\text{m}$, but very pure crystals of graphite have also been found which are transparent (Ref. 28) in the visible region. On the other hand, usual forms of carbon are opaque. One reason given for this is the density of dislocations in graphite crystals determines the ease with which light can pass through them. Another reason given is that most carbon is very porous, and the light entering it is multiply scattered before it can escape and is thus absorbed. Soot, which may have a density two order of magnitude below

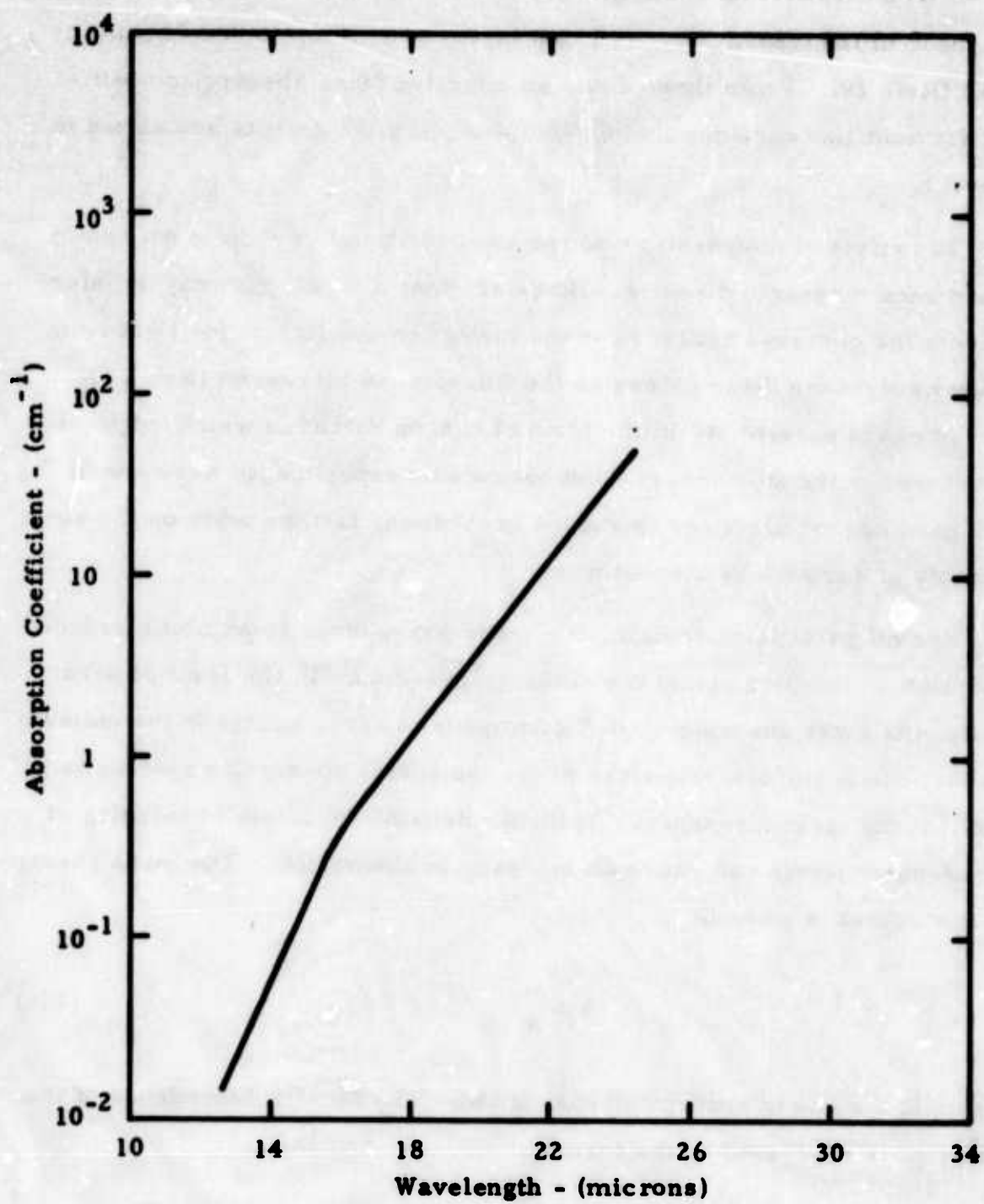


Figure 12. Absorption Coefficient for NaCl as a Function of Wavelength

solid graphite crystals, is particularly porous, and as a consequence is used as an antireflecting coating in the form of lampblack. A study has been made of the transmittance of thin layers of soot and other carbon blacks (Ref. 29). From these data, an effective mass absorption coefficient for soot like carbon may be calculated, and the results are shown in figure 13.

The effect of temperature on the absorptivity of carbon is not known to have been measured directly. However, that it increases may be inferred from the observed decrease in the reflection coefficient for light from intense neodymium laser pulses as the fluence was increased (Ref. 24). Because of the uncertainty in the form of carbon particles which might be encountered in the atmosphere, and because no experiments were known which used carbon particles to reduce breakdown, further work on the absorptivity of carbon was discontinued.

For all particle materials, the vapor phase tends to exhibit a reduced absorption as the band structure of the solid is lost. In the limit of zero density, the mass absorption coefficient goes to zero, except in the unlikely case that one of the discrete lines of the molecular absorption spectra is exactly at the laser frequency. At higher density, collision broadening of the molecular levels can cause an increase in absorption. The mass absorption coefficient is given by

$$A = \frac{a}{\rho} \quad (108)$$

where a is the linear absorption coefficient. The density dependence of the absorption is expressed in the form

$$a(\rho) = a_0 \left(\frac{\rho}{\rho_0} \right)^n \quad (109)$$

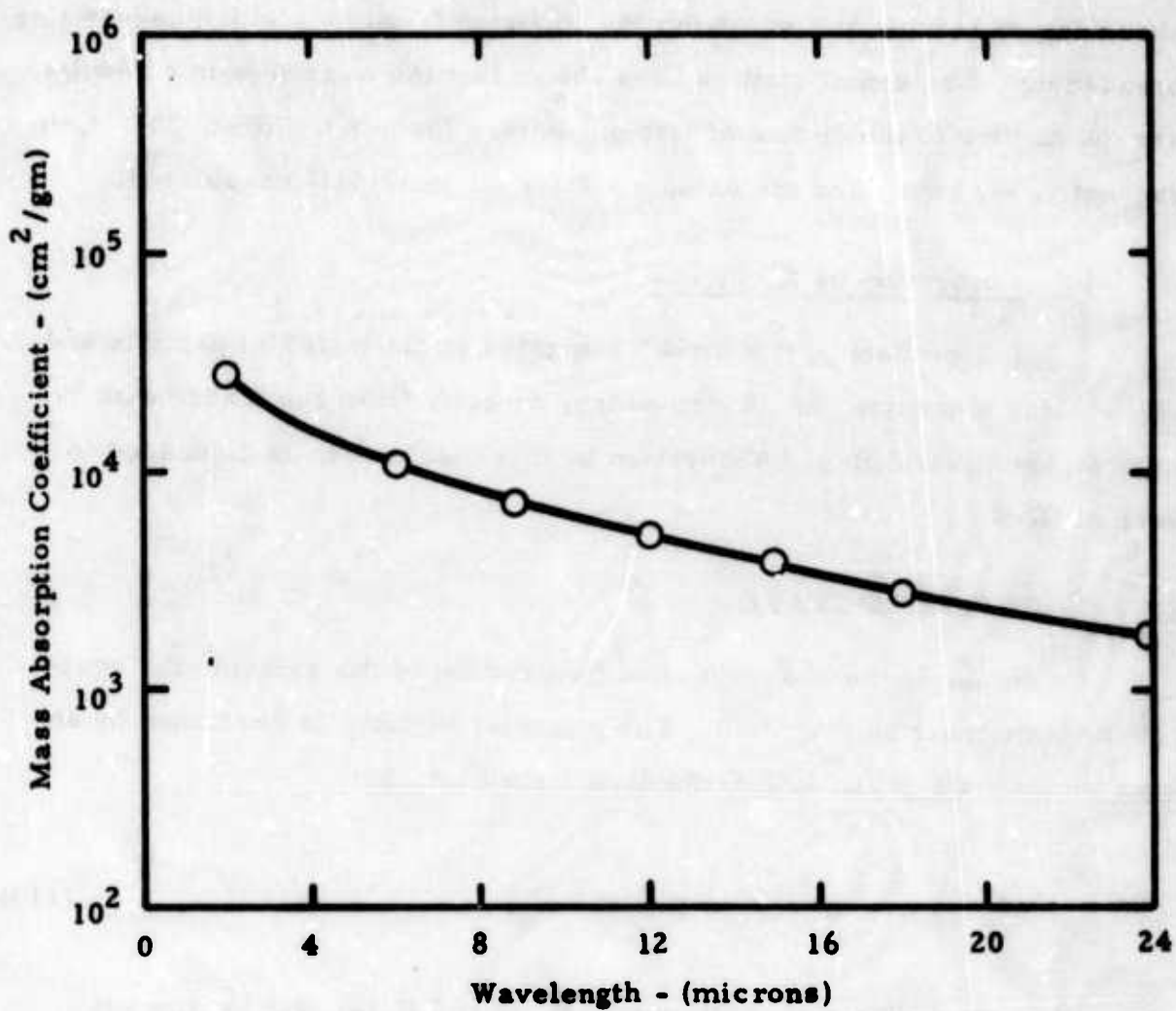


Figure 13. Mass Absorption Coefficient for Carbon (soot) as a Function of Wavelength

where a_0 is the absorptivity of the solid, ρ_0 is the density of the solid, and n is to be determined. For X-ray deposition, the energy is deposited in the atomic electrons, $n = 1$ and the mass absorption is independent of density. For laser deposition in the vapor from a quartz particle $n = 2$ (Ref. 23). For this diatomic molecule, one density factor is from the density of absorbing molecules and one from the collision frequency which causes line broadening. Numerical studies have shown that the hydrodynamic results are insensitive to the choice of this parameter for $n \geq 1.5$ (Ref. 30). Consequently, we have used the value $n = 2$ for all materials considered.

b. Absorption by Electrons

Independent of the mass absorption of the material particle and vapor, free electrons can absorb energy directly from the laser beam by inverse bremsstrahlung. Absorption by this mechanism is discussed in Section III-3.

2. EQUATION OF STATE

To complete the hydrodynamic description of the system, the equation of state must be specified. The material particle is described by an equation of state of the Mie-Grüneisen form (Ref. 31)

$$P = P_0 + \Gamma \rho (E - E_0) \quad (110)$$

where Γ is the Grüneisen coefficient. $P_0(\rho)$ and $E_0(\rho)$ give the density dependence of the pressure and energy density at a reference temperature. In the compressional region,

$$\mu = \frac{\rho}{\rho_0} - 1 > 0 \quad (111)$$

the pressure is given by

$$P = P_H(\mu) \left[1 - \frac{1}{2} \Gamma \mu \right] + \Gamma \rho \left[E - E_0 \right] \quad (112)$$

where

$$P_H(\mu) = C\mu + D\mu^2 + S\mu^3 \quad (113)$$

and the Hugoniot coefficients are determined from experimental data (Ref. 32). In the expansion region,

$$\eta = \frac{\rho}{\rho_0} < 1 \quad (114)$$

$$P = \rho \left[\gamma_1 + (\Gamma - \gamma_1) \eta^{\frac{1}{2}} \right] \left\{ E - E_S \left[1 - \exp \frac{F}{\eta} \left(1 - \frac{1}{\eta} \right) \right] \right\} \quad (115)$$

where E_S is the sublimation energy,

$$\gamma_1 = \gamma - 1 \quad (116)$$

and γ is the ratio of specific heats for the vapor. The factor

$$F = \frac{C}{\Gamma E_S \rho_0} \quad (117)$$

ensures continuity with the compressional equation as $\eta \rightarrow 1$.

The expansion equation must also allow for a change of phase as the material is heated. In the above expression, the phase transition is included only in an average or smoothed way as discussed in Ref. 32. Near normal density and energy density, the expansion equation gives a pressure appropriate to the solid. At low densities and high-energy density, the expansion pressure approaches that of an ideal gas. For the problem of dirty air breakdown, the region near the phase transition is critical for it controls

the rate of material vaporization, blowoff and subsequent shock heating. There is experimental evidence (Ref. 33) that for some materials the blow-off consists of macromolecular complexes rather than single molecules. This would completely change the above model; changing the effective sublimation energy of the solid and the γ of the vapor.

For the air surrounding the dust particle, two separate models have been used. In the first model, the air is assumed to be in local thermodynamic equilibrium, including the various molecular processes. The pressure, equilibrium electron density and effective specific heat ratio for shocks are computed as functions of density and energy density using an interpolation scheme on tables given by Gilmore (Ref. 34).

The validity of the equilibrium assumption is questionable since the rate constants for the molecular processes are often long compared to laser pulse times of a few microseconds. For example, at standard atmospheric density and 3000°K, the reaction



requires about 10^{-4} second to reach equilibrium (Ref. 35). This particular reaction is important for the equilibrium electron density because the ionization potential of NO at 9.25 ev (Ref. 36) is the lowest of the molecular species found in air.

For laser pulses that are short compared to the molecular reaction times, a better approximation to the air equation of state is obtained by assuming no molecular dissociation or reaction. This is the basis of the second model in which the pressure is given by the ideal gas equation. The equilibrium electron density is computed using the Saha equation with a single ionization potential of 12.05 ev for O_2 .

Calculations were carried out using both models. Over the times of the order of 10^{-7} sec. there was no significant difference in the answers

obtained from the two models. The results presented in later sections were all obtained from the second model.

The equation of state for the electron gas is just that of an ideal monatomic gas.

$$P_e = (\gamma_e - 1) \rho E_e \quad (119)$$

where $\gamma_e = \frac{5}{3}$ and E_e is the electron internal energy per gram of material.

Properties of the materials studied are listed in Table III. The parameter values employed in the CELAB computer runs are given.

3. THERMAL CONDUCTIVITY

In general, the thermal conductivity of the dust particle will depend on the temperature. We have assumed the functional form

$$\chi(T) = \chi_0 T^\beta \quad (120)$$

for the temperature dependence. We have fit limited experimental data on quartz and sapphire to determine values of χ_0 and β for the two materials. A plot of the fitted conductivity is shown in figure 14.

The thermal conductivity of air shows a general increase from room temperature to about 7000°K, then decreases between 7000 and 10,000°K as shown in figure 15. The data are too complicated to be fit with the functional form of equation (120) with a single value of the parameters over the entire temperature range. We have divided the data into four separate regions and fit each region with the form of equation (120). For any given temperature, a table look-up is used to determine the values of the coefficients and the conductivity computed from the above form.

The thermal conductivity of the free electron gas can be computed from the kinetic theory of gases (Ref. 37).

TABLE III
MATERIAL CONSTANTS

Property	Air	SiO_2	Al_2O_3
Density (gm/cc)	1.292×10^{-3}	2.65	3.97
γ	1.3802	1.25	1.25
Atomic Weight	28.98	60.06	102.0
Thermal Conductivity Constant (ergs/cm sec $^{\circ}\text{K}^{B+1}$)	31.4	1820	1820
β	0.78	0.74	0.74
Linear Absorption Coeff (cm^{-1})	0.	1×10^4	1×10^4
Grüneisen Coefficient	---	0.78	0.78
Hugoniot Constants			
C (dyne/cm ²)	---	8.7×10^{11}	4.65×10^{12}
D (dyne/cm ²)	---	0	0
S (dyne/cm ²)	---	0	0
Sublimation Energy (erg/gm)	---	2.35×10^{11}	2.35×10^{11}
Specific Heat Solid (erg/gm deg)	---	1.25×10^7	1.72×10^7
Vaporization Temp ($^{\circ}\text{K}$)	---	2503	3253
Work Function (ev)	---	4.58	3.77
Ionization Energy (ev)	12.05	10.8	7.7
Slope of Ionization Cross Section ($\pi a_0^2/\text{ev}$)	4.5×10^{-2}	8.3×10^{-2}	8.3×10^{-2}
Vibration Threshold (ev)	1.8	1.8	1.8
Vibration Bandwidth (ev)	1.4	1.4	1.4
Vibration Quanta (ev)	0.26	0.26	0.26
Vibrational Cross Section ($1 \times 10^{-15} \text{ cm}^2$)	26.60	26.60	26.60

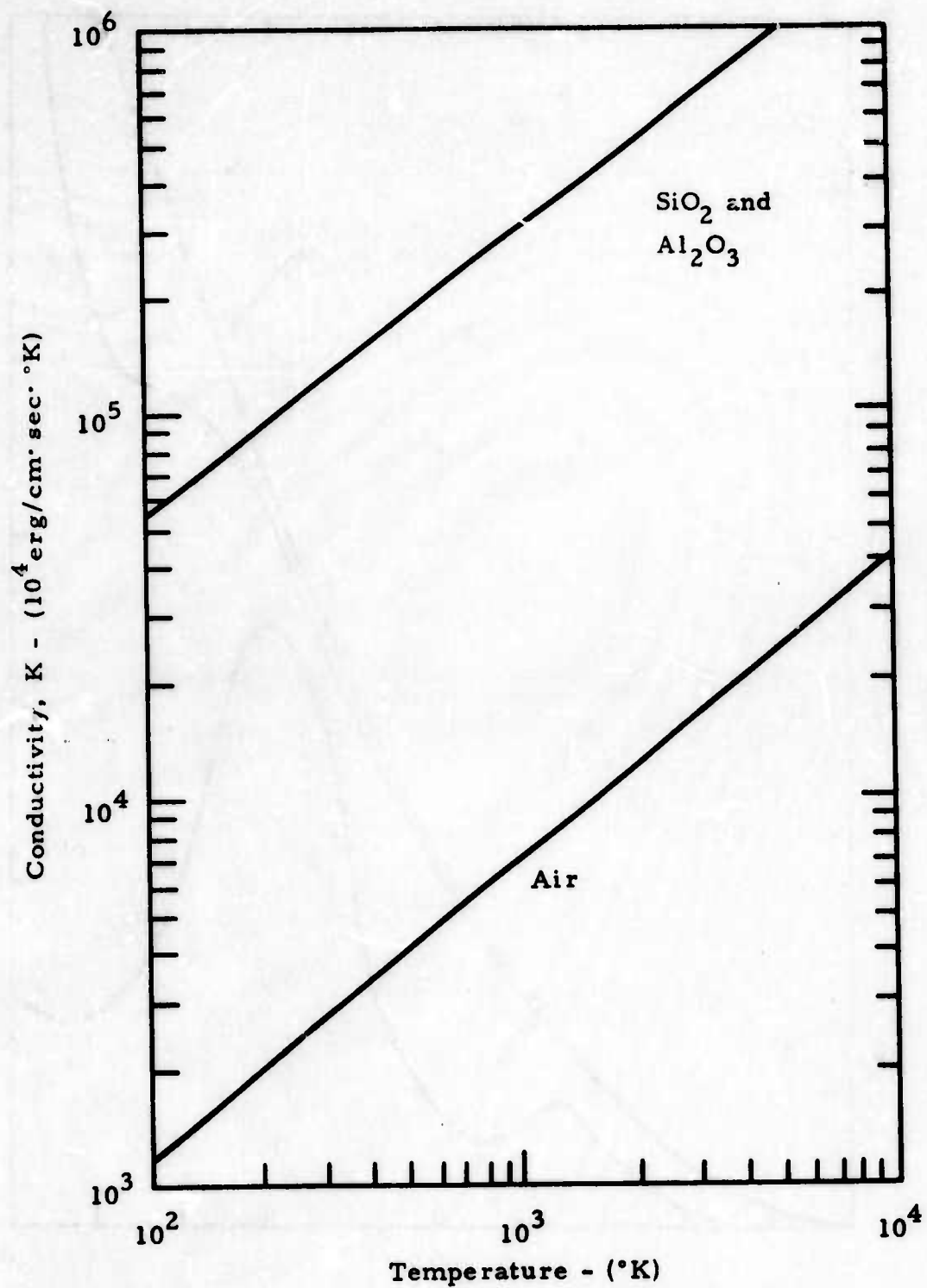


Figure 14. Thermal Conductivity of Various Material from Equation (1.0).

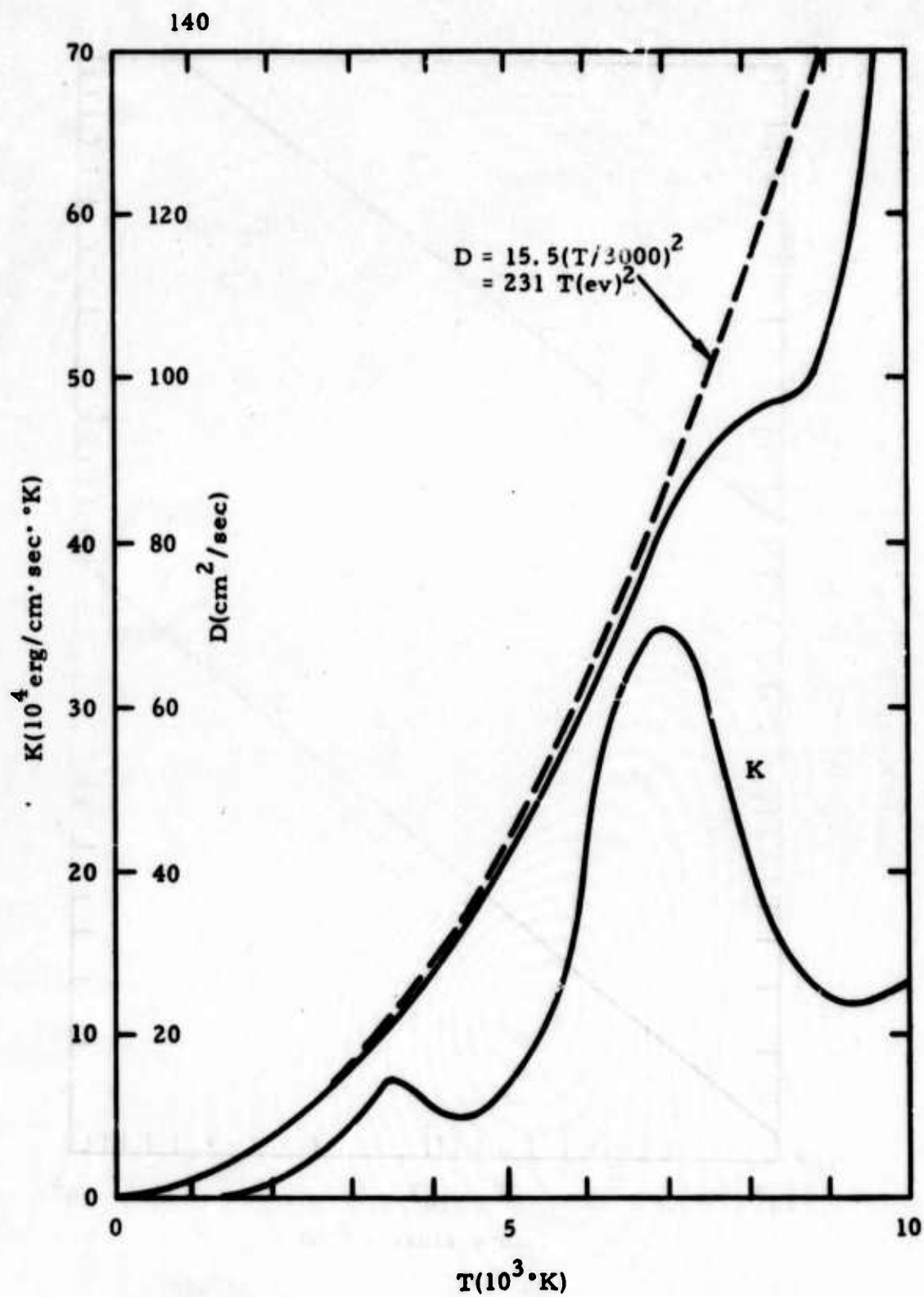


Figure 15. Air Conductivity, K, and Diffusivity, D, at One Atmosphere Pressure.

$$\chi_e = \frac{3}{2} N_e k D_e \quad (121)$$

where

$$D_e = \frac{1}{3} \bar{v} \lambda_e \quad (122)$$

is the electron diffusion coefficient, \bar{v} is the average electron velocity and λ_e is the mean free path. In terms of the collision frequency, the temperature-dependent diffusion coefficient is given by

$$D_e = \frac{kT_e}{m\nu_c} \quad (123)$$

Ambipolar diffusion is discussed in Section III-2.

4. THERMIONIC EMISSION

The thermionic emission (Ref. 38) from a material at high temperatures can be evaluated by assuming that the material emitted outside of the surface is in equilibrium with the material inside. Using the Fermi distribution for the electrons,

$$f(\epsilon + \epsilon_K) = \frac{1}{1 + e^{(W + \epsilon_K)/kT}} \quad (124)$$

where ϵ is the energy required to remove an electron from some reference energy level to a state of rest outside the metal, ϵ_K is the kinetic energy of an electron outside of the metal, and W is the work function. Multiplying equation (124) by $N_e v$, assuming that $(W + \epsilon_K) \gg kT$, and integrating over the density of states in phase space gives

$$J = \frac{m}{2\pi^3 h} (kT)^2 e^{-W/kT}$$

$$= 7.72 \times 10^{20} T^2 e^{-W/kT} \text{ cm}^{-2} \text{ sec}^{-1} \quad (125)$$

This is just the well known Richardson equation for thermionic emission.

On the basis of the derivation given above, one expects that the flux of electrons for different materials would depend on the density of electrons in the conduction band. Thus, to some degree, the difference in the conductivity between materials should indicate the difference to be expected in the thermionic emission. The conductivity of most metals is about 10^7 mhos/meter while the conductivity for quartz is $\sim 10^{-17}$ mhos/meter. Thus, one would expect the thermionic emission for quartz to be down several orders of magnitude from that given by the Richardson equation.

However, experimental evidence (Ref. 39) indicates that there is a substantial flux of electrons from quartz and borosilicate targets. This flux has been interpreted as being due to heating of surface contaminants. This effect would show up in the Richardson equation as a change in the constant factor. Since it is not clear, without further study, what value the constant factor should have for SiO_2 and Al_2O_3 , the value given in equation (125) has been used for the preliminary calculations given in this report. This provides an upper limit on the flux of electrons due to thermionic emission.

5. MACROMOLECULAR COMPLEXES

A further source of electrons may result from the interaction of a laser beam with naturally occurring molecular clusters. Such clusters generally have a substantially lower ionization potential. Of primary importance would be water clusters in the atmosphere. The evaluation of the density, size, and ionization potential of such clusters is a difficult problem for which there exists little information. The problem is neglected in the present report.

SECTION V

RESULTS

Calculations have been carried out to determine the effect of impurities on the breakdown of air by a CO_2 laser beam. The particular impurities considered were sapphire (Al_2O_3) and quartz (SiO_2), although the CELAB hydrodynamic code developed for this study is quite general and can be utilized for the study of other materials.

For numerical considerations in the present report, the only particle sizes considered were 12, 24, 48 and $96\ \mu$, although the code is capable of handling particles of any size. The code divides the particles into a number of zones, each zone having a width of approximately $10\ \mu$. In air, immediately outside the particle, the zone width is increased. The hydrodynamic time steps are of the order of 10^{-10} seconds. The temperatures, both ionic and electronic, are considered throughout the particle and into the air.

Figure 16 shows the calculated electron density in the first air zone as a function of the time for four different sizes of Al_2O_3 in the field of a $10.6\ \mu$ laser beam having an intensity of 3×10^8 watts/cm². The peak electron density is for the largest particle ($96\ \mu$), however, the difference in the electron density for the various sizes is not very significant. The electron density in the first zone reaches the steady state value of about 8×10^{16} electrons/cm³. This represents the degree of ionization of about 0.3%.

A similar pair of curves for SiO_2 and sizes 24 and $48\ \mu$ is shown in figure 17. Again, the laser is $10.6\ \mu$ with an intensity of 3×10^8 watts/cm². A steady-state value of the electron density in the first zone is apparently obtained at about 1.5×10^{-7} seconds.

The curves for SiO_2 , figure 17, show a pronounced maximum and minimum occurring at approximately 3.5 and 6×10^{-8} seconds. Again, the

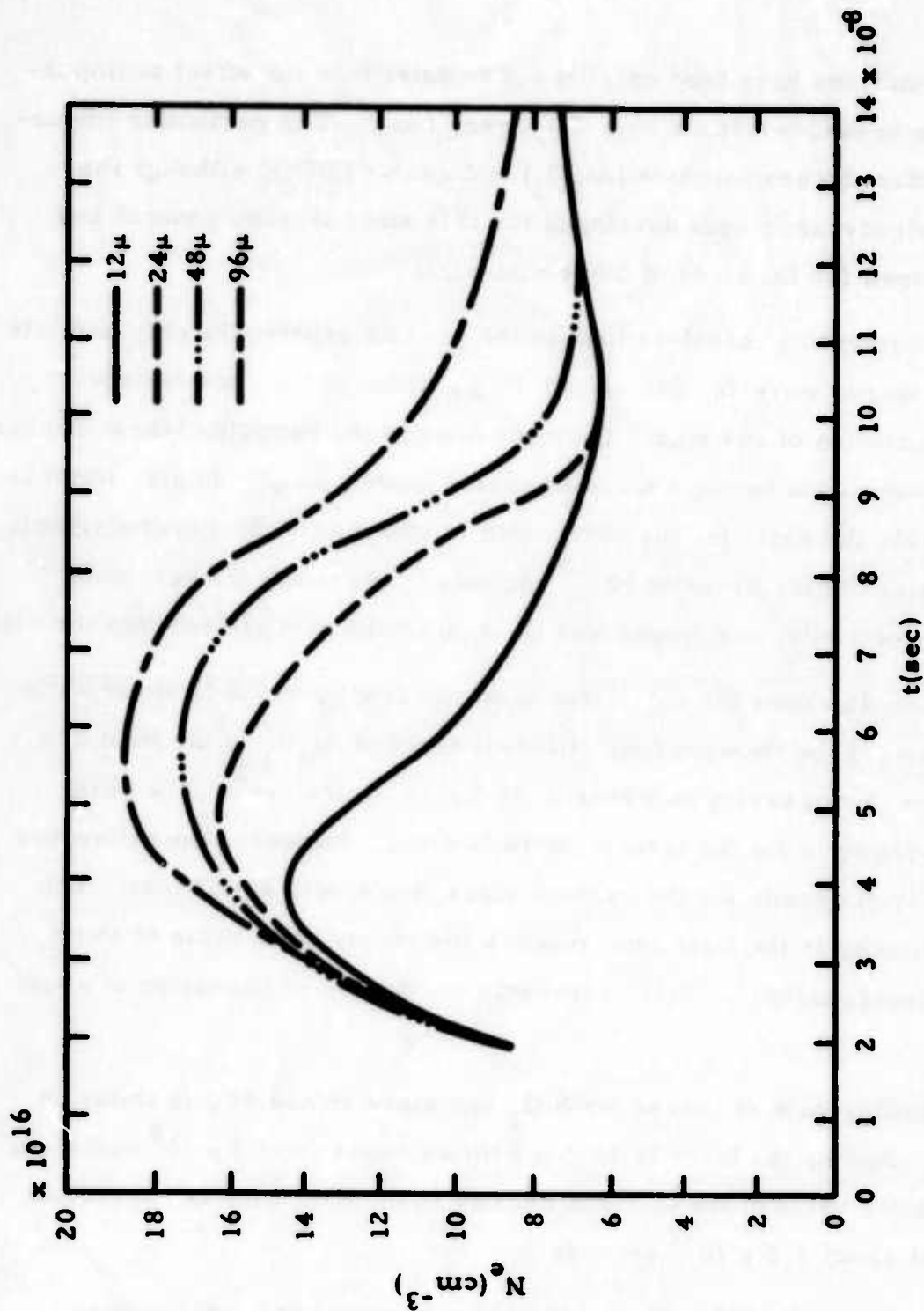


Figure 16. Electron Density vs Time for Different Size Al_2O_3 Particles in the Beam CO_2 Laser at an Intensity of 3×10^8 watts/ cm^2 .

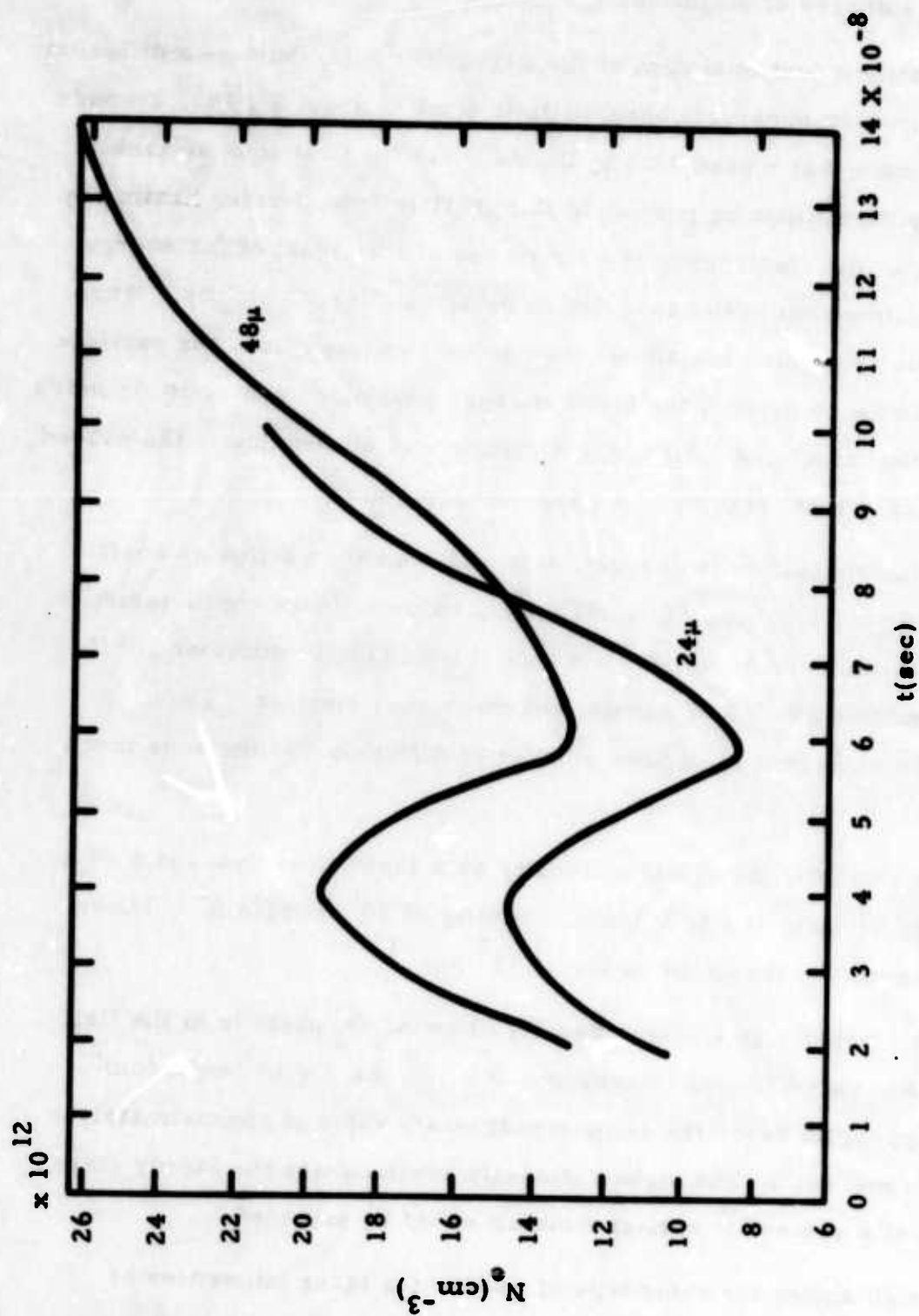


Figure 17. Electron Density vs Time for Different Size SiO_2 Particles in the Beam CO_2 Laser at an Intensity of $3 \times 10^8 \text{ watts/cm}^2$.

difference in the electron density for the two sizes is not substantial. However, the difference in the peak electron density for SiO_2 as compared to Al_2O_3 is about 4 orders of magnitude.

The maximum and minimum of the curves for SiO_2 indicate a diffusion type of motion with an apparent characteristic time of about 3×10^{-8} seconds. The curves indicate that a peak density builds up in the first zone at some point, shielding the remaining portion of the particle from further heating by the laser beam as the electrons in the first zone absorb most of the energy. The electrons diffuse out of the zone with a relatively large velocity. When the electron loss from the zone approaches some limiting value, the particle again begins to absorb most of the laser energy, heating up and emitting more electrons into the first zone. Since the diffusion has slowed down, the second peak is more persistent, leading to a quasi-steady state.

If this interpretation is correct, it would indicate a diffusion coefficient of approximately $10^2 \text{ cm}^2/\text{seconds}$. This value is more characteristic of the free electron diffusion coefficient than the ambipolar diffusion coefficient which would be about 2 to 3 orders of magnitude smaller. Thus, it appears that the electrons have been allowed to diffuse out of the zone much too rapidly.

Figure 18 shows the electron density as a function of time for a 24μ and 48μ quartz particle at a CO_2 laser intensity of 10^8 watts/cm^2 . These curves have a growth rate on the order of 10^7 sec^{-1} .

Figure 19 shows an electron density of an Al_2O_3 particle in the field of a CO_2 laser at two different intensities, 3×10^7 and $1 \times 10^7 \text{ watts/cm}^2$. Both curves appear to reach the same steady-state value of approximately $3 \times 10^{17} \text{ electrons/cm}^2$. The higher intensity beam causes the steady state to be reached at a somewhat earlier time as would be expected.

Figure 20 shows the same type of curves for laser intensities of 3×10^8 and $1 \times 10^8 \text{ watts/cm}^2$. The higher intensity again causes the peak

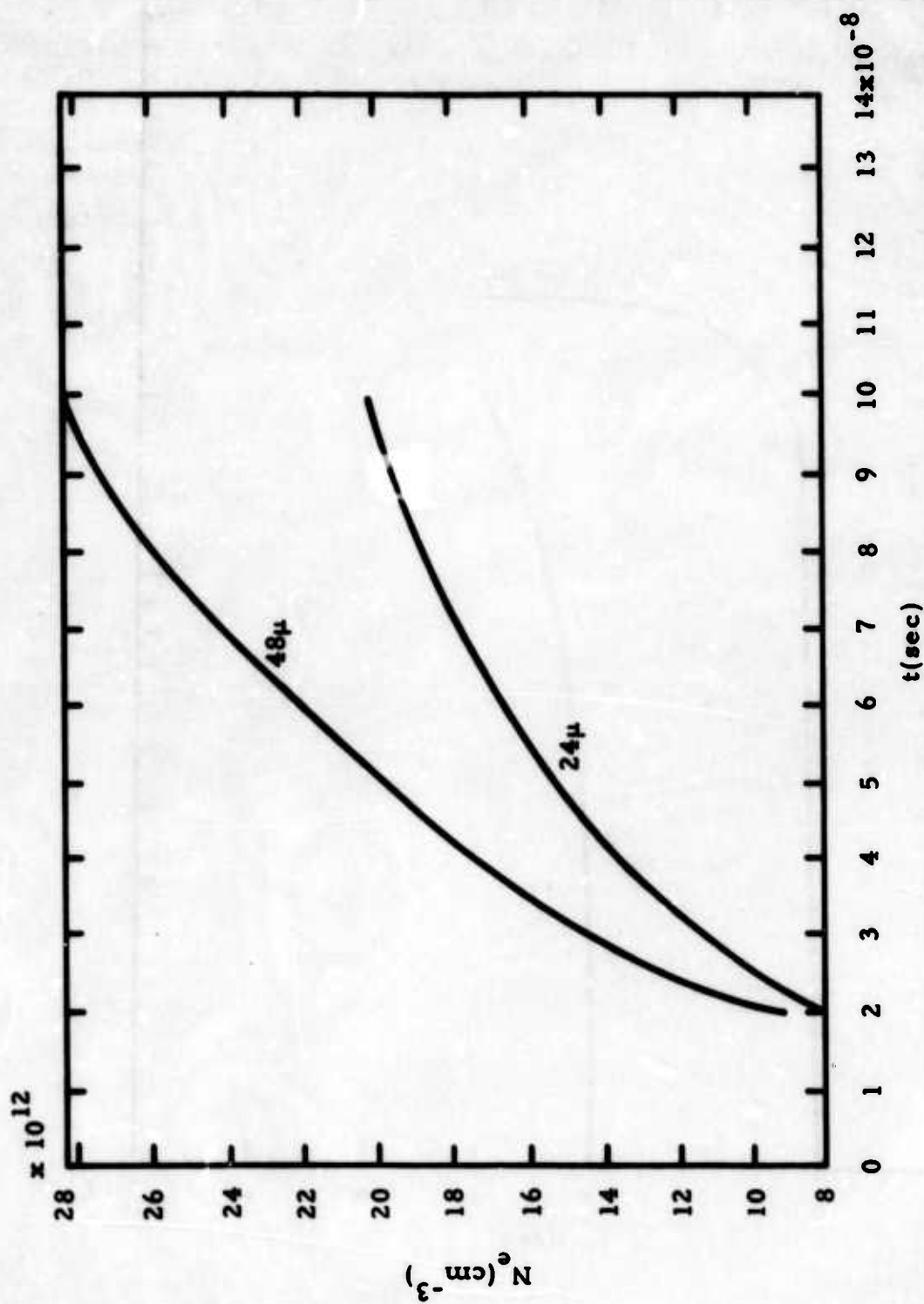


Figure 18. Electron Density vs Time for Different Size SiO_2 Particles in the Beam CO_2 Laser in an Intensity of $1 \times 10^8 \text{ watts/cm}^2$.

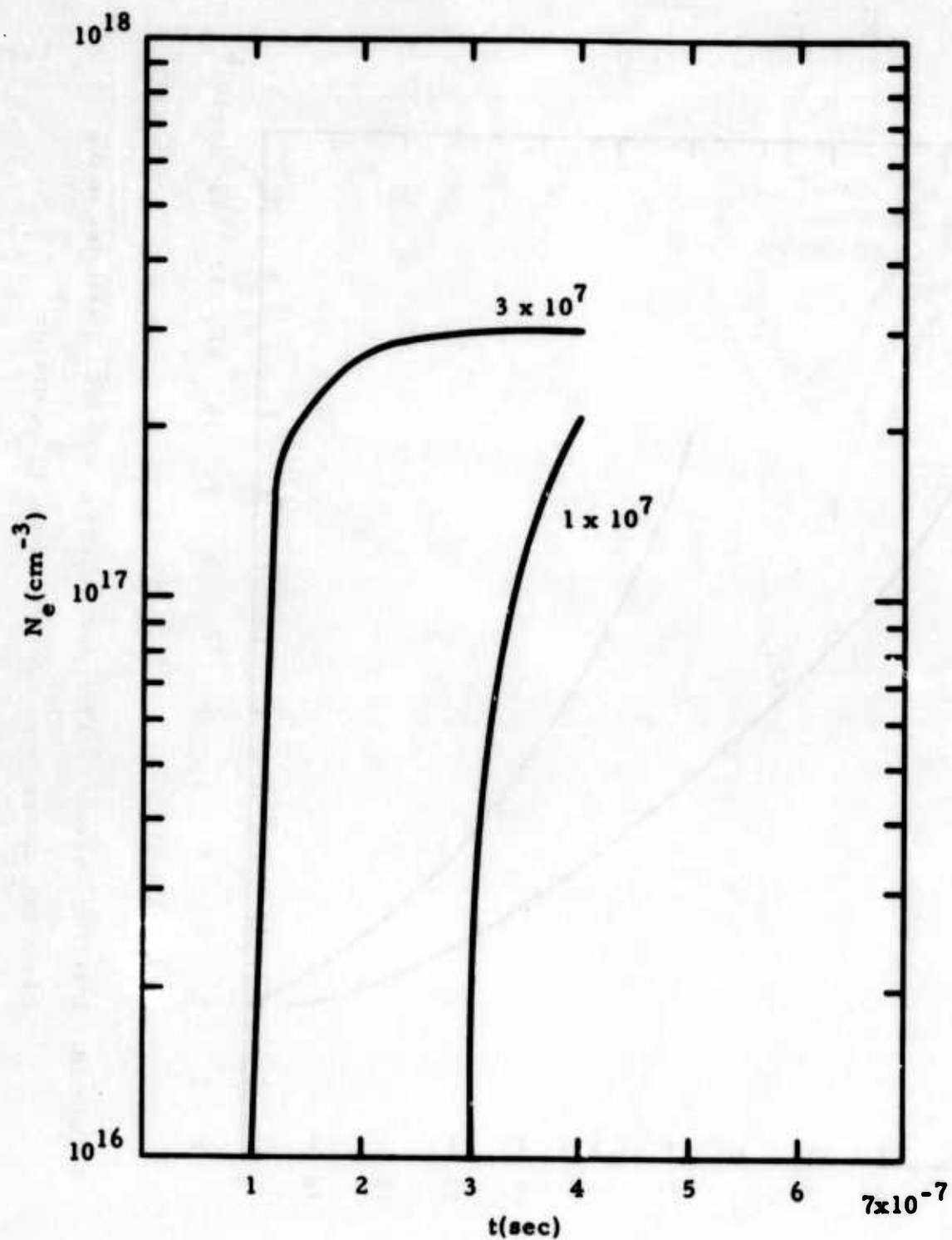


Figure 19. Electron Density vs Time for a 48μ Al_2O_3 Particle in the Beam of a CO_2 Laser at Two Different Intensities.

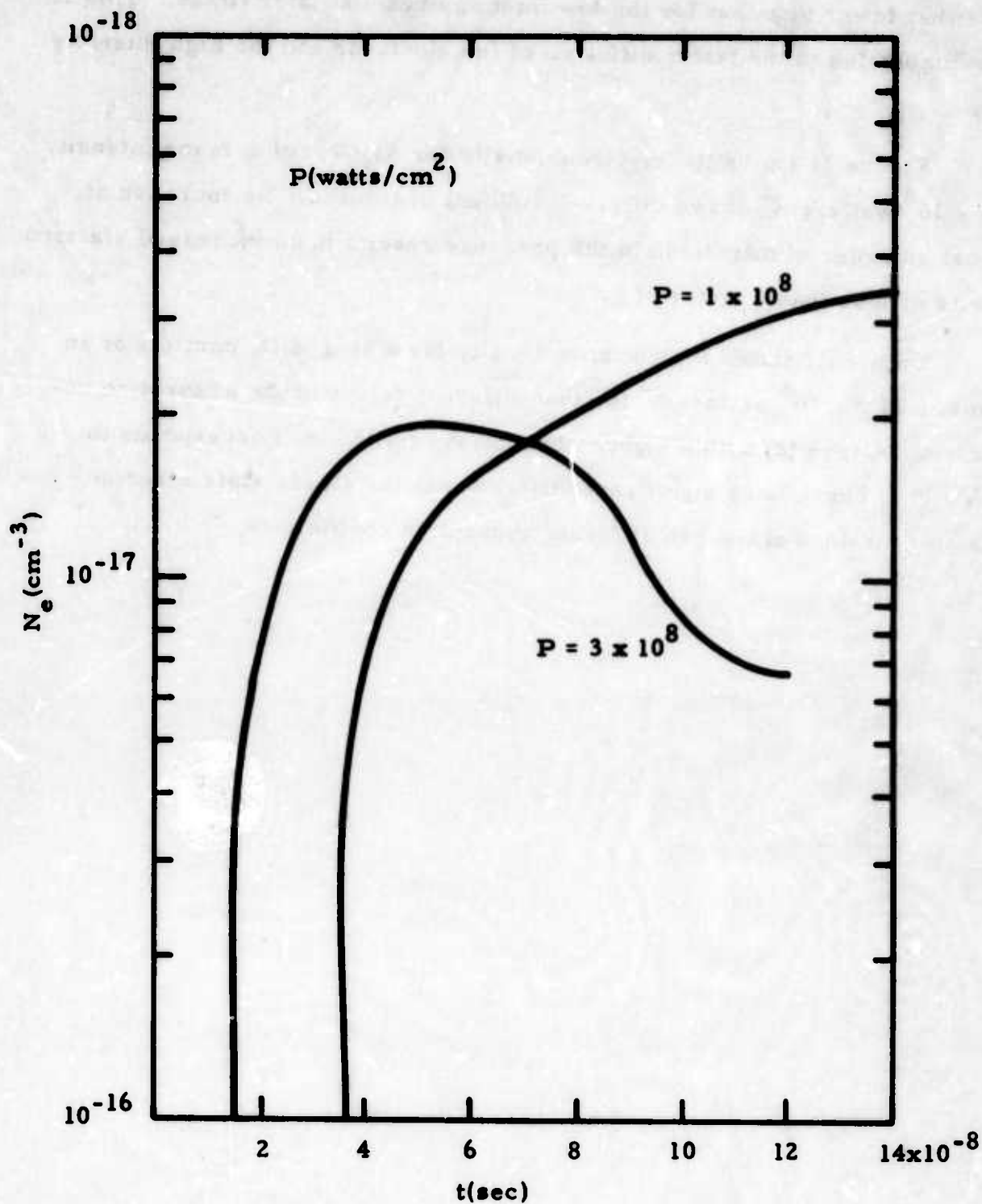


Figure 20. Electron Density vs Time for a $48\mu \text{ Al}_2\text{O}_3$ Particle in the Beam of a CO_2 Laser at Two Different Intensities.

electron density to be attained at an earlier time, however, the density is somewhat lower than that for the low intensity beam at later times. This is presumably due to the faster diffusion of the electrons and the high intensity beam.

Figure 21 shows the electron density for Al_2O_3 with a laser intensity of 3×10^8 watts/cm² at two different ambient pressures. An increase of almost an order of magnitude in the pressure results in an increased electron density of less than a factor of 2.

Figure 22 shows the electron density for a 48μ SiO_2 particle at an intensity of 3×10^8 watts/cm² for two different values of the absorption coefficient. Curve (2) with a higher absorption coefficient, corresponds to figure 17. There is no significant difference in the steady state electron densities attained at the two different absorption coefficients.

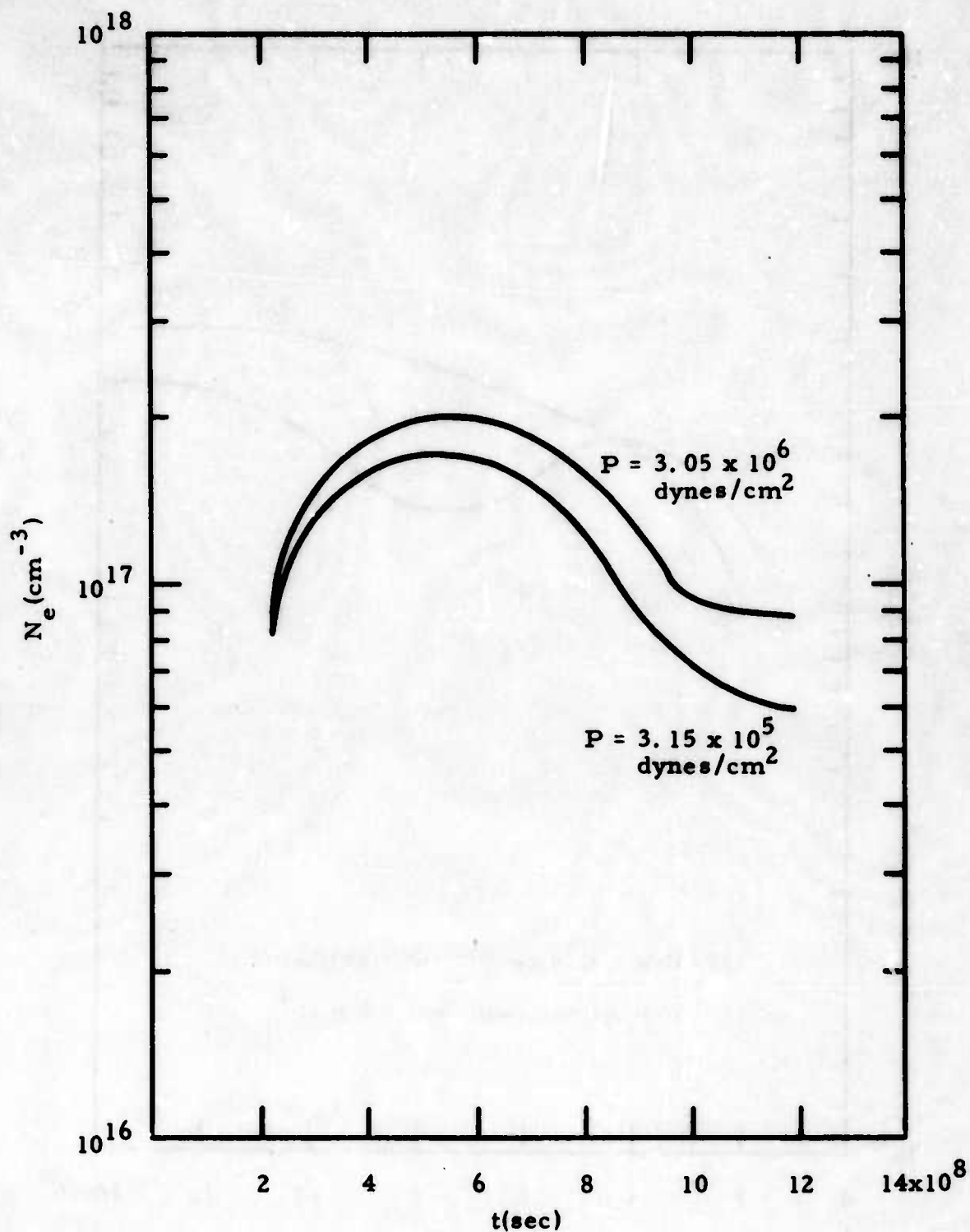


Figure 21. Electron Density vs Time for a $48\mu \text{ Al}_2\text{O}_3$ Particle in the Field of a CO_2 Laser at an Intensity of $3 \times 10^8 \text{ watts/cm}^2$ at Different Ambient Pressures.

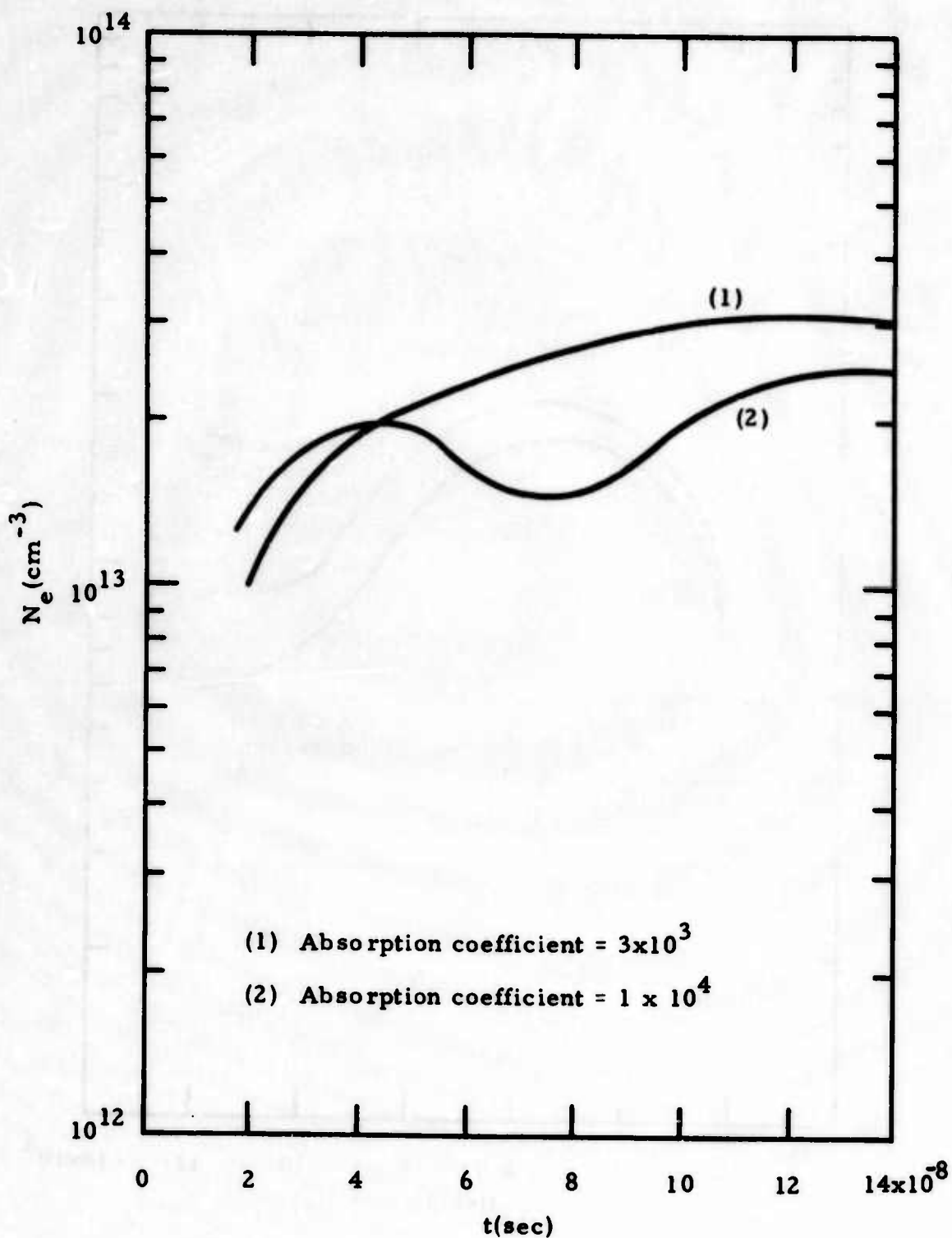


Figure 22. Electron Density vs Time for a 48μ SiO_2 Particle in the Field of a CO_2 Laser at an Intensity of 3×10^8 watts/cm² for Different Values of the SiO_2 Absorption Coefficient.

SECTION VI

CONCLUSIONS

It was shown in the theoretical analysis of the breakdown of air that the decrease in power required for breakdown is directly proportional to the increase in the total collision frequency. As the electron density is increased the total collision frequency is increased through electron-ion interaction. After the degree of ionization is increased beyond $\sim 10^{-3}$, the electron-ion interaction becomes dominant and the rate of energy absorption increases rapidly, leading to breakdown.

The results of the calculations performed for this report show that the atmospheric impurities are a source for a substantial density of free electrons as suggested in references 1 and 2. This is especially true for Al_2O_3 .

The temperatures calculated for the electrons were relatively low, about 10^3 °K, since the energy absorption was just compensated by the loss of electron energy to molecular vibration. Thus, the electron densities calculated were from the impurity particles and not from the atmospheric N_2 or O_2 . Under these conditions one cannot draw any conclusions about the relative effectiveness of the impurity particles in breaking down the atmosphere.

The electron diffusion coefficient used in the calculations was too large, being more consistent with the value for the free electron diffusion than the ambipolar diffusion. This would allow the electron density to decrease much too rapidly leading to the relatively low temperatures mentioned previously. On the other hand, the use of the Richardson equation to describe the thermionic emission for Al_2O_3 may have given too large an electron flux. These two possible overestimates tend to compensate each other; however, the large electron diffusion coefficient may lead to the more serious discrepancy. The electron density calculated for Al_2O_3 was

approaching values that could lead to substantial changes in the total collision frequency, thus, this area requires more study.

It was found during the course of this investigation that information on the material properties of atmospheric impurities was very difficult to find. Further studies of air breakdown should lead to a great deal of useful information on experimental measurements that are needed. An example of this was indicated by the lack of availability of information on the type of molecules formed by Al_2O_3 in the vapor phase.

The CELAB hydrodynamic code developed for this contract should be very useful for future investigations of the effectiveness of other impurities as a source of free electrons. It was originally intended that the present investigation would include calculations of the electron density resulting from clusters on macromolecules such as water vapor clusters. It is expected that the lower ionization potentials of such clusters might be a major source of electrons. Time, however, did not permit such studies at the present time. It is suggested that this potential source of electrons be investigated in the future along with other impurities existing in the atmosphere.

A second approach to the calculation of atmospheric breakdown was started but remained unfinished as the present investigation was terminated. In this approach a Monte Carlo calculation was used to follow the time dependent development of the electron distribution function including the effects of ionization. While the development of the code was not finished, enough progress had been made to justify its inclusion as an appendix in this report so that anyone wishing to follow this course of investigation could utilize the results obtained thus far.

APPENDIX I

DESCRIPTION OF CELAB CODE

This appendix gives a description of the difference methods used in the code CELAB. CELAB is a one-dimensional Lagrangian code which allows plane, cylindrical or spherical geometry through an input parameter $\alpha = 1, 2, 3$. We begin with a description of the difference equation approximation to the hydrodynamic equations. An implicit scheme is used to solve the energy equation including the thermal conductivity term. The method for control of the fundamental time step is given and the energy deposition is discussed.

1. DIFFERENCING FOR CELAB

The differential equations to be solved are:

Conservation of Momentum:

$$\frac{\partial U}{\partial t} = - R^{\alpha-1} \frac{\partial P + Q}{\partial M} \quad (126)$$

Definition of Velocity:

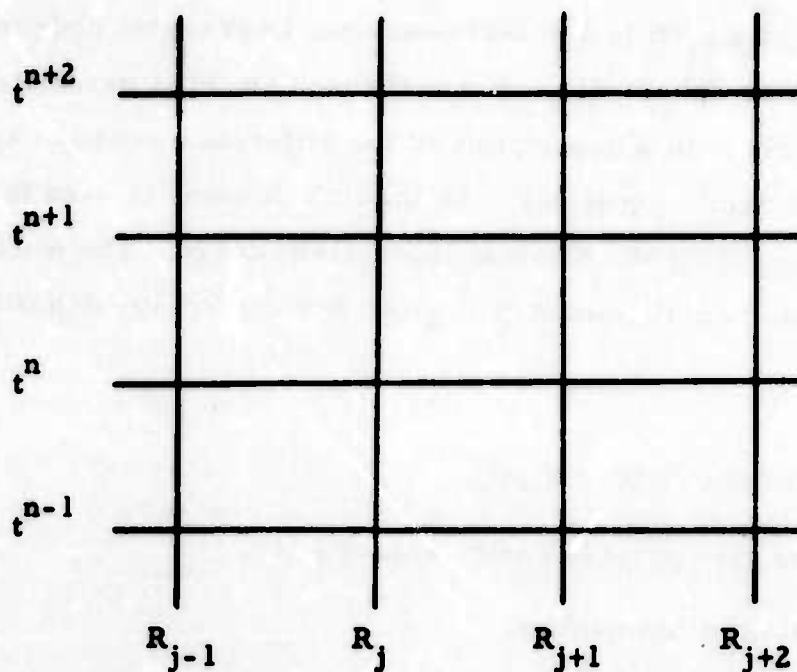
$$\frac{\partial R}{\partial t} = U \quad (127)$$

Conservation of Mass:

$$V = \frac{1}{D} = \frac{1}{\alpha} \frac{\partial R^{\alpha}}{\partial M} \quad (128)$$

Conservation of Energy:

$$\frac{\partial E}{\partial t} = -P \frac{\partial V}{\partial t} + \varphi \bar{K} + \frac{\partial}{\partial M} \left[\chi R^{\alpha-1} \frac{\partial T}{\partial R} \right] \quad (129)$$



- α = dimension of space
- R = coordinate
- U = velocity
- M = mass
- V = specific volume
- D = density
- E = specific energy
- P = pressure
- φ = laser flux
- \bar{K} = absorption coefficient
- χ = thermal conductivity
- T = temperature

Equation (126) can be differenced directly to give

$$U_j^{n+\frac{1}{2}} = U_j^{n-\frac{1}{2}} - (R_j^n)^{\alpha-1} \frac{P_{j+\frac{1}{2}}^n - P_{j-\frac{1}{2}}^n}{M_{j+\frac{1}{2}} + M_{j-\frac{1}{2}}} \cdot 2 \Delta t^n \quad (130)$$

where

$$\Delta t^n = \frac{1}{2} (t^{n+1} - t^{n-1}) \quad (131)$$

The second equation gives

$$R_j^{n+1} = R_j^n + U_j^{n+\frac{1}{2}} \Delta t^{n+\frac{1}{2}} \quad (132)$$

with

$$\Delta t^{n+\frac{1}{2}} = t^{n+1} - t^n \quad (133)$$

The conservation of mass becomes

$$V_{j-\frac{1}{2}}^{n+1} = \frac{1}{\alpha} \frac{(R_j^{n+1})^\alpha - (R_{j-1}^{n+1})^\alpha}{M_{j-\frac{1}{2}}} \quad (134)$$

or

$$D_{j-\frac{1}{2}}^{n+1} = \frac{\alpha M_{j-\frac{1}{2}}}{(R_j^{n+1})^\alpha - (R_{j-1}^{n+1})^\alpha} \quad (135)$$

For the energy equation, we use an implicit scheme to solve for the new energy and pressure, including the thermal conductivity terms. The left side of the energy equation is differenced directly

$$\left(\frac{\partial E}{\partial t}\right)_{j-\frac{1}{2}}^{n+\frac{1}{2}} = \frac{W_{j-\frac{1}{2}}^{n+\frac{1}{2}}}{\Delta t^{n+\frac{1}{2}}} \quad (136)$$

where

$$W_{j-\frac{1}{2}}^{n+\frac{1}{2}} = E_{j-\frac{1}{2}}^{n+1} - E_{j-\frac{1}{2}}^n \quad (137)$$

To compute the $P \cdot dV$ work implicitly, we assume that the pressure is a linear function of the internal energy

$$P = P_H + \Gamma DE \quad (138)$$

where Γ is the Grüneisen coefficient and P_H is the Hugoniot pressure which is a function of density only. For an ideal gas, $P_H = 0$ and $\Gamma = \gamma - 1$.

Including the artificial viscosity, the $P \cdot dV$ term gives

$$(P \cdot dV)_{j-\frac{1}{2}}^{n+\frac{1}{2}} = (\Gamma D_{j-\frac{1}{2}}^{n+1} E_{j-\frac{1}{2}}^{n+1} + P_{H,j-\frac{1}{2}}^{n+1} + P_{j-\frac{1}{2}}^n + 2Q_{j-\frac{1}{2}}^{n+\frac{1}{2}}) \cdot \frac{\Delta V_{j-\frac{1}{2}}^{n+\frac{1}{2}}}{2} \quad (139)$$

where

$$\Delta V_{j-\frac{1}{2}}^{n+\frac{1}{2}} = V_{j-\frac{1}{2}}^{n+1} - V_{j-\frac{1}{2}}^n \quad (140)$$

To avoid numerical cancellation in computing this difference, we use the relation

$$\Delta V_{j-\frac{1}{2}}^{n+\frac{1}{2}} = \left(\frac{\partial V}{\partial t}\right)_{j-\frac{1}{2}}^{n+\frac{1}{2}} \cdot \Delta t^{n+\frac{1}{2}} \quad (141)$$

and the conservation of mass to write

$$\Delta V_{j-\frac{1}{2}}^{n+\frac{1}{2}} = \frac{(R_j^{n+\frac{1}{2}})^{\alpha-1} U_j^{n+\frac{1}{2}} - (R_{j-1}^{n+\frac{1}{2}})^{\alpha-1} U_{j-1}^{n+\frac{1}{2}}}{M_{j-\frac{1}{2}}} \cdot \Delta t^{n+\frac{1}{2}} \quad (142)$$

For the laser deposition we write,

$$(\overline{\phi K})_{j-\frac{1}{2}}^{n+\frac{1}{2}} = F_{j-\frac{1}{2}}^{n+\frac{1}{2}} \quad (143)$$

where $F_{j-\frac{1}{2}}^{n+\frac{1}{2}}$ will be computed using Bier's law and an appropriate absorption coefficient.

For the thermal conductivity term of the energy equation, we assume a power law for the temperature dependence of the conductivity,

$$\chi(T) = \chi_0 T^\beta \quad (144)$$

where χ_0 and β depend on material and may be slowly varying functions of temperature and density. We further assume that the relation between temperature and internal energy is linear

$$E - E_0 = C (T - T_0) \quad (145)$$

where C is a specific heat and E_0 is the internal energy at a reference temperature T_0 . Let

$$E_1 = E_0 - C T_0$$

so that

$$T = \frac{1}{C} (E - E_1) \quad (146)$$

The conductivity term

$$\dot{E}_c = \frac{\partial}{\partial M} \left[\chi(T) R^{\alpha-1} \frac{\partial T}{\partial R} \right] \quad (147)$$

can be differenced implicitly,

$$(\dot{E}_c)_{j-\frac{1}{2}}^{n+\frac{1}{2}} = \frac{1}{M_{j-\frac{1}{2}}} \left\{ (R_j^{n+\frac{1}{2}})^{\alpha-1} \left[\chi \frac{\partial T}{\partial R} \right]_j^{n+\frac{1}{2}} - (R_{j-1}^{n+\frac{1}{2}})^{\alpha-1} \left[\chi \frac{\partial T}{\partial R} \right]_{j-1}^{n+\frac{1}{2}} \right\} \quad (148)$$

The direct method of determining the energy flow at the zone boundary

$$\left[\chi(T) \frac{\partial T}{\partial R} \right]_j^{n+\frac{1}{2}}$$

is to use the conservation of energy

$$\left[\chi(T) \frac{\partial T}{\partial R} \right]_{j-} = \left[\chi(T) \frac{\partial T}{\partial R} \right]_{j+} \quad (149)$$

and the approximation

$$\chi_{j\pm} = \chi_{j\pm\frac{1}{2}}$$

to solve for the temperature at the zone boundary,

$$T_j^{n+\frac{1}{2}} = \frac{X_{j-\frac{1}{2}}^{n+\frac{1}{2}} T_{j-\frac{1}{2}}^{n+\frac{1}{2}} + X_{j+\frac{1}{2}}^{n+\frac{1}{2}} T_{j+\frac{1}{2}}^{n+\frac{1}{2}}}{X_{j-\frac{1}{2}}^{n+\frac{1}{2}} + X_{j+\frac{1}{2}}^{n+\frac{1}{2}}} \quad (150)$$

where

$$X_{j-\frac{1}{2}}^{n+\frac{1}{2}} = \frac{\chi_{j-\frac{1}{2}}^{n+\frac{1}{2}}}{R_j^{n+\frac{1}{2}} - R_{j-1}^{n+\frac{1}{2}}} \quad (151)$$

This temperature can then be used to compute the energy flow at the zone boundary.

$$\left[\chi \frac{\partial T}{\partial R} \right]_j^{n+\frac{1}{2}} = \frac{2 X_{j-\frac{1}{2}}^{n+\frac{1}{2}} X_{j+\frac{1}{2}}^{n+\frac{1}{2}} (T_{j+\frac{1}{2}}^{n+\frac{1}{2}} - T_{j-\frac{1}{2}}^{n+\frac{1}{2}})}{X_{j-\frac{1}{2}}^{n+\frac{1}{2}} + X_{j+\frac{1}{2}}^{n+\frac{1}{2}}}$$

Using equations (144) and (146), the implicit dependence of $T_{j-\frac{1}{2}}^{n+\frac{1}{2}}$ and $\chi_{j-\frac{1}{2}}^{n+\frac{1}{2}}$ on the energy differences can be determined

$$T_{j-\frac{1}{2}}^{n+\frac{1}{2}} = T_{j-\frac{1}{2}}^n + \frac{1}{2C_{j-\frac{1}{2}}} W_{j-\frac{1}{2}}^{n+\frac{1}{2}} \quad (151)$$

$$\chi_{j-\frac{1}{2}}^{n+\frac{1}{2}} = \chi_{j-\frac{1}{2}}^n \left\{ 1 + \frac{\beta_{j-\frac{1}{2}}}{2C_{j-\frac{1}{2}} T_{j-\frac{1}{2}}^n} W_{j-\frac{1}{2}}^{n+\frac{1}{2}} \right\} \quad (152)$$

Then to first order in the energy differences, the energy flow at the zone boundary is

$$\left[\chi \frac{\partial T}{\partial R} \right]_j^{n+\frac{1}{2}} = \frac{2(T_{j+\frac{1}{2}}^n - T_{j-\frac{1}{2}}^n) + W_{j+\frac{1}{2}}^{n+\frac{1}{2}}/C_{j+\frac{1}{2}} - W_{j-\frac{1}{2}}^{n+\frac{1}{2}}/C_{j-\frac{1}{2}}}{Y_{j-\frac{1}{2}}^n \left[1 - \beta_{j-\frac{1}{2}} W_{j-\frac{1}{2}}^{n+\frac{1}{2}}/2C_{j-\frac{1}{2}} T_{j-\frac{1}{2}}^n \right] + Y_{j+\frac{1}{2}}^n \left[1 - \beta_{j+\frac{1}{2}} W_{j+\frac{1}{2}}^{n+\frac{1}{2}}/2C_{j+\frac{1}{2}} T_{j+\frac{1}{2}}^n \right]} \quad (153)$$

where

$$Y_{j-\frac{1}{2}}^n = \frac{R_j^{n+\frac{1}{2}} - R_{j-1}^{n+\frac{1}{2}}}{\chi_{j-\frac{1}{2}}^n} \quad (154)$$

Expanding to first order in the energy differences and collecting terms we obtain

$$\begin{aligned}
\left[\chi \frac{\partial T}{\partial R} \right]_j^{n+\frac{1}{2}} &= \frac{1}{Y_{j-\frac{1}{2}}^n + Y_{j+\frac{1}{2}}^n} \left\{ 2(T_{j+\frac{1}{2}}^n - T_{j-\frac{1}{2}}^n) \right. \\
&\quad + \left[1 + \frac{T_{j+\frac{1}{2}}^n - T_{j-\frac{1}{2}}^n}{Y_{j-\frac{1}{2}}^n + Y_{j+\frac{1}{2}}^n} \cdot \frac{\beta_{j+\frac{1}{2}} Y_{j+\frac{1}{2}}^n}{T_{j+\frac{1}{2}}^n} \right] \frac{W_{j+\frac{1}{2}}^{n+\frac{1}{2}}}{C_{j+\frac{1}{2}}} \\
&\quad \left. - \left[1 - \frac{T_{j+\frac{1}{2}}^n - T_{j-\frac{1}{2}}^n}{Y_{j-\frac{1}{2}}^n + Y_{j+\frac{1}{2}}^n} \cdot \frac{\beta_{j-\frac{1}{2}} Y_{j-\frac{1}{2}}^n}{T_{j-\frac{1}{2}}^n} \right] \frac{W_{j-\frac{1}{2}}^{n+\frac{1}{2}}}{C_{j-\frac{1}{2}}} \right\} \quad (155)
\end{aligned}$$

Combining this result with equation(148) and using the notation

$$Z_j^n = \frac{(R_j^{n+\frac{1}{2}})^{\alpha-1}}{Y_{j-\frac{1}{2}}^n + Y_{j+\frac{1}{2}}^n} \quad (156)$$

gives an expression for the heat conductivity of the form

$$\begin{aligned}
(\dot{E}_c)_{j-\frac{1}{2}}^{n+\frac{1}{2}} &= \frac{1}{M_{j-\frac{1}{2}}} \left\{ 2Z_j^n (T_{j+\frac{1}{2}}^n - T_{j-\frac{1}{2}}^n) - 2Z_{j-1}^n (T_{j-\frac{1}{2}}^n - T_{j-\frac{3}{2}}^n) \right. \\
&\quad + \left(1 - \frac{T_{j-\frac{1}{2}}^n - T_{j-\frac{3}{2}}^n}{Y_{j-\frac{3}{2}}^n + Y_{j-\frac{1}{2}}^n} \cdot \frac{\beta_{j-\frac{3}{2}} Y_{j-\frac{3}{2}}^n}{T_{j-\frac{3}{2}}^n} \right) Z_{j-1}^n \cdot \frac{W_{j-\frac{3}{2}}^{n+\frac{1}{2}}}{C_{j-\frac{3}{2}}} \\
&\quad - \left[\left(1 - \frac{T_{j+\frac{1}{2}}^n - T_{j-\frac{1}{2}}^n}{Y_{j-\frac{1}{2}}^n + Y_{j+\frac{1}{2}}^n} \cdot \frac{\beta_{j-\frac{1}{2}} Y_{j-\frac{1}{2}}^n}{T_{j-\frac{1}{2}}^n} \right) Z_j^n \right. \\
&\quad \left. + \left(1 + \frac{T_{j-\frac{1}{2}}^n - T_{j-\frac{3}{2}}^n}{Y_{j-\frac{3}{2}}^n + Y_{j-\frac{1}{2}}^n} \cdot \frac{\beta_{j-\frac{1}{2}} Y_{j-\frac{1}{2}}^n}{T_{j-\frac{1}{2}}^n} \right) Z_{j-1}^n \right] \frac{W_{j-\frac{1}{2}}^{n+\frac{1}{2}}}{C_{j-\frac{1}{2}}} \\
&\quad \left. + \left(1 + \frac{T_{j+\frac{1}{2}}^n - T_{j-\frac{1}{2}}^n}{Y_{j-\frac{1}{2}}^n + Y_{j+\frac{1}{2}}^n} \cdot \frac{\beta_{j+\frac{1}{2}} Y_{j+\frac{1}{2}}^n}{T_{j+\frac{1}{2}}^n} \right) Z_j^n \cdot \frac{W_{j+\frac{1}{2}}^{n+\frac{1}{2}}}{C_{j+\frac{1}{2}}} \right\} \quad (157)
\end{aligned}$$

Combining equations(129), (136), (139), (143) and (157) yields an expression for the energy differences which can be written in the form

$$-A_j W_{j-\frac{3}{2}}^{n+\frac{1}{2}} + B_j W_{j-\frac{1}{2}}^{n+\frac{1}{2}} - C_j W_{j+\frac{1}{2}}^{n+\frac{1}{2}} = D_j \quad (158)$$

where

$$A_j = \left(1 - \frac{T_{j-\frac{1}{2}}^n - T_{j-\frac{3}{2}}^n}{Y_{j-\frac{3}{2}}^n + Y_{j-\frac{1}{2}}^n} \cdot \frac{\beta_{j-\frac{3}{2}} Y_{j-\frac{3}{2}}^n}{T_{j-\frac{3}{2}}^n} \right) Z_{j-1}^n \cdot \frac{\Delta t^{n+\frac{1}{2}}}{M_{j-\frac{1}{2}} C_{j-\frac{3}{2}}} \quad (159)$$

$$B_j = 1 + \frac{1}{2} \Gamma D_{j-\frac{1}{2}}^{n+1} \cdot \Delta V_{j-\frac{1}{2}}^{n+\frac{1}{2}} + \left[\left(1 - \frac{T_{j+\frac{1}{2}}^n - T_{j-\frac{1}{2}}^n}{Y_{j-\frac{1}{2}}^n - Y_{j+\frac{1}{2}}^n} \cdot \frac{\beta_{j-\frac{1}{2}} Y_{j-\frac{1}{2}}^n}{T_{j-\frac{1}{2}}^n} \right) Z_j^n \right. \\ \left. + \left(1 + \frac{T_{j-\frac{1}{2}}^n - T_{j-\frac{3}{2}}^n}{Y_{j-\frac{3}{2}}^n - Y_{j-\frac{1}{2}}^n} \cdot \frac{\beta_{j-\frac{1}{2}} Y_{j-\frac{1}{2}}^n}{T_{j-\frac{1}{2}}^n} \right) Z_{j-1}^n \right] \cdot \frac{\Delta t^{n+\frac{1}{2}}}{M_{j-\frac{1}{2}} C_{j-\frac{1}{2}}} \quad (160)$$

$$C_j = \left(1 + \frac{T_{j+\frac{1}{2}}^n - T_{j-\frac{1}{2}}^n}{Y_{j-\frac{1}{2}}^n + Y_{j+\frac{1}{2}}^n} \cdot \frac{\beta_{j+\frac{1}{2}} Y_{j+\frac{1}{2}}^n}{T_{j+\frac{1}{2}}^n} \right) Z_j^n \cdot \frac{\Delta t^{n+\frac{1}{2}}}{M_{j-\frac{1}{2}} C_{j+\frac{1}{2}}} \quad (161)$$

$$D_j = F_{j-\frac{1}{2}}^{n+\frac{1}{2}} \Delta t^{n+\frac{1}{2}} - \left(\Gamma D_{j-\frac{1}{2}}^{n+1} E_{j-\frac{1}{2}}^n + P_{H_{j-\frac{1}{2}}}^{n+1} + P_{j-\frac{1}{2}}^n + 2Q_{j-\frac{1}{2}}^{n+\frac{1}{2}} \right) \frac{\Delta V_{j-\frac{1}{2}}^{n+\frac{1}{2}}}{2} \\ + \left[Z_j^n (T_{j+\frac{1}{2}}^n - T_{j-\frac{1}{2}}^n) - Z_{j-1}^n (T_{j-\frac{1}{2}}^n - T_{j-\frac{3}{2}}^n) \right] \cdot \frac{2\Delta t^{n+\frac{1}{2}}}{M_{j-\frac{1}{2}}} \quad (162)$$

When the boundary condition at the origin

$$W_{-\frac{1}{2}}^{n+\frac{1}{2}} = 0 \quad (163)$$

is used in equation (158) for $j = 1$, a linear relation between $W_{1/2}^{n+1/2}$ and $W_{3/2}^{n+1/2}$ is obtained. This linear relation can then be used in equation (158) for $j = 2$ to obtain a linear relation between $W_{3/2}^{n+1/2}$ and $W_{5/2}^{n+1/2}$. This process can be repeated throughout the mesh. The general form of the linear relation can be deduced in the following manner. Let

$$W_{j-\frac{1}{2}}^{n+\frac{1}{2}} = G_{j-\frac{1}{2}} W_{j+\frac{1}{2}}^{n+\frac{1}{2}} + H_{j-\frac{1}{2}} \quad (164)$$

Substituting this expression into equation (156) and collecting terms gives

$$\begin{aligned} & [-A_j G_{j-\frac{3}{2}} G_{j-\frac{1}{2}} + B_j G_{j-\frac{1}{2}} - C_j] W_{j+\frac{1}{2}}^{n+\frac{1}{2}} \\ & + [-A_j G_{j-\frac{3}{2}} H_{j-\frac{1}{2}} - A_j H_{j-\frac{3}{2}} + B_j H_{j-\frac{1}{2}} - D_j] = 0 \end{aligned}$$

These relations are the desired equations when the equality is an identity, i. e., when

$$G_{j-\frac{1}{2}} = \frac{C_j}{B_j - A_j G_{j-\frac{3}{2}}} \quad (165)$$

$$H_{j-\frac{1}{2}} = \frac{D_j + A_j H_{j-\frac{3}{2}}}{B_j - A_j G_{j-\frac{3}{2}}} \quad (166)$$

These recursion relations along with the boundary condition at the origin,

$$G_{-\frac{1}{2}} = H_{-\frac{1}{2}} = 0 \quad (167)$$

can be used to determine the G s and H s by an outward sweep through the mesh. Then using the boundary condition at the outer boundary and equation (164), the energy differences $W_{j-\frac{1}{2}}^{n+\frac{1}{2}}$ can be determined by an inward sweep through the mesh. For the outer boundary condition, we take

$$W_{j+\frac{1}{2}}^{n+\frac{1}{2}} = 0 \quad (168)$$

which corresponds to no conductivity across the outer boundary.

2. TIME STEP CONTROL

For stability of the hydrodynamic difference equations, we use an artificial viscosity similar to that discussed in Richtmeyer and Morton, and including a linear term in the velocity. If the material is in the solid state we use

$$Q = -D [C_0^2 |\delta U| + C_1 C_s] \cdot \delta U \quad (169)$$

where $\delta U = \frac{\partial U}{\partial R} \delta R$, C_s is the sound velocity

$$C_s^2 = \left(\frac{\partial P}{\partial D} \right)_s \quad (170)$$

and C_0 and C_1 are constants with typical values

$$C_0 = 2.0 \quad C_1 = 0.25$$

The artificial viscosity in the form of equation(169) can exert a tension in a zone undergoing expansion, $\delta U > 0$. In the gas state a tensile artificial viscosity is not allowed and the modified form is used

$$Q = \begin{cases} -D [C_0^2 |\delta U| + C_1 C_s] \cdot \delta U & \delta U < 0 \\ 0 & \delta U > 0 \end{cases} \quad (171)$$

Corresponding to the linear artificial viscosity, the time step for hydrodynamic stability is determined by a generalized Courant condition

$$\Delta t_s = \frac{\delta R}{C_s} \left\{ \left[1 + \left(C_1 + \frac{2 C_0^2 |\delta U|}{C_s} \right)^2 \right]^{\frac{1}{2}} - \left(C_1 + \frac{2 C_0^2 |\delta U|}{C_s} \right) \right\} \quad (172)$$

The time step determined by equation (172) along with the artificial viscosity assure the stability of the hydrodynamic difference equations and the implicit solution of the energy equation guarantees the stability of the thermal conductivity. However, the accuracy of the energy equation suffers if the time step is so large that the thermal front is conducted across more than one zone. The time step for accuracy of thermal conduction is

$$\Delta t_A = \frac{\delta R}{V_{th}} \quad (173)$$

where the velocity of the thermal front is estimated from the similarity solution

$$V_{th} = \frac{\partial T / \partial t}{\partial T / \partial R} \quad (174)$$

Combining equations (173) & (174) and making use of the thermal conductivity term of the energy equation gives

$$\begin{aligned} \frac{1}{\Delta t_A} &= \frac{1}{\delta T} \frac{\partial T}{\partial t} \\ \frac{1}{\Delta t_A} &= \frac{1}{C \delta T} \frac{\partial}{\partial M} \left[\chi R^{\alpha-1} \frac{\partial T}{\partial R} \right] \end{aligned} \quad (175)$$

The corresponding difference equation is

$$\frac{1}{\Delta t_A} = \frac{1}{C_{j-\frac{1}{2}} M_{j-\frac{1}{2}} (T_{j-1}^n)} \frac{(R_j^n)^{\alpha-1} X_{j-\frac{1}{2}}^n X_{j+\frac{1}{2}}^n (T_{j+\frac{1}{2}}^n - T_{j-\frac{1}{2}}^n)}{X_{j-\frac{1}{2}}^n + X_{j+\frac{1}{2}}^n} - \frac{(R_{j-1}^n)^{\alpha-1} X_{j-3/2}^n X_{j-\frac{1}{2}}^n (T_{j-\frac{1}{2}}^n - T_{j-3/2}^n)}{X_{j-3/2}^n + X_{j-\frac{1}{2}}^n} \quad (176)$$

3. INPUT VARIABLES AND FORMATS

- a. (Problem description in columns 1-60) Format (12A5)
- b. NCYCS, NMAT, IALPH, NEDIT, LINMX, INPUT, NELOP, NEPRN, Format (8I10)

NCYCS	= maximum number of hydro cycles to be run
NMAT	= number of material layers, up to four
IALPH	= geometry factor; 1 for slab, 2 for cylindrical and 3 for spherical
NEDIT	= cycle interval at which EDITS is called
LINMX	= maximum number of lines printed per page 55 is recommended for CDC
INPUT	= parameter controlling source of input for cards. INPUT = 0 reads from cards, INPUT = K, input from Kth record on TAPE8.
NELOP	= maximum number of electron-ion interaction loops in ELECT for each hydroloop. Usual value is 100-200.

NEPRN = control parameter for printing partial values
of electron loop. Usual volume is NELOP-
10.

c. NTAPE, NPRIN, IPRIN, JINT, JMIN, JMAX Format (8I10)

NTAPE = Interval for taping time edits of mesh
NTAPE = 0 no time edits taped
NTAPE = -1 only last time edit taped for
for restart

NPRIN = Interval for printing and plotting time edits
NPRIN = 0 no time edits printed
NPRIN = -1 only last time edit printed

IPRIN = control parameter for type of time edit print
IPRIN = 0 print and plot
IPRIN = 1 print only
IPRIN = 2 plot only

JINT = interval for plotting and printing mesh points
in time edit
JINT = 0 active zones greater than JMIN
are plotted

JMIN = minimum mesh point plotted

JMAX = maximum mesh point plotted unless JINT = 0.

d. TSTOP, DTMIN, TEDIT, REDIT, DTEDT, TMAX, RTMAX
Format (8 E10.4)

TSTOP = maximum problem time

DIMIN = first hydro time step, not used when re-
starting from tape.

TEDIT = time of first time edit. Additional time
edits at times given by

TEDIT = TEDIT * (1 + REDIT) + DTEDT

The run is stopped if the temperature at point RTMAX exceeds TMAX.

e. PΦWW, WLM, TEMP, PRESA Format (8 E10.4)

PΦWW = Laser power in watts/cm²
 WLM = Laser wavelength in micron
 TEMP = Ambient temperature in degrees Kelvin
 PRESA = Ambient pressure in atmospheres

f. IZT, NZ, THIK, RAT Format (2I10, 6E10.4)(one for each material layer)

IZT = control parameter for type of zoning
 IZT = 0, 1 determined by ΔR
 IZT = 2 determined by $\Delta V \approx R^{\alpha-1} \Delta R$
 NZ = number of zones in layer
 THIK = material thickness or radius in centimeters
 RAT = ratio for geometric series of changing zone size.

g. MATRL, MMΦD, RHΦ, GAM1, AMWT, VIΦNE, SIGIE
 Format (2A5, I10, 6E10.4)

MATRL = material name in 10 characters
 MMΦD = material model parameter
 MMΦD = -1 Gilmore tables for air
 = 0 ideal gas
 = 1 Hugoniot equation of state
 RHΦ = material density at standard conditions
 GAM1 = ratio of specific heats of vapor
 AMWT = atomic or molecular weight
 VIΦNE = ionization energy in ev
 SIGIE = slope of electron impact ionization cross section in units $\pi a_{\text{Bohr}}^2 / \text{ev}$

h. CHIΦ, BETA, ACL, AEXΦ, VIBΦE, VIBWE, VHNUE, SIGV
 Format (8E10.4)

CHI Φ = factor in computing temperature dependent thermal conductivity

CHI(J) = CHI Φ (M) * T(J) ** BETA(M)

$$\chi(T) = \chi_0 T^\beta$$

ACL = linear absorption coefficient at standard density

AEXO = power of density dependence in linear absorption coefficient

$$\alpha(\rho) = \alpha_0 \left(\frac{\rho}{\rho_0} \right)^{AEXO}$$

VIBOE = threshold for molecular vibrational excitation by electron impact in ev

VIBWE = bandwidth for molecular vibrational excitation by electron impact in ev.

VANUE = molecular vibrational quanta in ev

SIGV = cross section for molecular vibrational excitation by electron impact at center of band

i. GRUN, HUGC, HUGD, HUGS, ESUB, CVS, TVAP, WFUNE

Format (8E10.4)

GRUN = Grüneisen coefficient for solid

HUGC = C coefficient in Hugoniot equation of state

HUGD = D coefficient in Hugoniot equation of state

HUGS = S coefficient in Hugoniot equation of state

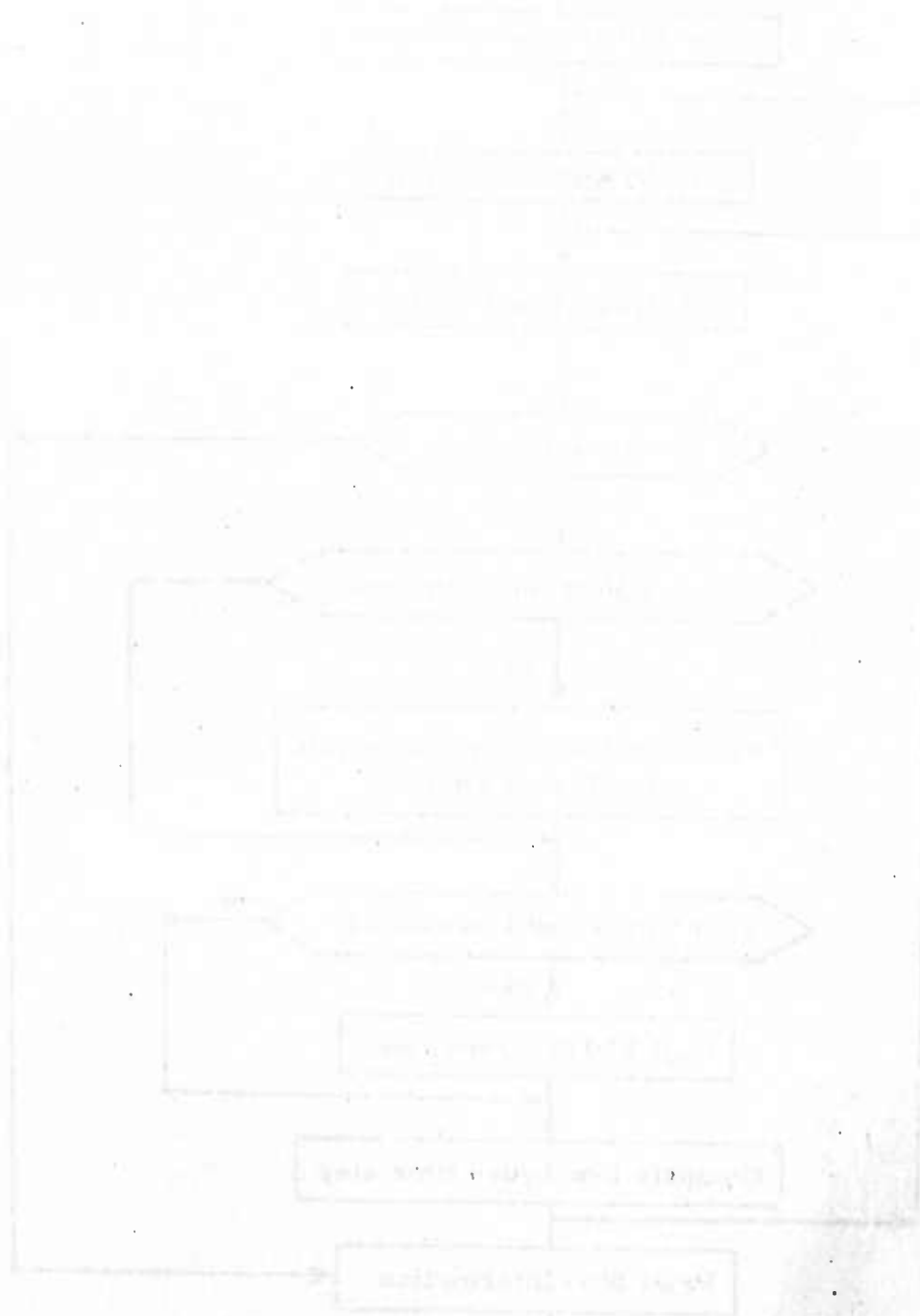
$$PH(J) = C_\mu + D_\mu^2 + S_\mu^3 \text{ in dyne/cm}^2$$

ESUB = sublimation energy of solid in ergs/gm

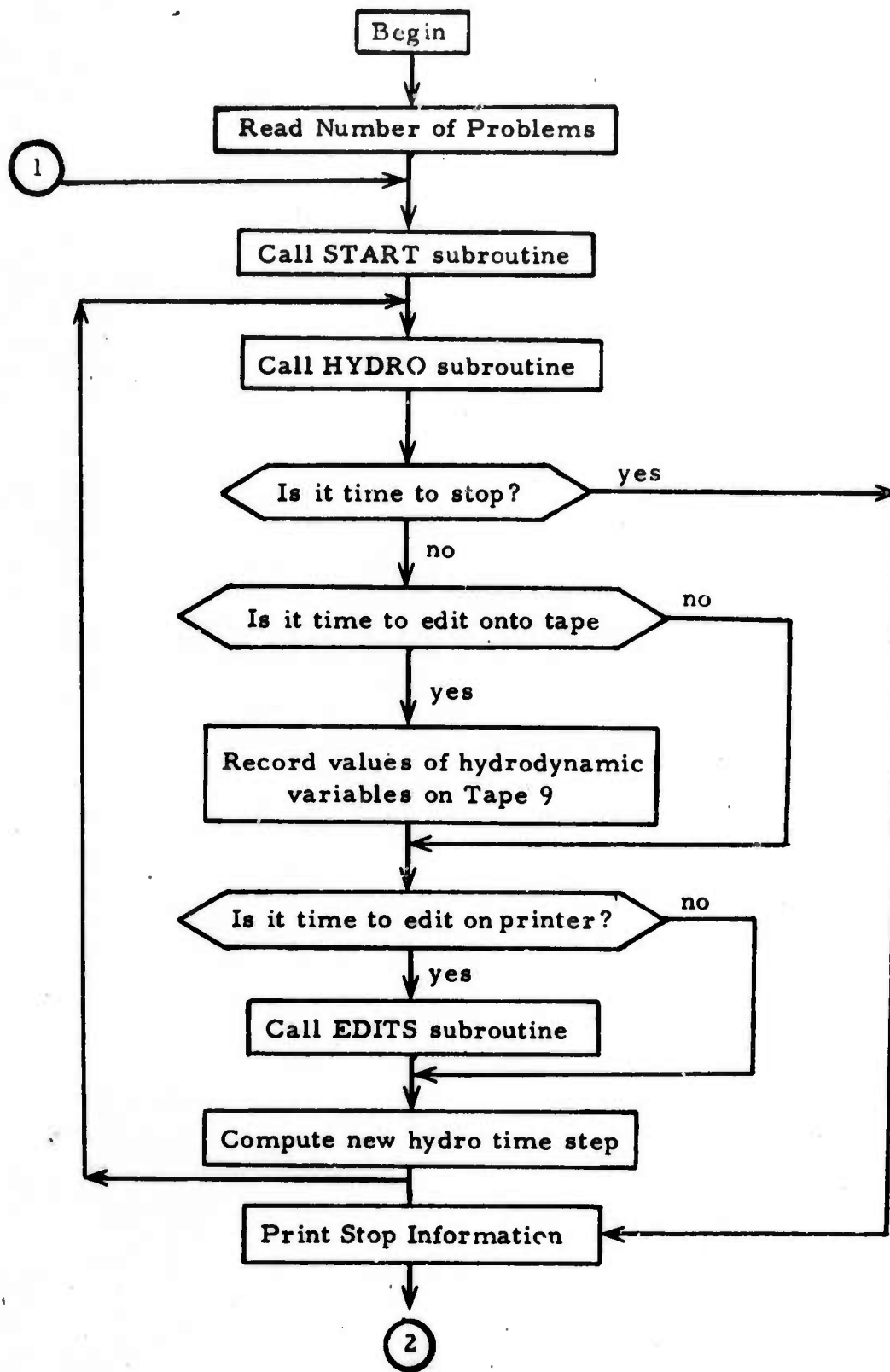
CVS = specific heat of solid in ergs/gm degree

TVAP = vaporization temperature in degrees Kelvin

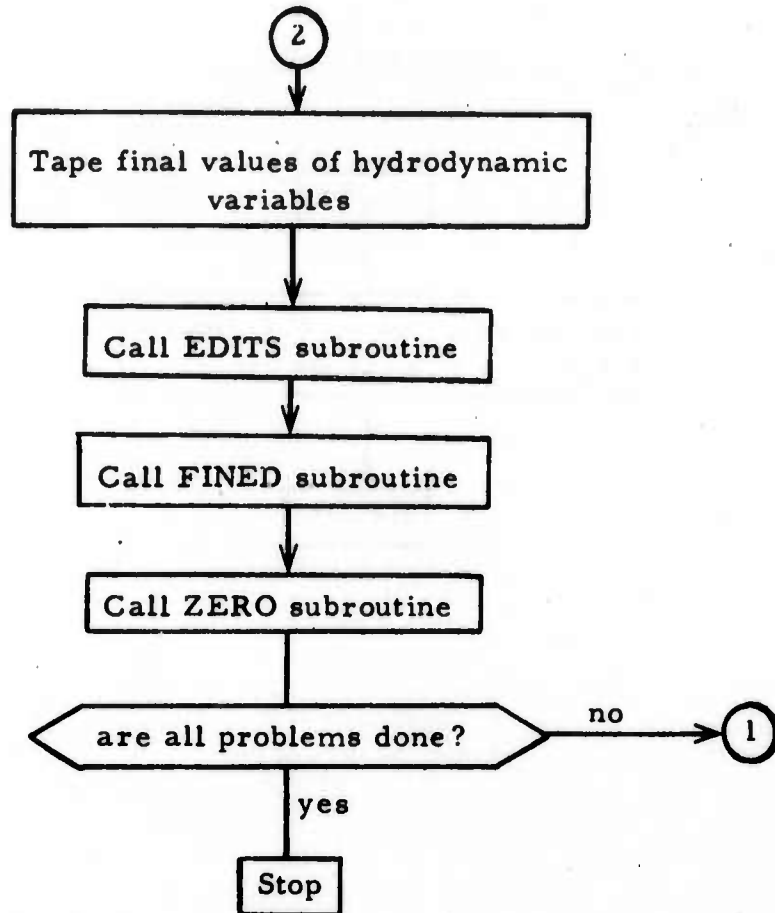
WFUNE = work function for thermionic emission



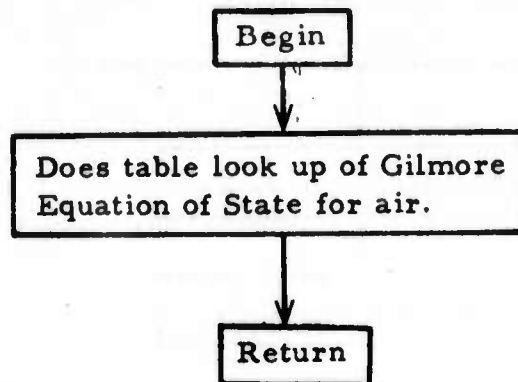
Logical Flow Chart for CELAB Program



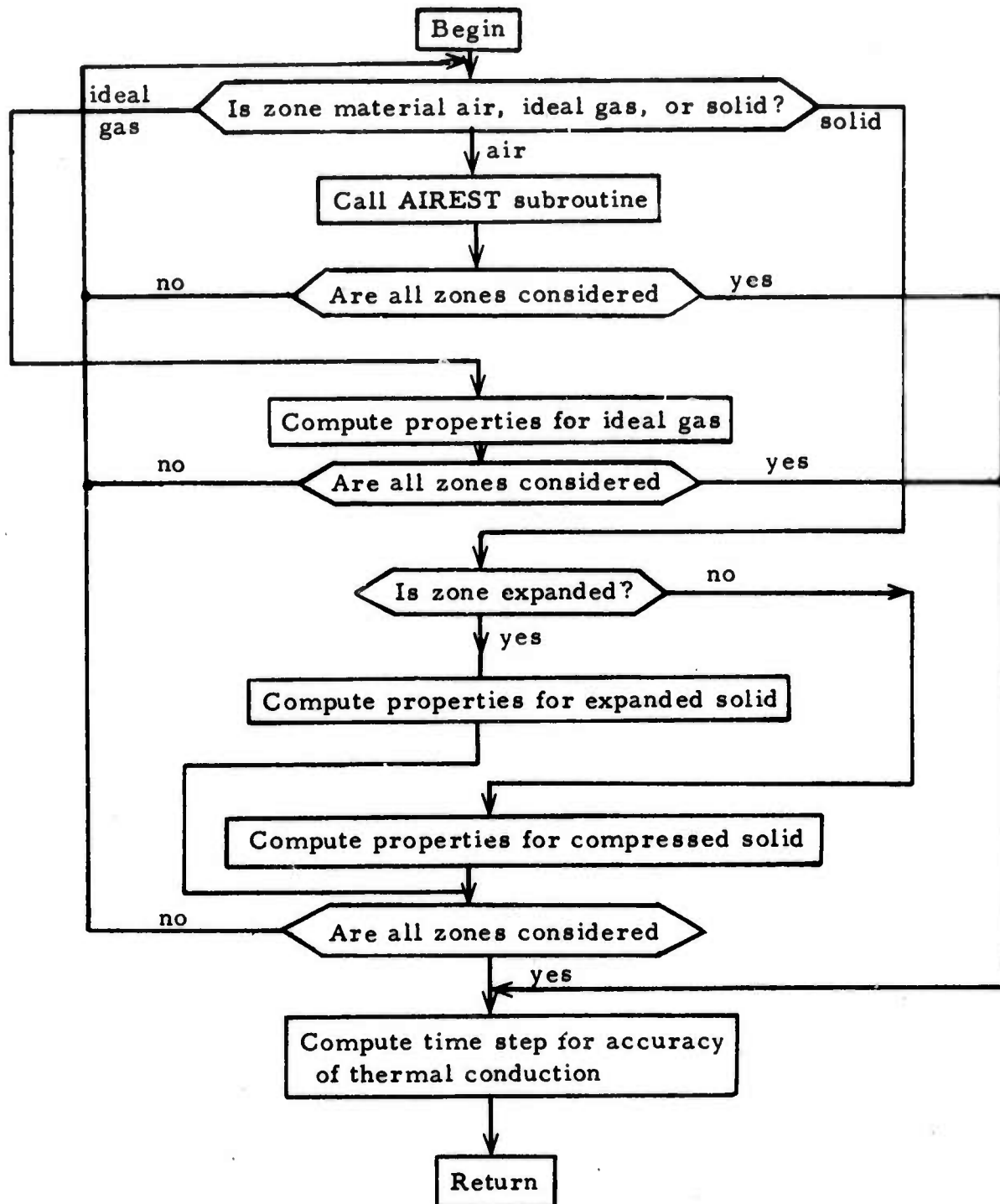
CELAB (CONT)



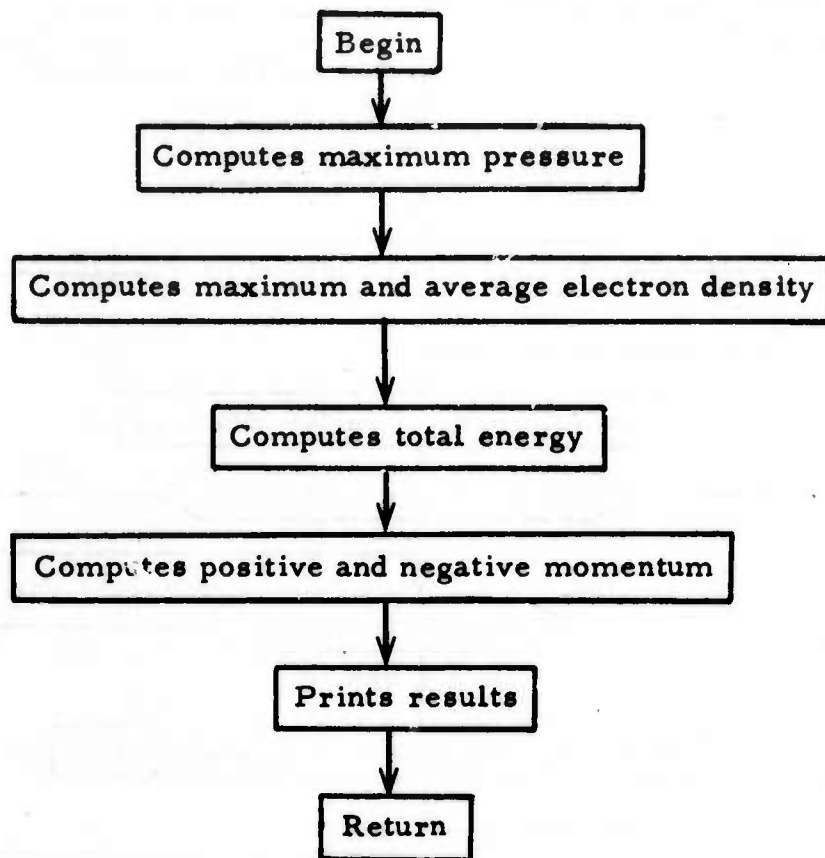
AIREST Subroutine



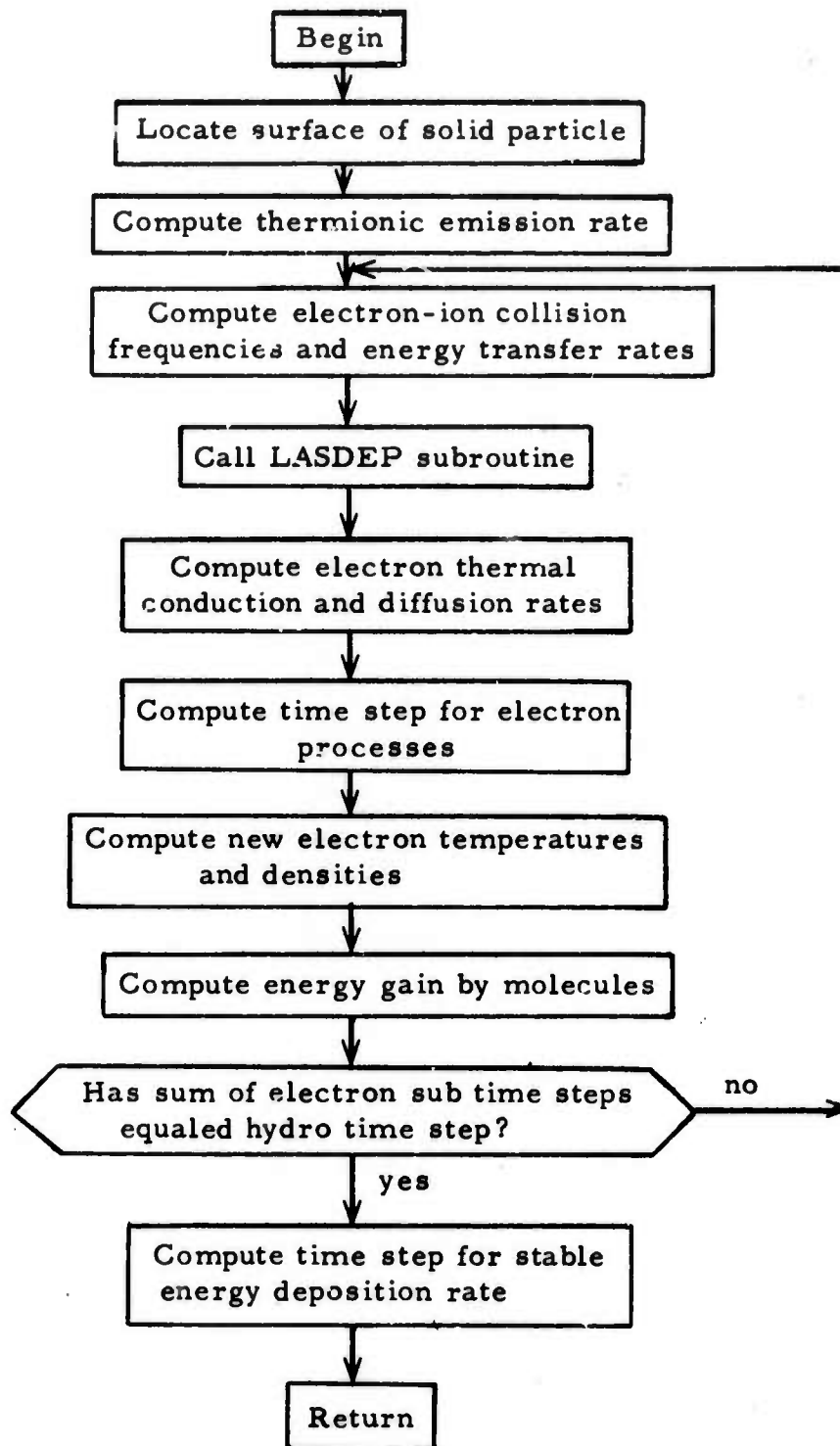
C SOUND Subroutine



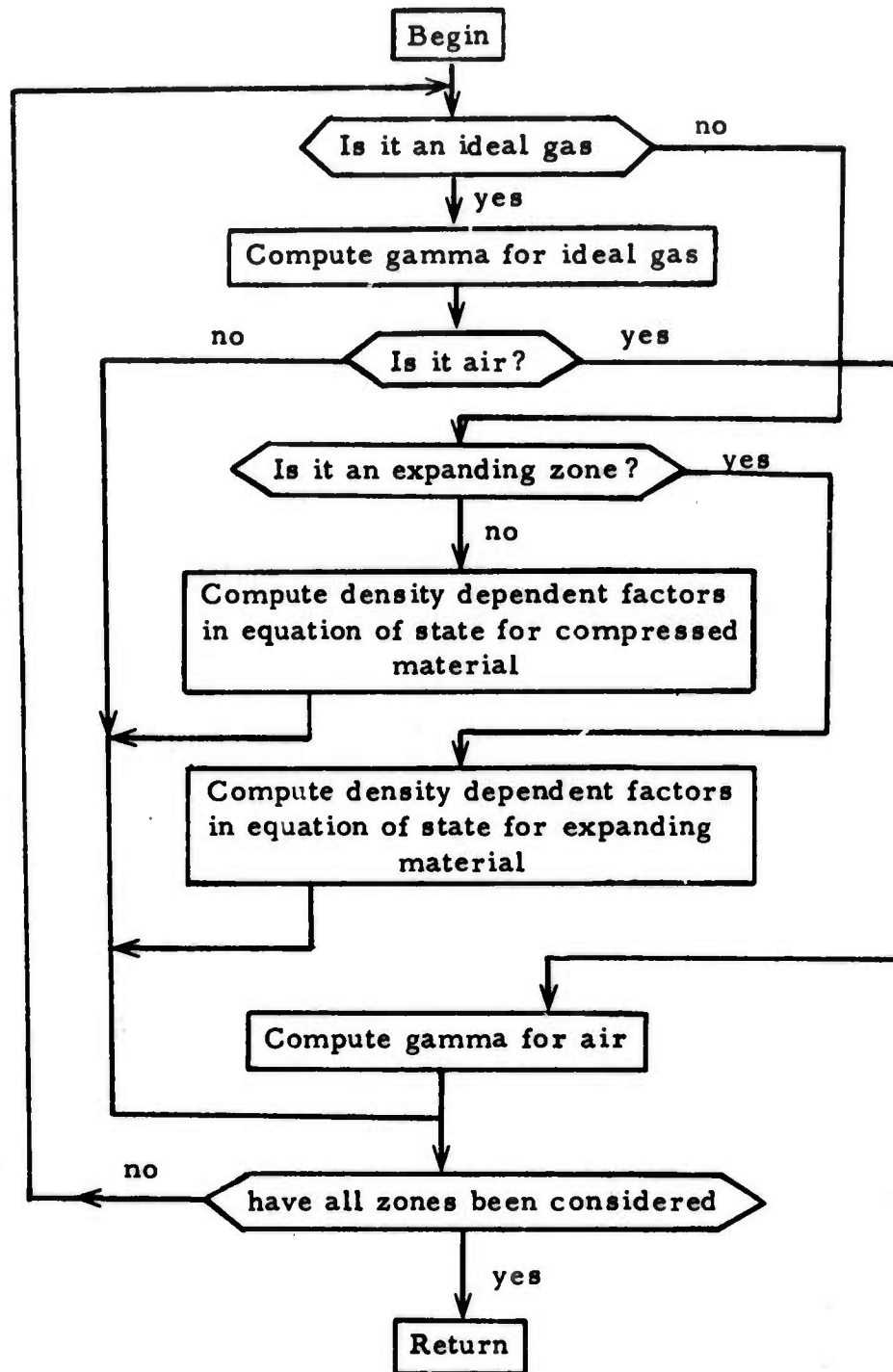
EDITS Subroutine



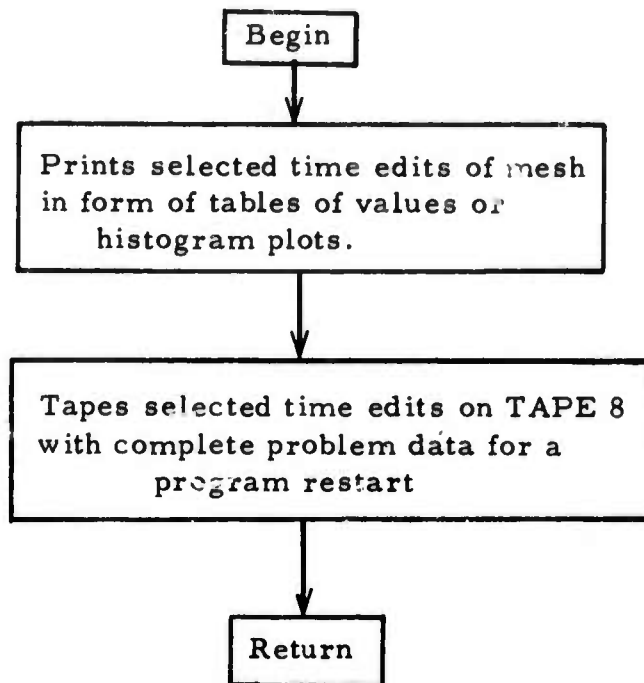
ELECT Subroutine



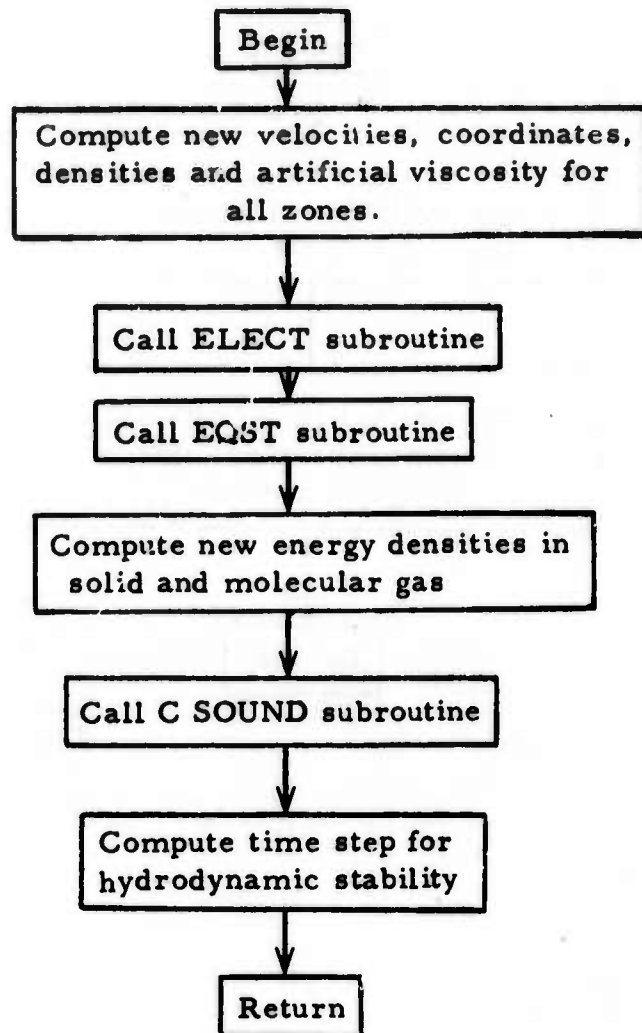
EQST Subroutine



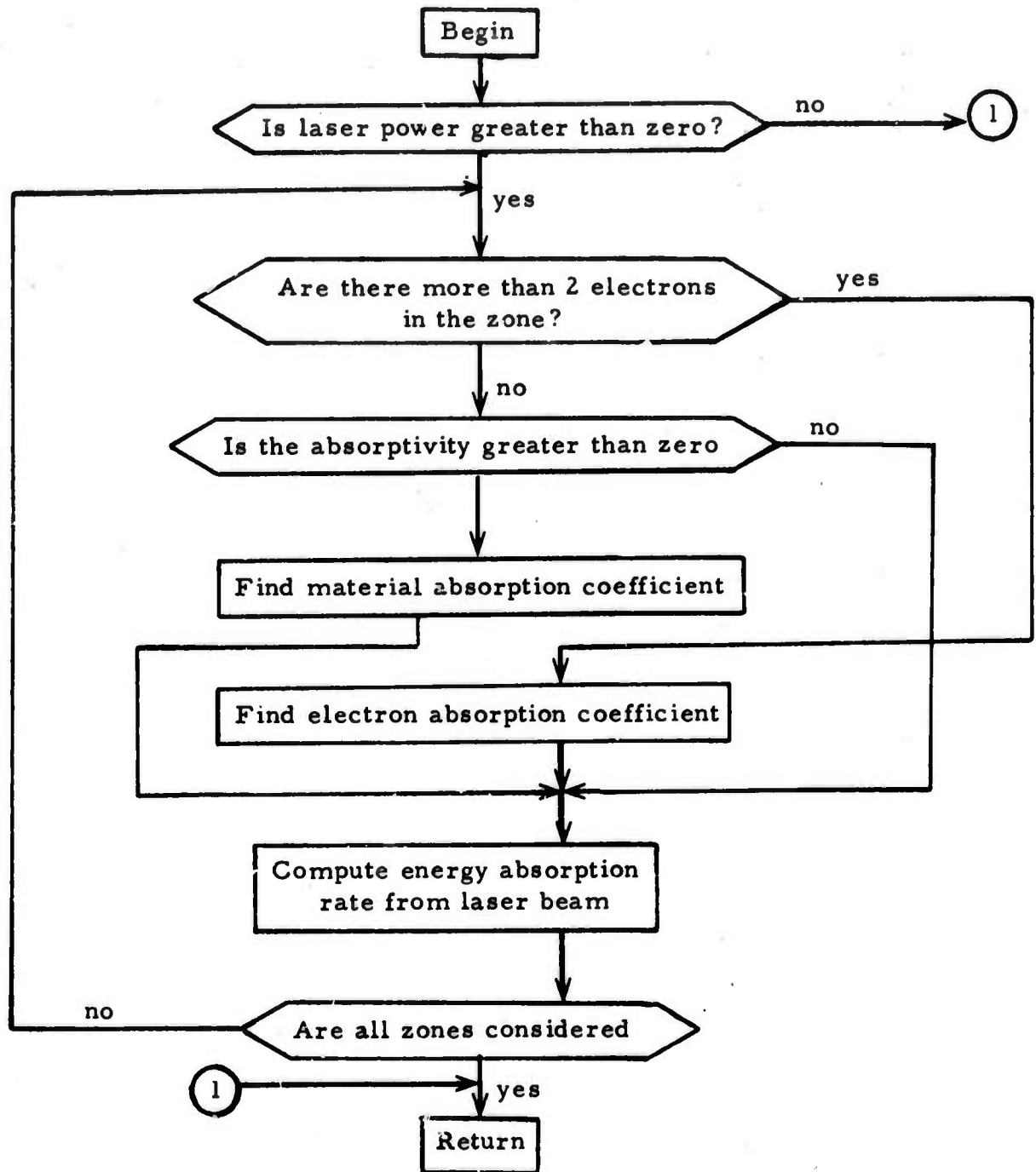
FINED Subroutine



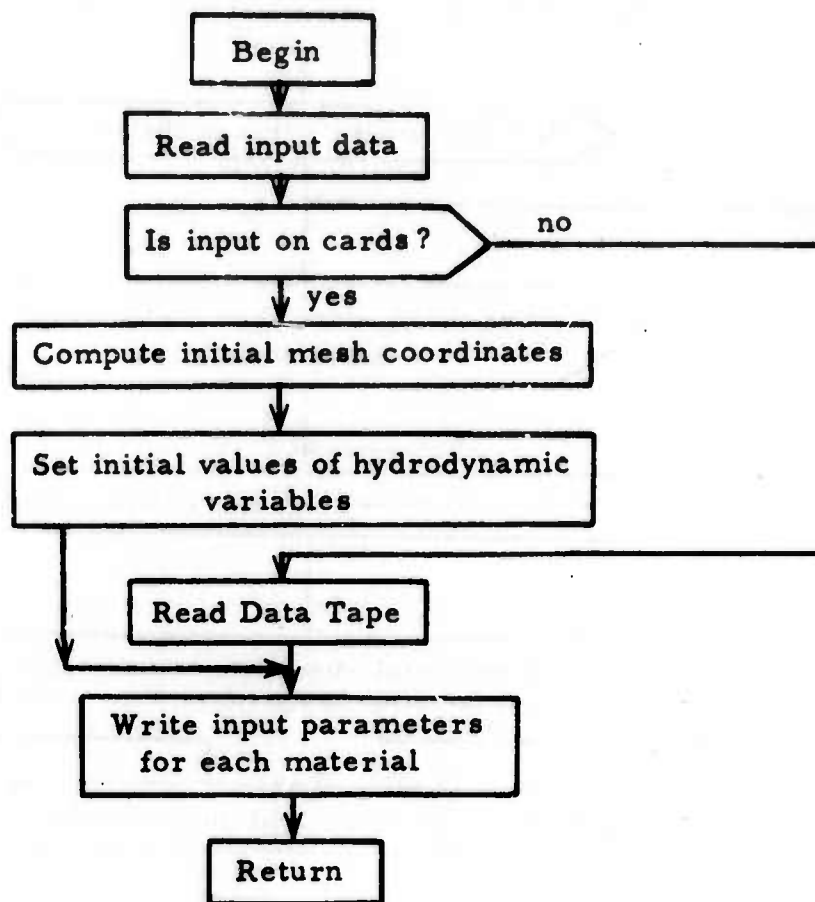
HYDRO Subroutine



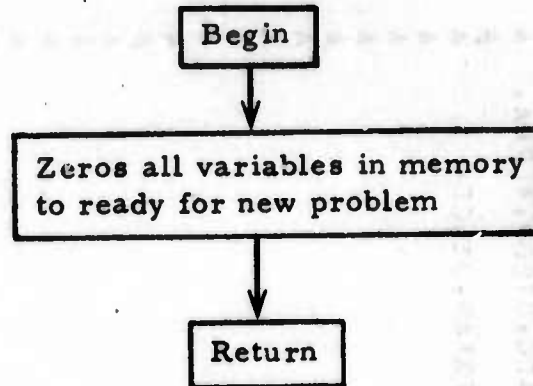
LASDEP Sub-routine



START Subroutine



ZERO Subroutine




```

34 IF (NTAPE) 35,38,35
35 CALL FINED
   CALL ZERO
36 CONTINUE
   IF (NTAPE) 37,38,37
37 END FILE &
   REWIND 8
38 STOP
39 FORMAT (/,130(1H*),/,130(1H*))
40 FORMAT (4X,21H MAXIMUM CYCLE NUMBER,15,15H WAS REACHED AT,E10.3,
   4H SEC)
41 FORMAT (4X,7H TIME =,E10.3,
   38H EXCEEDED MAXIMUM TIME AT CYCLE NUMBER,15)
42 FORMAT (4X,10H DENSITY =,E10.3,15H OF ZONE NUMBER,14,
   28H IS NEGATIVE AT CYCLE NUMBER,15,11H AND TIME =,E10.3)
43 FORMAT (4X,7H TEMP =,E10.3,15H OF ZONE NUMBER,14,9H EXCEEDS ,
   E10.3,16H AT CYCLE NUMBER,15,11H AND TIME =,E10.3)
44 FORMAT (1H1)
45 FORMAT (4X,9H ENERGY =,E10.3,15H OF ZONE NUMBER,14,
   28H IS NEGATIVE AT CYCLE NUMBER,15,11H AND TIME =,E10.3)
46 FORMAT (4X,8H KTAPE =,13,22H TIME EDITS WERE TAPED,/)
47 FORMAT (4X,6H NEL =,14,24H EXCEEDS MAXIMUM NELOP =,14)
48 FORMAT (8140)
   END

```

```

A 107
A 108
A 109
A 110
A 111
A 112
A 113
A 114
A 115
A 116
A 117
A 118
A 119
A 120
A 121
A 122
A 123
A 124
A 125
A 126
A 127
A 128
A 129
A 130

```

```

SUBROUTINE HYDRO (JDEN)
COMMON /RVAR/ R(512),P(512),Q(512),U(512),D(512),E(512),T(512),
    PE(512),EE(512),TE(512),ANE(512),FM(512),CS(512)
COMMON /RMAS/ ZM(512),ZMHI(512),RNH(512),RA(512),RANH(512)
COMMON /MPROP/ PH(512),GAMD(512),CHI(512),BET(512),CI(512)
COMMON /GJHJ/ GJ(512),HJ(512),DVDT(512)
COMMON /PMAT/ THIK(4),RAT(4),UV(4),ESUB(4),ERAT(4),GAMC(4),AMWT(4),
    HUGD(4),HUGS(4),GAMJ(4),AEX(4),ACL(4),AEXO(4),TOE(4),TVAP(4),
    CHIN(4),BETA(4),AMU(4),CVSI(4),CVGI(4),VIONE(4),VIONK(4),SIGIE(4),
    SIGIK(4),VIBOE(4),VIBOK(4),VIRWE(4),VIRWK(4),VHNUE(4),
    HNUSQ(4),SIGV(4),SEO(4),SEC(4),WFUNE(4),WFUNK(4),DNM(4)
COMMON /MPAR/ NMAT,MMOD(7),JBND(4),IZT(4),NZ(4)
COMMON /JPAP/ JOR,JORP,JACM,JAC,JACP,JTMAX,IALPM,JTSTAB,JTACC,
    JTEDP,JSR
COMMON /NTIME/ NCYCS,N,NELOP,NEL,NEDIT,LINE,LINMX,NTAPE,NPRIN,
    IPRIN,JINT,JMIN,JMAX,NTED,KTAPE,NETP
COMMON /CTIME/ TSTOP,TIME,DTN,DTNH,DTNHS,DTSTAB,DTACC,DTEDP,ALPHA,
    TMAX,TEMP,PRES,EINTI,EDPT,EDP,SOS
DATA COSQH,COSQ2,CIH,CI/2,.8,.0,125,U.250/
BEGIN HYDRO LOOP **
J2=1
PJP=P(2)+PE(2)+Q(2)
RUJP=U.
DO 10 M=1,NMAT
    J1=J2+1
    J2=JBND(M)
    DO 10 J=J1,J2
        PJP=P(J+1)+PE(J+1)+Q(J+1)
        U(J)=U(J)-RA(J)+DTN*ZMHI(J)+(PJP-PJM)
        IF (ABS(U(J))-U) 1,1,2
1 U(J)=0.
GO TO 3
2 RNH(J)=R(J)
R(J)=R(J)+DTNH*U(J)

```

C

109
110
111
112
113
114
115
116
117

8 8 8 8 8 8 8 8 8

JTSTAB=J
20 CONTINUE
 UTSTAB=1./DTSTAB
 RETURN
21 JDEN=-J
 RETURN
22 JDEN=J
23 RETURN
 END

```

SUBROUTINE ELECT (JDEN)
COMMON /RVAR/ R(512),P(512),Q(512),U(512),D(512),E(512),T(512),
. PE(512),EE(512),TE(512),ANE(512),FM(512),CS(512)
COMMON /RMAS/ ZM(512),ZMHI(512),RNH(512),RA(512),RANH(512)
COMMON /GJHJ/ DNE(512),DEE(512),DVDI(512)
COMMON /FREQ/ CNU(512),FE(512)
COMMON /PMAT/ THIK(4),RAT(4),DV(4),RHO(4),GRUN(4),HUGC(4),
. HUGD(4),HUGS(4),GAM1(4),ESUB(4),ERAT(4),GAMC(4),AMWT(4),
. CHTO(4),BETA(4),AMU(4),AEX(4),ACL(4),AEXO(4),TOE(4),TVAP(4),
. CVS(4),CVG(4),CVSI(4),CVGI(4),VIONE(4),VIONK(4),SIGIE(4),
. SIGIK(4),VIBOE(4),VIROK(4),VIRWE(4),VIRWK(4),VHNUE(4),
. HNUSQ(4),SIGV(4),SEO(4),SEC(4),WFUNE(4),WFUNK(4),DNM(4)
COMMON /MPAR/ NMAT,MMOD(7),JBND(4),IZT(4),NZ(4)
COMMON /JPAP/ JOR,JORP,JACH,JAC,JACP,JTMAX,IALPH,JTSTAB,JTACC,
. JTEDP,JSR
COMMON /NTIME/ NCYCS,N,NEL,NEDIT,LINE,LINMX,NTAPE,NPRIN,
. IPRIN,JINT,JMIN,JMAX,NTED,KTAPE,NETP
COMMON /CTIME/ TSTOP,TIME,DTN,DTNH,DTNHS,DTSTAB,DTACC,DTEDP,ALPHA,
. THAX,TEMP,PRES,EINTI,EDPT,EDP,SOS
COMMON /EPAR/ ACPAO,REC,SIGO,SIGC,DIFI,ATIE,AIO,AKBT,AKB,GAME,
. FNEL,NEPRN
. ICON=0
NEL=0
DTFN=DTNH*FNEL
DTFNT=DTFN*DTFN
DTFNO=10.*DTFNT
ETIME=TIME-DTNH
DO 1 J=2,JAC
CNU(J)=0,
FE(J)=0,
FM(J)=0,
1 DETERMINE SURFACE OF SOLID PARTICLE **
J2=1
DO 2 MS=1,NMAT
J1=J2+1
J2=JHND(MS)
C

```



```

J1=J2+1
J2=MINO(JBND(M),JEL)
DO 21 J=J1,J2
  IDO=0
  ANN=DNM(M)*D(J)
  TEJ=TE(J)
  IF (EE(J)) 14,14,13
13 TH=SQRT(TEJ)
  FFAC=ACPAO*TH
  CFI=SIGIK(M)*(VIONK(M)+TEJ+TEJ)
  AA=EXP(-VIONK(M)/TEJ)
  DNR=FFAC*CFI
  DNI=DNM*AA*ANN
  DNR=DNR*ANF(J)*REC*ANE(J)/(TH*TEJ)
  DNE(J)=ANE(J)*(DNI-DNR)
  CFI=CFI*AA
  DEI=AKB*VIONK(M)*DNE(J)/D(J)
  AA=VIBOK(M)/TEJ
  BB=VIBWK(M)/TEJ
  VFAC=EXP(-AA)*(1+AA*BB)*EXP(-BB)
  CFV=SIGV(M)*VFAC
  DEV=HNUSQ(M)*CFV/(TEJ*T(J))
  AL=(ALO+ALOG(TEJ**3/ANE(J)))/TEJ
  CFC=SIGC*AL**2
  DEC=SEC(M)*AL/TEJ
  CNU(J)=FFAC*(ANE(J)*CFC*ANN*(SIGO*CFV*CFI))
  FE(J)=FFAC*AKB*(TEJ-T(J))*ANE(J)*DEC*ANN*(SEO(M)+DEV))/
    D(J)
  DEE(J)=FE(J)-DEI
  DKT=DEE(J)/EE(J)-DNI+DNR
  DTT=ABS(0.1/DKT)
  IF (DTT-DTFNT) 14,14,15
14 TE(J)=T(J)
  AA=FE(J)
  EE(J)=AKBT*ANE(J)*TE(J)/D(J)
  FE(J)=0.

```

```

73 C
74 C
75 C
76 C
77 C
78 C
79 C
80 C
81 C
82 C
83 C
84 C
85 C
86 C
87 C
88 C
89 C
90 C
91 C
92 C
93 C
94 C
95 C
96 C
97 C
98 C
99 C
100 C
101 C
102 C
103 C
104 C
105 C
106 C
107 C
108 C

```



```

J1=JS+1
DTDIF=0.
DTCON=0.
DYJP=DIFI*(CNU(J1)*(RNH(J1)-RNH(J1-1)))/TE(J1)
CYJP=AKRT*ANE(J1)/DYJP
IF (CYJP) 22,23,22
22 CYJP=1./CYJP
23 DNEJP=0.
CEEJP=0.
DO 30 J=J1,JEL
DYJM=DYJP
CYJM=CYJP
DNEJM=DNEJP
CEEJM=CEEJP
DYJP=DIFI*(CNU(J+1)*(RNH(J+1)-RNH(J)))/TE(J)
DNEJP=RNH(J)/(DYJM+DYJP)
IF (DTDIF-DNEJP*(ZMHI(J))) 24,25,25
24 DTDIF=DNEJP*(ZMHI(J))
25 CEEJP=DNEJP*(EE(J+1)-EE(J))
DNEJP=DNEJP*(ANE(J+1)-ANE(J))
DNE(J)=DNE(J)+D(J)*(DNEJP-DNEJM)/ZM(J)
CYJP=AKRT*ANE(J+1)/DYJP
IF (CYJP) 26,29,26
26 CYJP=1./CYJP
CEEJP=RNH(J)/(CYJM+CYJP)
IF (DTCON-CEEJP*(ZMHI(J))) 27,28,28
27 DTCON=CEEJP*(ZMHI(J))
28 CEEJP=CEEJP*(TE(J+1)-TE(J))
GO TO 30
29 CEEJP=0.
30 DEE(J)=DEE(J)+(CEEJP-CEEJM)/ZM(J)
IF (DNEJP) 31,32,32
31 DNE(JELP)=-D(J)*(DNEJP/ZM(J))
32 IF (CEEJP) 33,34,34
33 UEE(JELP)=-CEEJP/ZM(J)
34 DTEE=1.

```

```

145 C
146 C
147 C
148 C
149 C
150 C
151 C
152 C
153 C
154 C
155 C
156 C
157 C
158 C
159 C
160 C
161 C
162 C
163 C
164 C
165 C
166 C
167 C
168 C
169 C
170 C
171 C
172 C
173 C
174 C
175 C
176 C
177 C
178 C
179 C
180 C

```

```

DTNE=1.
00 40 J=J1,JEL
IF (DEE(J)) 35,37,37
35 DTEST=EE(J)/DEE(J)
IF (DTEST-DTEE) 36,37,37
36 DTEE=DTEST
37 IF (DNE(J)) 38,40,40
38 DTEST=-ANE(J)/DNE(J)
IF (DTEST-DTNE) 39,40,40
39 DTNE=DTEST
40 CONTINUE
UTEL=AMAX1(2,DTTE,DTFM)
DTEL=0.51*AMIN1(DTEL,DTNE,DTEE,DTNH)
IF (TIME-ETIME-DTEL) 41,42,43
41 DTEL=TIME-ETIME
42 ICON=1
43 ETIME=ETIME+DTEL
00 46 J=J1,JELP
ANE(J)=ANE(J)+DNE(J)*DTEL
IF (ANE(J)) 56,46,44
44 EE(J)=EE(J)+DEE(J)*DTEL
IF (EE(J)) 57,46,45
45 AA=D(J)*EE(J)
TE(J)=0.5*(TE(J)+AA/(AKBT*ANE(J)))
PE(J)=GAME*AA
46 CONTINUE
EDPT=EDPT+EDP*DTEL
00 47 J=2,JAC
FM(J)=FM(J)+FE(J)*DTEL
IF (ICON) 51,48,51
48 IF (NEL-NELOP) 49,49,58
49 00 50 J=2,JS
50 FE(J)=0.
GO TO 12
51 DTEDP=0.
J2=1

```



```

SUBROUTINE LASDEF
COMMON /RVAR/ R(512),P(512),Q(512),U(512),D(512),E(512),T(512),
PE(512),EE(512),TE(512),ANE(512),FM(512),CS(512)
COMMON /RMAS/ ZM(512),ZMHI(512),RNH(512),RA(512),RANH(512)
COMMON /GJHJ/ DEE(512),DNE(512),DVT(512)
COMMON /FREQ/ CNU(512),FE(512)
COMMON /PMAT/ THIK(4),RAT(4),DV(4),RHO(4),GRUN(4),HUGC(4),
HUGD(4),HUGS(4),GAM(4),ESUB(4),ERAT(4),GAMC(4),AMWT(4),
CHIO(4),BETA(4),AMU(4),AEX(4),ACL(4),AEXO(4),TOE(4),TVAP(4),
CVS(4),CVG(4),CVSI(4),CVGI(4),VIONE(4),VIONK(4),SIGIE(4),
SIGIK(4),VIBOE(4),VIBOK(4),VIRWE(4),VIRWK(4),VHNUE(4),
HNUSQ(4),SIGV(4),SEO(4),SEC(4),WFUNE(4),WFUNK(4),DNH(4)
COMMON /MPAR/ NMAT,MMOD(7),JBND(4),IZT(4),NZ(4)
COMMON /JPAR/ JOR,JORP,JACM,JAC,JACP,JTMAX,IALPM,JTSTAB,JTACC,
JTENP,JSR
COMMON /CTIME/ TSTOP,TIME,DTN,DTNH,DTNHS,DTSTAB,DTACC,DTEDP,ALPHA,
TMAX,TEMP,PRES,EINTI,EDPT,EDP,SOS
COMMON /LASER/ POW,WL,WF,CRITE,EC
DATA ZX4,ZEXP,C2,C6,C24/0.020,88.72,0.5,0.166666667,0.0416666667/
DTEDP=0.
EDP=0.
P'=POW
M=NMAT
IF (POW) 14,14,1
BEGIN ENERGY DEPOSITION LOOP **
1 I2=JAC-JBND(M-1)
I1=MAX0(1,JACP-JBND(M))
DO 12 I=I1,I2
J=JACP-I
IF (ANE(J)-2.) 2,4,4
2 IF (AMU(M)) 11,11,3
3 A=AMU(M)*D(J)**AEX(M)
AE=0.
GO TO 6
4 A=ANE(J)*CNU(J)*EC
AE=A

```



```

SUBROUTINE EQST
COMMON /RVAR/ R(512),P(512),Q(512),U(512),D(512),E(512),T(512),
PE(512),EE(512),TE(512),ANE(512),FM(512),CS(512)
COMMON /MPROP/ PH(512),GAMD(512),CHI(512),BET(512),CI(512)
COMMON /EQSF/ EXFAC(512),SQFAC(512)
COMMON /PMAT/ THIK(4),RAT(4),DV(4),RHO1(4),RHO(4),GRUN(4),HUGC(4),
HUGD(4),HUGS(4),GAM1(4),ESUB(4),ERAT(4),GAMC(4),AMWT(4),
CHIO(4),BETA(4),AMU(4),AEX(4),ACL(4),AEXO(4),TOE(4),TVAP(4),
CVS(4),CVG(4),CVSI(4),CVGI(4),VIONE(4),VIONK(4),SIGIE(4),
SIGIK(4),VIBOE(4),VIBOK(4),VIRWE(4),VIRWK(4),VHNUE(4),
HNUSQ(4),SIGV(4),SEO(4),SEC(4),WFUNE(4),WFUNK(4),DNM(4)
COMMON /MPAR/ NMAT,MMOD(7),JBND(4),IZT(4),NZ(4)
COMMON /JPAP/ JOR,JORP,JACH,JAC,JACP,JTMAX,IALPM,JTSTAB,JTACC,
JTEDP,JSR
M=0
J2=1
1 M=M+1
J1=J2+1
J2=MIN0(JAC,JBND(M))
IF (MMOD(M)) 8,2,4
C IDEAL GAS EQUATION OF STATE **
2 DO 3 J=J1,J2
3 GAMD(J)=GAM1(M)*D(J)
IF (M-NMAT) 1,10,10
C HUGONOT EQUATION OF STATE **
4 DO 7 J=J1,J2
EMU=D(J)/RHO(M)-1.
IF (EMU) 5,6,6
C FOR EXPANDED ZONES **
5 V1=RHO(M)/D(J)
EXFAC(J)=ESUB(M)*EXP(ERAT(M)*(1.-V1)*V1)
PH(J)=ESUB(M)-EXFAC(J)
SQFAC(J)=(GRUN(M)-GAM1(M))*SQRT(D(J)/RHO(M))
GAMD(J)=(GAM1(M)+SQFAC(J))*D(J)
PH(J)=-GAMD(J)+PH(J)
GO TO 7

```

```

C      FOR COMPRESSED ZONES **
6      PH(J)=((HUGS(M)*EMU+HUGD(M))*EMU+HUGC(M))*EMU
      PH(J)=PH(J)*(1.-0.5*GRUN(M)*EMU+RHO(M)/D(J))
      GAMD(J)=GRUN(M)*D(J)
7      CONTINUE

C      IF (M-NMAT) 1,10,10
      USE EQUATION OF STATE FOR AIR **
8      DO 9 J=J1,J2
9      GAMD(J)=GAMD(J)*D(J)
      IF (M-NMAT) 1,10,10
10     RETURN
      END

```

```

37
38
39
40
41
42
43
44
45
46
47
48
E E E E E E E E E E E E E E

```

```

SUBROUTINE CSOUND
COMMON /HVAR/ R(512),P(512),Q(512),U(512),D(512),E(512),T(512),
PE(512),EE(512),TE(512),ANE(512),FM(512),CS(512)
COMMON /RMAS/ ZM(512),ZMHI(512),RNH(512),RA(512),RANH(512)
COMMON /MPROP/ PH(512),GAMD(512),CHI(512),BET(512),CI(512)
COMMON /EOSF/ EXFAC(512),SQFAC(512)
COMMON /PMAT/ THIK(4),RAT(4),DV(4),RHO1(4),RHO(4),GRUN(4),HUGC(4),
HUGD(4),HUGS(4),GAMI(4),ESUB(4),ERAT(4),GAMC(4),AMWT(4),
CHIO(4),BETA(4),AMU(4),AEX(4),ACL(4),AEXO(4),TOE(4),TVAP(4),
CVS(4),CVG(4),CVSI(4),CVGI(4),VIONE(4),VIONK(4),SIGIE(4),
SIGIK(4),VIBOE(4),VIBOK(4),VIRWE(4),VIRWK(4),VHNUE(4),
HNUSQ(4),SIGV(4),SEO(4),SEC(4),WFUNE(4),WFUNK(4),DNM(4)
COMMON /MPAR/ NMAT,MMOD(7),JBND(4),IZT(4),NZ(4)
COMMON /JPAR/ JOR,JORP,JACM,JAC,JACP,JTMAX,IALPM,JTSTAB,JTACC,
JTDP,JSR
COMMON /CTIME/ TSTOP,TIME,DTN,DTNH,DTNHS,DTSTAB,DTACC,DTEDP,ALPHA,
TMAX,TEMP,PRES,EINTI,EDPT,ENDP,SOS
M=0
J2=1
1 M=M+1
J1=J2+1
J2=MIN0(JAC,JBND(M))
IF (MMOD(M)) 2,3,5
CALL GILMORE EQUATION OF STATE FOR AIR **
2 CALL AIREST (M,J1,J2)
IF (M-NMAT) 1,13,13
IDEAL GAS EQUATION OF STATE **
3 DO 4 J=J1,J2
CS(J)=SQRT(GAMC(M)*E(J))
T(J)=E(J)/CVG(M)
4 CHI(J)=CHIO(M)*T(J)**BETA(M)
IF (M-NMAT) 1,13,13
HUGONOT EQUATION OF STATE **
5 DO 12 J=J1,J2
EMU=D(J)/RHO(M)-1.
IF (EMU) 6,8,8

```

1 F
2 F
3 F
4 F
5 F
6 F
7 F
8 F
9 F
10 F
11 F
12 F
13 F
14 F
15 F
16 F
17 F
18 F
19 F
20 F
21 F
22 F
23 F
24 F
25 F
26 F
27 F
28 F
29 F
30 F
31 F
32 F
33 F
34 F
35 F
36 F

```

C      FOR EXPANDED ZONES **
6      V1=RHO(M)/D(J)
      E=U3=ERAT'M*(1.-2.*V1)*V1
      CSQ=P(J)/D(J)+0.5*SQFAC(J)*(E(J)-ESUB(M)*EXFAC(J))-(GAM1(M)+
      .      SOFAC(J))*ENU3*EXFAC(J)
      IF (CSQ) 7,7,9
7      CSQ=GAM1(M)*(1.+GAM1(M))*E(J)
      GO TO 9
C      FOR COMPRESSED ZONES **
8      CSQ=GRUN(M)*E(J)+((3.*HUGS(M)*EMU+2.*HUGD(M))*EMU+HUGC(M)-GAM1(M)*
      .      ((2.*HUGS(M)*EMU+1.5*HUGD(M))*EMU+HUGC(M))*EMU)/RHO(M)
9      CS(J)=SORT(CSQ)
      IF (ESUR(M)-E(J)) 10,11,11
10     CI(J)=CVGI(M)
      T(J)=TVAP(M)+(E(J)-ESUB(M))*CI(J)
      GO TO 12
11     CI(J)=CVSI(M)
      T(J)=AMIN1(TVAP(M),TOE(M)+E(J)*CI(J))
12     CHI(J)=CHIO(M)+T(J)*BETA(M)
      IF (M-NMAT) 1,13,13
C      COMPUTE TIME STEP FOR THERMAL CONDUCTIVITY **
13     DTACC=0.
      TJP=T(2)
      YJP=R(2)/CHI(2)
      XTRP=.
      DO 16 J=2,JACM
      TJM=TJP
      YJM=YJP
      XTRM=XTRP
      YJP=(R(J+1)-R(J))/CHI(J+1)
      DEN=YJM-YJP
      TJP=(T(J)+YJP+T(J+1)+YJM)/DEN
      XTRP=RA(J)*(T(J+1)-T(J))/DEN
      DT=ABS(TJP-TJM)
      IF (DT-0.01*TJP) 16,16,14
14     DTI=A95(XTRP-XTRM)*CI(J)/(ZM(J)*DT)

```

F 37
 F 38
 F 39
 F 40
 F 41
 F 42
 F 43
 F 44
 F 45
 F 46
 F 47
 F 48
 F 49
 F 50
 F 51
 F 52
 F 53
 F 54
 F 55
 F 56
 F 57
 F 58
 F 59
 F 60
 F 61
 F 62
 F 63
 F 64
 F 65
 F 66
 F 67
 F 68
 F 69
 F 70
 F 71
 F 72

```

IF (DTI-DTACC) 16,16,15
15 DTACC=DTI
   JTACC=J
16 CONTINUE
   IF (DTACC-1.) 17,17,18
17 DTACC=1.
   RETURN
18 DTACC=0.125/DTACC
   RETURN
   END

```

```

73
74
75
76
77
78
79
80
81
82
F F F F F F F F F F

```

```

SUBROUTINE AIREST (M,J1,J2)
COMMON /RVAR/ R(512),P(512),Q(512),U(512),D(512),E(512),T(512),
PE(512),EEL(512),TE(512),ANE(512),FM(512),CS(512)
COMMON /MPROP/ PH(512),GAMD(512),CHI(512),BET(512),CI(512)
COMMON /PMAT/ THIK(4),RAT(4),DV(4),RHO1(4),RHO(4),GRUN(4),HUGC(4),
HUGD(4),HUGS(4),GAMI(4),ESUB(4),ERAT(4),GAMC(4),AMWT(4),
CHIN(4),BETA(4),AMU(4),AEX(4),ACL(4),AEXO(4),TOE(4),TVAP(4),
CVS(4),CVG(4),CVSI(4),CVGI(4),VIONE(4),VIONK(4),SIGIE(4),
SIGIK(4),VIBOE(4),VIBOK(4),VIRWE(4),VIRWK(4),VHNUE(4),
HNUSQ(4),SIGV(4),SEO(4),SEC(4),WFUNE(4),WFUNK(4),DNM(4)
DIMENSION EE(10,8),TT(10),DTT(10),RD(8)
DIMENSION GAM(10,8),TC(4),DTCI(4),COND(5),RC(4)
DATA TCO,TC/2000.,3200.,4100.,7000.,9000./
DATA DTCI/.83333333E-03,1.111111E-03,.3448276E-03,.5E-03/
DATA TT/200.,300.,400.,500.,600.,700.,800.,1200.,1800.,
2400./
DATA DTT/100.,100.,100.,100.,100.,100.,100.,100.,400.,600.,
600./
DATA COND/11787.,7000.,4500.,35000.,141568./
DATA CONE,BE/1.3682E-05,2.5/
DATA RC/3.88,-1.84,3.81,-3.60/
DATA RD/-6.,-5.,-4.,-3.,-2.,-1.,0.,1./
DATA EE/.25283E11,.63209E11,.12956E12,.32257E12,.35229E12,
.41705E12,.62957E12,.14559E13,.21642E13,.38892E13,
.19867E11,.61743E11,.91757E11,.26456E12,.34438E12,
.37620E12,.46088E12,.14023E13,.16849E13,.35347E13,
.17929E11,.59274E11,.78111E11,.17020E12,.32048E12,
.36100E12,.39943E12,.11419E13,.15911E13,.25865E13,
.17297E11,.50106E11,.73171E11,.11382E12,.23927E12,
.34053E12,.37661E12,.76269E12,.15455E13,.18866E13,
.17096E11,.38122E11,.69488E11,.91632E11,.15396E12,
.26769E12,.34899E12,.54795E12,.13349E13,.16991E13,
.17029E11,.31667E11,.60990E11,.82506E11,.11231E12,
.17552E12,.26803E12,.46423E12,.93725E12,.15049E13,
.17008E11,.29239E11,.49897E11,.73757E11,.94813E11,
.12591E12,.17786E12,.41944E12,.67395E12,.11089E13,

```


37	.16999E11..28444E11..43618E11..62874E11..82673E11,	G
38	.10344E12..13081E12..33367E12..56176E12..82046E12/	G
39	DATA GAM/.23810..16500..12310..08699..09805..10170..09126..09393,	G
40	.10820..10510..29410..16840..15910..09635..09939..10840,	G
41	.16310..09495..12510..10960..32210..17310..18070..12510,	G
42	.10290..11120..11780..10160..12940..12730..33260..19500,	G
43	.19000..16500..11980..11440..12210..11910..13080..15130,	G
44	.33610..23980..19670..19380..15670..12890..12680..13980,	G
45	.13620..15940..33750..27800..21350..20870..19440..16390,	G
46	.14390..15300..15310..16500..33760..29670..24470..22290,	G
47	.21780..20280..18080..16080..17510..17810..33770..30360,	G
48	.26940..24490..23500..22860..21760..17640..18980..19500/	G
49	DATA EEO,ALDO/7.55154E+09,-2.888637,	G
50	DO 7 J=J1,J2	G
51	IF (E(J)-EEO) 1,1,2	G
52	1 CI(J)=CVGI(M)	G
53	T(J)=CI(J)*E(J)	G
54	GAMD(J)=GAMI(M)	G
55	CS(J)=SORT(GAMC(M)*E(J))	G
56	GO TO 7	G
57	2 RDL=ALOG10(D(J))-ALDO	G
58	DO 3 K=2,8	G
59	IF (RD(K)-RDL) 3,4,4	G
60	3 CONTINUE	G
61	4 RM=RD(K)-RDL	G
62	BP=1.-RM	G
63	EP=EEO	G
64	DO 5 I=1,10	G
65	EM=EP	G
66	EP=RM*EF(I,K-1)+BP*EE(I,K)	G
67	IF (EP-E(J)) 5,6,6	G
68	5 CONTINUE	G
69	6 CI(J)=DTT(I)/(EP-EM)	G
70	AM=(EP-F(J))/(EP-EM)	G
71	AP=1.-AM	G
72	T(J)=TT(I)-DTT(I)*AM	G

```

GAMD(J)=AP*BP*GAM(I,K)+AP*BM*GAM(I,K-1)+AM*BP*GAM(I-1,K)+AM*BM*
      GAM(I-1,K-1)
      CS(J)=SORT(GAMD(J)*(1.+GAMD(J))*E(J))
7 CONTINUE
      IF (CHIO(M)) 14,14,8
      R DO 13 J=J1,J2
      IF (T(J)-TCO) 9,9,10
      CHI(J)=CHIO(M)*T(J)**BETA(M)
      BET(J)=BETA(M)
      GO TO 13
10 DO 11 K=1,4
      IF (T(J)-TC(K)) 12,12,11
11 CONTINUE
      CHI(J)=CONE*SQRT(T(J))*T(J)**2
      BET(J)=BE
      GO TO 13
12 AM=(TC(K)-T(J))*DTCI(K)
      CHI(J)=AM*COND(K)+(1.-AM)*COND(K+1)
      BET(J)=BC(K)
13 CONTINUE
14 RETURN
      END

```

G 73
 G 74
 G 75
 G 76
 G 77
 G 78
 G 79
 G 80
 G 81
 G 82
 G 83
 G 84
 G 85
 G 86
 G 87
 G 88
 G 89
 G 90
 G 91
 G 92
 G 93
 G 94

```

SUBROUTINE START
COMMON /RVAR/ R(512),P(512),Q(512),U(512),D(512),E(512),7(512),
PE(512),EE(512),TE(512),ANE(512),FM(512),CS(512)
COMMON /RMAS/ ZM(512),ZMH(512),RNH(512),RA(512),RANH(512)
COMMON /MPROP/ PH(512),GAMD(512),CHI(512),BET(512),CI(512)
COMMON /PMAT/ THIK(4),RAT(4),DV(4),RHO1(4),RHO(4),GRUN(4),HUGC(4),
HUGD(4),HUGS(4),GAM1(4),ESUB(4),ERAT(4),GAMC(4),AMWT(4),
CHIO(4),BETA(4),AMU(4),AEX(4),ACL(4),AEXO(4),TOE(4),TVAP(4),
CVS(4),CVG(4),CVSI(4),CVGI(4),VIONE(4),VIONK(4),SIGIE(4),
SIGIK(4),VIBOE(4),VIBOK(4),VIRWE(4),VIBWK(4),VHNUE(4),
HNUSQ(4),SIGV(4),SEO(4),SEC(4),WFUNE(4),WFUNK(4),DNM(4)
COMMON /MPAR/ NMAT,MMOD(7),JBND(4),IZT(4),NZ(4)
COMMON /JPAP/ JOR,JORP,JACM,JAC,JACP,JTMAX,IALPM,JTSTAB,JTACC,
JTEDP,JSR
COMMON /NTIME/ NCYCS,N,NELOP,NEL,NEDIT,LINE,LINMX,NTAPE,NPRIN,
IPRIN,JINT,JMIN,JMAX,NTED,KTAPE,NETP
COMMON /CTIME/ TSTOP,TIME,DTN,DTNH,DTNHS,DTSTAB,DTACC,DTEDP,ALPHA,
TMAX,TEMP,PRES,EINTI,EDPT,EDP,SOS
COMMON /NAME/ IDT(12),MATN(8)
COMMON /LASER/ POW,WL,WF,CRI TE,EC
COMMON /EPAR/ ACPAD,REC,SIGO,SIGC,DIFI,ATIE,ALO,AKBT,AKB,GAME,
FNEL,NEPRN
COMMON /EDTIME/ TEDIT,REDIT,DTEDT
DATA AO,C,RMC2,RE,ALPHA1,PI/6.02252E+23,2.997925E+10,0.511006E+06,
2.81777E-13,137.0388,3.1415927/
DATA AKB,GAME,RATM,SIGO/1.3806E-16,0.66666667,1836.,11.346/
DATA AODEG,CTEV,TO,ATM/8.3143E+07,11605.7,277.144,1.01325E+06/
DATA ABOHR,RYD/0.52967E-08,13.605/
READ INPUT PARAMETERS **
READ 39, (IDT(I),I=1,12)
READ 40, NCYCS,NMAT,IALPH,NEDIT,LINMX,INPUT,NELOP,NEPRN
READ 40, NTAPE,NPRIN,IPRIN,JINT,JMIN,JMAX
READ 41, TSTOP,DTMIN,TEDIT,REDIT,DTEDT,TMAX,RTMAX
LINMX=MAX0(LINMX,30)
JMIN=MAX0(JMIN,1)
FNEL=4.1/FLOAT(NELOP)

```

C


```

12 J1=JOR+1
   JOR=JOR+NZ(M)-1
   IF (RAT(M)-1.0) 13,14,13
13 DV(M)=(V2-V1)*(RAT(M)-1.)/(RAT(M)*NZ(M)-1.)
   GO TO 15
14 DV(M)=(V2-V1)/FLOAT(NZ(M))
15 DVV=DV(M)
   VR=V1
   DO 16 J=J1,JOR
   VR=VR+DVV
   R(J)=VR*ALP1Z
   RNH(J)=R(J)+R(J)
   RA(J)=R(J)*IALPM
   RANH(J)=RA(J)+RA(J)
16 DVV=DVV+RAT(M)
   JOR=JOR+1
   JBND(M)=JOR
   R(JOR)=R2
   RNH(JOR)=R(JOR)+R(JOR)
   RA(JOR)=R(JOR)*IALPM
17 RANH(JOR)=RA(JOR)+RA(JOR)
   JORP=JOR+1
   VR=V2+DVV+RAT(M)
   R(JORP)=VR*ALP1Z
   RNH(JORP)=R(JORP)+R(JORP)
   RA(JORP)=R(JORP)*IALPM
   RANH(JORP)=RA(JORP)+RA(JORP)
   DO 18 J=J1,JORP
   IF (R(J)-RTMAX) 18,19,19
18 CONTINUE
19 JTMAX=J
C COMPUTE ELECTRON SCATTERING AND ABSORPTION COEFFICIENTS **
RO=RYD*CTEV
ACPA0=2.*C*PI*ABOHR**2/(ALPHA1*SQRT(PI*RO))
HEC=4.*ABOHR**3*PI*RO*SQRT(PI*RO)
SIGC=2.*RO**2

```

```

73 H
74 H
75 H
76 H
77 H
78 H
79 H
80 H
81 H
82 H
83 H
84 H
85 H
86 H
87 H
88 H
89 H
90 H
91 H
92 H
93 H
94 H
95 H
96 H
97 H
98 H
99 H
100 H
101 H
102 H
103 H
104 H
105 H
106 H
107 H
108 H

```

```

DIFI=RO*(ALPHAI/C)**2
AKBT=AKB/GAME
ATIE=0.125*C/(ALPHAI*ABOHR*(RO*PI*ABOHR)**2)
ATIE=ALOG(ATIE)
ALO=-ALOG(32.*PI*(ABOHR*RO)**3/9.)
WF=2.*PI*C/WL
CRITE=(WF*ALPHAI/C)**2/(4.*PI*ABOHR)
EC=RE*WL**2/(PI*C)
J2=0
M=0
READ MATERIAL PROPERTIES **
20 M=M+1
M2=2*M
M1=M2-1
READ 42, MATN(M), MATN(M2), MMOD(M), RHO(M), GAM1(M), AMWT(M), VIONE(M),
, SIGIE(M)
, READ 41, CHIO(M), RETA(M), ACL(M), AEXO(M), VIBOE(M), VIBWE(M), VHNUE(M),
, SIGV(M)
, VIONK(M)=VIONE(M)*CTEV
SIGIK(M)=SIGIE(M)/CTEV
VIBOK(M)=VIBOE(M)*CTEV
VIBWK(M)=VIBWE(M)*CTEV
HNUSQ(M)=(VHNUE(M)*CTEV)**2
SEO(M)=0.5*SIGN/(RATM*AMWT(M))
SEC(M)=2.*SIGC/(RATM*AMWT(M))
DNM(M)=AO/AMWT(M)
CVG(M)=AODEG/(AMWT(M)*GAM1(M))
CVGI(M)=1./CVG(M)
IF (MMOD(M)) 21,21,22
21 GAMC(M)=GAM1(M)*(GAM1(M)+1.)
CVS(M)=CVG(M)
GRUN(M)=GAM1(M)
EJ=CVG(M)*TEMP
RHO1(M)=PRES/(GRUN(M)*CVG(M)*TEMP)
GO TO 23
22 READ 41, GRUN(M), HUGC(M), HUGD(M), HUGS(M), ESUB(M), CVS(M), TVAP(M),

```

109
110
111
112
113
114
115
116
117
118
119
120
121
122
123
124
125
126
127
128
129
130
131
132
133
134
135
136
137
138
139
140
141
142
143
144


```

      WFUNK(M)=CTEV*WFUNE(M)
      ERAT(M)=HUGC(M)/(GRUN(M)*ESUB(M)*RHO(M))
      EJ=ATM/(GRUN(M)*RHO(M))
      TOE(M)=TO-EJ/CVS(M)
      EJ=CVS(M)*(TEMP-TOE(M))
      RHO1(M)=RHO(M)*(HUGC(M)*PRES)/(HUGC(M)*GRUN(M)*RHO(M)*EJ)
23  AEX(M)=AEX0(M)+1.
      AMU(M)=ACL(M)/RHO(M)*AEX(M)
      CVSI(M)=1./CVS(M)
      CHIJ=CHIO(M)*TEMP*BETA(M)
      SET INITIAL VALUES INTO MESH **
      J1=J2+1
      J2=JBND(M)*M/NMAT
      DO 24 J=J1,J2
        D(J)=RHO1(M)
        E(J)=EJ
        T(J)=TEMP
        TE(J)=TEMP
        CHI(J)=CHIJ
        CI(J)=CVSI(M)
        GAMD(J)=GRUN(M)
        BET(J)=BETA(M)
24  IF (M-NMAT) 20,25,25
25  JAC=JOR
      CALL EQST
      J2=1
      DO 26 M=1,NMAT
        J1=J2+1
        J2=JBND(M)*M/NMAT
        DO 26 J=J1,J2
          P(J)=PH(J)*GAMD(J)*E(J)
          GAMD(J)=GRUN(M)
          ZM(J)=ALPHI*RHO1(M)*(RA(J)*R(J)-RA(J-1)*R(J-1))
26  ZMHI(J-1)=1./(ZM(J-1)+ZM(J))
          P(1)=P(2)

```

C

```

P(JORP)=P(JOR)
DTNH=DTMIN
DTN=DTMIN
DTNHS=DTMIN
JACH=JBND(1)
JAC=JACH+1
JACP=JAC+1
DETERMINE SURFACE OF SOLID PARTICLE **
J2=1
DO 27 M=1,NMAT
  J1=J2+1
  J2=JBND(M)
  DO 27 J=J1,J2
    IF (E(J)-ESUB(M)) 27,27,28
27 CONTINUE
28 JSR=J-1
28 COMPUTE INITIAL INTERNAL ENERGY **
SOS=0.
EDPT=0.
EINTI=0.
DO 29 J=2,JOR
  EINTI=EINTI+E(J)*ZM(J)
  GO TO 35
29 READ INPUT FROM TAPE **
30 DO 34 IN=1,INPUT
  READ (8) (IDT(I),I=1,20),KTAPE,JOR,JORP,JACH,JAC,JACP,JTMAX,JSR,
.   IALPM,NMAT,(MMOD(J),J=1,19),ALPHA,TMAX,TEMP,PRES,EINTI,
.   EDPT,POW,WL,WFCRITE,ACPAO,REC,SIGC,DIFI,ATIE,ALO,AKBT,
.   (THIK(K),K=1,168)
  IF (KTAPE-1) 33,33,31
31 KDO=KTAPE-1
  DO 32 K=1,KDO
32 READ (8) TIME,DTNHS
33 READ (8) TIME,DTNHS,DTNH,N,JORP,(R(J),P(J),Q(J),U(J),D(J),E(J),
.   T(J),PE(J),EE(J),TE(J),ANE(J),FM(J),CS(J),J=1,JORP)
34 READ (8) DTN,DTNH,(PH(J),GAMD(J),CHI(J),BET(J),CI(J),ZM(J),ZMHI(J)

```

```

181 H
182 H
183 H
184 H
185 H
186 H
187 H
188 H
189 H
190 H
191 H
192 H
193 H
194 H
195 H
196 H
197 H
198 H
199 H
200 H
201 H
202 H
203 H
204 H
205 H
206 H
207 H
208 H
209 H
210 H
211 H
212 H
213 H
214 H
215 H
216 H

```

```

      ,RNH(J),RA(J),RANH(J),J=1,JORP)
      REWIND 8
      POWW=POW*1.E-07
      WLM=W*1.E-04
      PRESA=PRES/ATM
      NCYCS=N*NCYCS
      PRINT INPUT PARAMETERS **
35  PRINT 48, (IDT(I),I=1,12)
      PRINT 49
      PRINT 44, NCYCS,NMAT,IALPH,NEOIT,LINMX,INPUT,NELOP,NEPRN
      PRINT 50
      PRINT 44, NTAPE,NPRIN,IPRIN,JINT,JMIN,JMAX
      PRINT 51
      PRINT 45, TSTOP,DTMIN,TEOIT,REDIT,DTEDI,TMAX,RTMAX
      PRINT 52
      PRINT 45, POWW,WLM,TEMP,PRESA
      PRINT 53
      PRINT 54
      DO 36 M=1,NMAT
36  PRINT 46, M,IZT(M),NZ(M),THIK(M),RAT(M),DV(M)
      DO 38 M=1,NMAT
      M2=2*M
      M1=M2-1
      PRINT 47
      PRINT 55, MATN(M1),MATN(M2),MMOD(M)
      PRINT 56
      PRINT 45, RHO(M),GAM1(M),AMWT(M),CHIO(M),BETA(M),ACL(M),AEXO(M)
      PRINT 58
      PRINT 45, VIONE(M),SIGIE(M),VIBOE(M),VIBWE(M),VHNUE(M),SIGV(M)
      IF (MMOD(M)) 38,38,37
37  PRINT 57
      PRINT 45, GRUN(M),HUGC(M),HUGD(M),HUGS(M),ESUB(M),ERAT(M),CVS(M),
      TVAP(M),WFUNE(M)
38  CONTINUE
      WRITE (9) (IDT(I),I=1,12),POW,WLM,TEMP,PRES,JOR
      RETURN

```

```

39 FORMAT (12A5)
40 FORMAT (8I10)
41 FORMAT (8E10.4)
42 FORMAT (2A5,I10,6E10.4)
43 FORMAT (2I10,7E10.4)
44 FORMAT (18,10I12)
45 FORMAT (10E12.3)
46 FORMAT (18,2I12,4X,8E12.3)
47 FORMAT (///)
48 FORMAT (1M1,3X,12A5,/)
49 FORMAT (/,.4X,6H NCYCS,7X,5H NMAT,6X,6H IALPH,6X,6H NEDIT,6X,
        6H LINMX,6X,6H INPUT,6X,6H NELOP,6X,6H NERPNI)
50 FORMAT (/,.4X,6H NTAPE,6X,6H NPRIN,6X,6H IPRIN,6X,5H JINT,7X,
        5H JMIN,7X,5H JMAX)
51 FORMAT (/,.4X,6H TSTOP,6X,6H DTMIN,6X,6H TEDIT,6X,6H REDIT,6X,
        6H DTEDT,7X,5H TMAX,6X,6H RTMAX)
52 FORMAT (/,.5X,4H POW,8X,3H WL,8X,5H TEMP,7X,5H PRES)
53 FORMAT (///,4X,48H ZONING DETERMINED BY RADIUS AND NUMBER OF ZONES)
54 FORMAT (/,.6X,2H M,9X,4H IZT,8X,3H NZ,8X,5H THIK,8X,4H RAT,11X,
        2MDV)
55 FORMAT (4X,25H MATERIAL PROPERTIES FOR ,2A5,8X,7H MMOD =,I2)
56 FORMAT (/,.5X,4H RHO,7X,5H GAM1,7X,5H AMWT,7X,5H CHIO,7X,5H BETA,
        8X,4H ACL,8X,4H AEX)
57 FORMAT (/,.4X,5H GRUN,7X,5H HUGC,7X,5H HUGD,7X,5H HUGS,7X,5H ESUB,
        7X,5H ERAT,8X,4H CVS,7X,5H TVAP,7X,5H WFUN)
58 FORMAT (/,.4X,5H VION,7X,5H SIGI,7X,5H VI80,7X,5H VIBW,7X,5H VHNU,
        7X,5H SIGV)
        . END

```

```

253 H
254 H
255 H
256 H
257 H
258 H
259 H
260 H
261 H
262 H
263 H
264 H
265 H
266 H
267 H
268 H
269 H
270 H
271 H
272 H
273 H
274 H
275 H
276 H
277 H
278 H
279 H
280 H

```



```

6 EINT=EINT+(E(J)+EE(J))*ZM(J)
7 PMV=U(J)*(ZM(J)+ZM(J+1))
7 EGIN=EGIN+U(J)*PMV
8 IF (JAC-JOR) 8,10,10
8 DO 9 J=JACP,JOR
9 EINT=EINT+E(J)*ZM(J)
10 PMVNEG=0.5*PMVNEG
10 PMVPOS=0.5*PMVPOS
EGIN=0.25*FKIN
ENEW=EGIN+EINT-EINTI
IF (VOL) 12,12,11
11 ANAVG=ANAVG/VOL
12 PRINT 19
12 PRINT 16, N,JAC,JTSTAB,JTACC,JTEDP,JPMAX,NEL,JNMAX,EDP,EKIN,ENEW
PRINT 20
PRINT 17, TIME,DTNH,DTSTAB,DTACC,DTEDP,PMAX,SOS,ANMAX,ANAVG,EINT,
. EDP
LINE=LINE+6
IF (LINMX-LINE) 13,14,13
13 PRINT 18
14 LINE=6
15 RETURN
16 FORMAT (18,7I12,4X,3E12.3)
17 FORMAT (11E12.3,/)
18 FORMAT (1H)
19 FORMAT (/,6X,2H N,8X,4H JAC,7X,7H JTSTAB,6X,6H JTACC,6X,6H JTEDP,
. 6X,6H JPMAX,6X,4H NEL,6X,6H JNMAX,5X,7H EDP,7X,
. 5H EGIN,7X,5H ENEW)
20 FORMAT (4X,5H TIME,7X,5H DTNH,6X,7H DTSTAB,6X,6H DTACC,6X,
. 6H DTEDP,7X,5H PMAX,7X,5H SOS,6X,6H ANMAX,5X,7H ANAVG,7X,
. 5H EINT,7X,5H EDP)
. END

```

```

37 I
38 I
39 I
40 I
41 I
42 I
43 I
44 I
45 I
46 I
47 I
48 I
49 I
50 I
51 I
52 I
53 I
54 I
55 I
56 I
57 I
58 I
59 I
60 I
61 I
62 I
63 I
64 I
65 I
66 I
67 I
68 I

```



```

1 SUBROUTINE FINED
2 COMMON /RVAR/ R(512),P(512),Q(512),U(512),O(512),E(512),T(512),
3 PE(512),EE(512),TE(512),ANE(512),FM(512),CS(512)
4 COMMON /RMAS/ ZM(512),ZMHI(512),RNH(512),RA(512),RANH(512)
5 COMMON /MPROP/ PH(512),GAMD(512),CHI(512),BET(512),CI(512)
6 COMMON /PMAT/ THIK(4),RAT(4),DV(4),PHOI(4),RHO(4),GRUN(4),HUGC(4),
7 HUGD(4),HUGS(4),GAM1(4),ESUB(4),ERAT(4),GAMC(4),AMWT(4),
8 CHIO(4),BETA(4),AMU(4),AEX(4),ACL(4),AEXO(4),TOE(4),TVAP(4),
9 CVS(4),CVG(4),CVSI(4),CVGI(4),VIONE(4),VIONK(4),SIGIE(4),
10 SIGIK(4),VIBOE(4),VIBOK(4),VIRWE(4),VIRWK(4),VHNUE(4),
11 HNUSQ(4),SIGV(4),SEO(4),SEC(4),WFUNE(4),WFUNK(4),DNM(4)
12 COMMON /MPAR/ NMAT,MMOD(7),JBND(4),IZT(4),NZ(4)
13 COMMON /JPAP/ JOR,JORP,JACH,JACP,JTMAX,IALPM,JTSTAB,JTACC,
14 JTEDP,JSR
15 COMMON /N/IME/ NCYCS,N,NELOP,NEL,NEDIT,LINE,LINMX,NTAPE,NPRIN,
16 IPRIN,JINT,JMIN,JMAX,NTED,KTAPE,NETP
17 COMMON /CTIME/ TSTOP,TIME,DTN,DTNH,DTNHS,DTSTAB,DTACC,DTEDP,ALPHA,
18 TMAX,TEMP,PRES,EINTI,EDPT,EDP,SOS
19 COMMON /NAME/ IDT(12),MATN(8)
20 COMMON /LASER/ POW,WL,WF,CRITE,EC
21 COMMON /EPAR/ ACPAO,REC,SIGO,SIGC,DIFI,ATIE,ALO,AKBT,AKB,GAME,
22 FNEL,NEPRN
23 DIMENSION A(121)
24 DATA AMICRN,BARI,HLANK,DASH,PLUS/1.E+04,1.E-06,1H,1H-,1H+/
25 DATA SMP,SMU,SMT,SMN,KP,KU,KT,KN/1HP,1HU,1HT,1HN,61,61,1,1/
26 DATA SME/1HE/
27 IF (NTAPE) 1,2,1
28 1 WRITE (8,64) (IDT(I),I=1,20),KTAPE,JOR,JORP,JACH,JACP,JTMAX,
29 JSR,IALPM,NMAT,(MMOD(J),J=1,19),ALPHA,TMAX,TEMP,PRES,EINTI,
30 EDPT,POW,WL,WF,CRITE,ACPAO,REC,SIGC,DIFI,ATIE,ALO,AKBT,
31 (THIK(K),K=1,168)
32 2 NEPR=0
33 IF (NPRIN) 3,5,4
34 3 NEPR=NTED
35 GO TO 5
36 4 NEPR=1

```

```

5 READ (9) (IDT(I),I=1,12),POW,WL,TEMP,PRES,JOR
  IF (JINT) 7,7,6
6 JLIN=2+(JMAX-JMIN-1)/JINT
  JLIN=(JLIN-1)/6
  JLIN=7+6*JLIN
  JIN=JINT
7 DO 56 NE=1,NTED
  READ (9) TIME,DTNHS,DTNH,N,JAC,(R(J),P(J),Q(J),U(J),D(J),E(J),T(J),
    .PE(J),EE(J),TE(J),ANE(J),FM(J),CS(J),J=1,JAC)
    FM(J)=FM(J)/DTNH
    P(J)=P(J)+Q(J)
    IF (JINT) 8,8,11
8 IF (N) 1,10,9
9 JMAX=MAX0(JMAX,JAC)
10 JIN=1+(JMAX-JMIN)/54
  JLIN=2+(JMAX-JMIN-1)/JIN
  JLIN=(JLIN-1)/6
  JLIN=7+6*JLIN
11 IF (IPRIN-1) 12,12,55
12 PRINT 59, TIME,DTNHS,N,NE,(IDT(I),I=1,12)
  JSIX=1
  J=JMIN
  DO 54 JL=1,JLIN
  IF (JSIX-JL) 15,13,15
13 DO 14 K=1,11,10
  A(K)=PLUS
  DO 14 L=1,9
  A(K+L)=DASH
  A(121)=PLUS
15 IF (J-JOR) 17,17,16
16 RJ=0.
  GO TO 4R
17 PA=RAHI*ABS(P(J))
  IF (PA-1.12) 18,18,19
18 LP=KP
  GO TO 22

```

```

19 PB=10.*ALOG10(PA)+0.5
   L=INT(PR)
   IF (P(J)) 20,20,21
20 LP=KP-L
   GO TO 22
21 LP=KP+L
22 IF (T(J)-100.) 23,24,24
23 LT=KT
   GO TO 25
24 TB=20.*ALOG10(T(J))-39.5
   LT=KT+INT(TB)
25 UA=ABS(U(J))
   IF (UA-1.06) 26,27,27
26 LU=KU
   GO TO 30
27 UB=10.*ALOG10(UA)+0.5
   L=INT(UB)
   IF (U(J)) 28,28,29
28 LU=KU-L
   GO TO 30
29 LU=KU+L
30 IF (ANE(J)-1.25) 31,31,32
31 LN=KN
   GO TO 33
32 ANB=5.*ALOG10(ANE(J))+0.5
   LN=KN+INT(ANB)
33 IF (TE(J)-100.) 34,35,35
34 LE=KT
   GO TO 36
35 EB=20.*ALOG10(TE(J))-39.5
   LE=KT+INT(EB)
36 IF (LP-LT) 38,37,38
37 LT=LT+1
38 IF (LU-LP) 42,39,42
39 IF (LU+1-LT) 41,40,41
40 LU=LU-1

```

```

73
74
75
76
77
78
79
80
81
82
83
84
85
86
87
88
89
90
91
92
93
94
95
96
97
98
99
100
101
102
103
104
105
106
107
108

```

```

GO TO 46
41 LU=LU+1
GO TO 46
42 IF (LU-LT) 46,43,46
43 IF (LU-1-LP) 44,45,44
44 LU=LU-1
GO TO 46
45 LU=LU+1
46 LU=MAX0(2,LU)
LP=MAX0(2,LP)
LT=MAX0(2,LT)
LN=MAX0(2,LN)
LE=MAX0(2,LE)
LU=MIN0(LU,120)
LP=MIN0(LP,120)
LT=MIN0(LT,120)
LN=MIN0(LN,120)
LE=MIN0(LE,120)
AE=A(LE)
AP=A(LP)
AT=A(LT)
AU=A(LU)
AN=A(LN)
A(LE)=SME
A(LP)=SMP
A(LT)=SMT
A(LU)=SMU
A(LN)=SMN
RJ=AMICRN*(R(J)
IF (RJ-100000.) 48,47,47
47 RJ=RJ-100000.
48 PRINT 61, J,(A(I),I=1,121),RJ
IF (JSIX-JL) 51,49,51
49 JSIX=JSIX+6
DO 50 K=1,111,10
A(K)=DASH

```

```

109
110
111
112
113
114
115
116
117
118
119
120
121
122
123
124
125
126
127
128
129
130
131
132
133
134
135
136
137
138
139
140
141
142
143
144

```

```

DO 50 L=1,9
50 A(K+L)=BLANK
   A(121)=DASH
   GO TO 54
51 IF (J-1) 54,54,52
52 IF (J-JOR) 53,53,54
53 A(LP)=AP
   A(LT)=AT
   A(LU)=AU
   A(LN)=AN
   A(LE)=AE
54 J=J+JIN
   PRINT 63, SMP
   IF (IPRIN-1) 55,56,55
   PRINT TABLE OF VALUES **
55 PRINT 59, TIME,DTNHS,N,NE,(IDT(I),I=1,12)
   PRINT 60
   PRINT 62, (J,R(J),P(J),PE(J),U(J),D(J),E(J),T(J),TE(J),EE(J),
     ANE(J),FM(J),J,J=JMIN,JMAX,JIN)
56 CONTINUE
   IF (NTAPE) 57,58,57
57 WRITE (8,64) DTN,DTNH,(PH(J),GAMD(J),CHI(J),BET(J),CI(J),ZM(J),
     ZMHI(J),RNH(J),RA(J),RANH(J),J=1,JORP)
58 REWIND 9
   RETURN
59 FORMAT (7H1TIME =,E10.4,2X,6H DTS =,E10.4,2X,4H N =,I4.3X,5H NE =,
     I3.3X,12A5,/)
60 FORMAT (2X,2H J,5X,2H R,9X,2H P,8X,3H PE,9X,2H U,9X,2H D,9X,2H E,
     9X,2H T,8X,3H TE,8X,3H EE,8X,4H ANE,7X,3H FM,8X,2H J,/)
61 FORMAT (I4,12I1A1,F7,1)
62 FORMAT (I4,11E11.4,I6)
63 FORMAT (3X,2H 6.8X,2H 5.8X,2H 4.8X,2H 3.8X,2H 2.8X,2H 1.8X,2H 0.
     8X,2H 1.8X,2H 2.8X,2H 3.8X,2H 4.8X,2H 5.8X,2H 6.5H LOG(.A1,
     1H))
64 FORMAT (8A10)
   END

```

```

145 J
146 J
147 J
148 J
149 J
150 J
151 J
152 J
153 J
154 J
155 J
156 J
157 J
158 J
159 J
160 J
161 J
162 J
163 J
164 J
165 J
166 J
167 J
168 J
169 J
170 J
171 J
172 J
173 J
174 J
175 J
176 J
177 J
178 J
179 J
180 J

```

```

SUBROUTINE ZERO
COMMON /RVAR/ R(6656)
COMMON /GJHJ/ A(1536)
COMMON /RMAS/ Z(2560)
COMMON /MPROP/ PH(2560)
COMMON /FREQ/ C(1024)
COMMON /EQSF/ E(1024)
DO 1 J=1,6656
1 R(J)=0.
DO 2 J=1,1536
2 A(J)=0.
DO 3 J=1,2560
3 PH(J)=0.
DO 4 J=1,1024
4 C(J)=0.
DO 5 J=1,1024
5 E(J)=0.
RETURN
END

```

```

1 2 3 4 5 6 7 8 9 10 11 12 13 14 15 16 17 18 19
X X X X X X X X X X X X X X X X X X X X

```


APPENDIX II

AIR BREAKDOWN REDUCTION BY TRANSPARENT PARTICLES

The experimentally observed fact that particles of NaCl cause a reduction in the air breakdown threshold by an amount comparable to that of much more opaque materials is difficult to reconcile with a postulated mechanism that requires heating of the particle as an essential step since the heating rate in nearly transparent NaCl is relatively very slow. A lowering of the breakdown threshold occurs when the population of free electrons having kinetic energies above the nitrogen vibrational excitation region is large enough to ensure at least one or more of these is in the laser focal volume to initiate the cascade process. The mechanisms by which electrons can more easily overcome the barrier to energy growth presented by the nitrogen vibrational excitation region usually depend on an air temperature rise induced by the laser heated particle as a result of conduction, shock compression or radiative transfer. Such a temperature rise increases the free electron density and with it the probability an electron will overcome the barrier. In addition, it makes it easier for electrons to thermalize over the barrier, and shifts the balance of energy loss to gain rates in the direction favoring easier breakdown. Without heating, however, these mechanisms are inoperative.

Another mechanism which could allow electrons to overcome this energy barrier without heating could be the result of the presence of a relatively high density of very low-energy electrons in at least a small region close to the surface of the particle. These electrons might be the result of thermionic emission at the particle surface, perhaps consisting of a cloud extending outward no more than the order of a Debye length. Whatever the source of these relatively numerous low-energy electrons, their presence could allow the energy barrier to be overcome as a result of electron-electron collisions alone without the necessity of air heating.

In order to investigate what magnitude of an effect electron-electron collisions might have on easing the penetration of the vibrational excitation barrier, it was necessary to compute electron energy distribution curves with and without electron-electron collisions, and to determine from these whether or not equivalent densities of electrons with energies above the barrier could occur at lower laser powers when electron-electron scattering was taken into account. Although a method for integrating the Boltzman equation directly taking into account electron-electron scattering was available to us (Ref. 40), it required considerable amounts of computer time per case to use. Instead a Monte Carlo method was chosen as a relatively direct approach employing a minimum of simplifying assumptions.

It turned out that, although this direct approach is reasonably effective in treating the case with no electron-electron scattering, it is quite inefficient for the electron-electron scattering case unless a number of more sophisticated Monte Carlo refinements are employed. Resources available to us in this study did not allow completion of incorporation of these refinements, and as a consequence this covers only the work which was done along with an indication of the direction further effort might take.

At the time the Monte Carlo approach was adapted, electron distribution curves had been computed by AFWL (Ref. 30) for the case of no electron-electron scattering utilizing a differencing technique. This technique was subsequently refined by AFWL to include electron-electron scattering effects (Ref. 16). It was hoped that by making comparisons the importance of some simplifying assumptions made in the AFWL approach could be evaluated since they were not made in the Monte Carlo approach. In particular, the differencing approach employed an average power input from the laser, and did not take into account the fact that electrons oscillate in the laser electric field only in the field direction. The kinetic energy of a 2 ev electron in a 10^9 watt/cm² laser field may actually range from 1.6 to 2.4 ev during a laser cycle when its initial velocity is aligned with the field. Interaction cross sections can vary significantly over this 0.8 ev energy range,

and this in turn could significantly influence the effectiveness of barrier penetration, and thus the shape of the electron energy distribution curves.

1. MONTE CARLO CALCULATION OF ELECTRON ENERGY DISTRIBUTIONS

In the application of the Monte Carlo technique, the straightforward approach of following the time history of a single electron starting at some initial kinetic energy was chosen. This electron was followed until it was lost by some process such as attachment, or until it caused an ionization event. After an ionization event, one of the resultant electrons was picked to follow further. The total time spent by the electron at each energy (in practice the time spent in one of the preselected energy intervals) was recorded. From this information, the energy distribution function was calculated.

The ergodic hypothesis assures the validity of this method of determining energy distributions for steady state distributions. It states that the time average for the properties of any system of interest equal the averages of those same properties for the members of the ensemble (Ref. 41). That is, any quantity, $A(p, q)$ will have a time average,

$$\bar{A} = \lim_{T \rightarrow \infty} \frac{1}{T} \int_0^T A(p(t), q(t)) dt \quad (177)$$

and an ensemble average

$$\langle A \rangle = \int A(p, q) f(p, q) dp dq \quad (178)$$

where $f(p, q)$ = the distribution function

$p(t) \equiv p(p_0, q_0, t)$, momentum coordinates

$q(t) \equiv q(p_0, q_0, t)$, position coordinates

the ergodic hypothesis guarantees the ultimate equality of these two average values, \bar{A} and $\langle A \rangle$ at sufficiently long times.

When the distribution is changing in time, these two average values are equal only if the time variation is slow compared with the time for the distribution function to relax to its quasi-equilibrium form. It will be assumed that this is true for the cases of interest here, although this assumption needs further verification at least in the late stages of breakdown, when electron-electron collisions, superelastic collisions, etc., are becoming increasingly important at a rapid rate.

If the quantity, A , is taken to be the electron kinetic energy, E , and if further the integrals are replaced with summations, these results are

$$\bar{E} = \lim_{T \rightarrow \infty} \sum_i E_i \left(\frac{\Delta t_i}{T} \right) \quad (179)$$

and

$$\langle E \rangle = \sum_i E_i f(E_i) \quad (180)$$

where Δt_i is the time spent by the electron in the i th energy bin represented by energy, E_i . The ergodic hypothesis states that $\bar{E} = \langle E \rangle$ for all ensembles. For this to be true for all arbitrary E_i requires from equations (179) and (180) that

$$f(E_i) = \lim_{T \rightarrow \infty} \left(\frac{\Delta t_i}{T} \right) \quad (181)$$

Equation (181) proves that the results of following one electron's history, as described above, gives asymptotically the energy distribution function desired. The statistical uncertainties in the distribution at any finite time are equivalent to those inherent in the corresponding Monte Carlo calculation.

In following the history of a single electron, its interactions with molecules were simulated. The reactions with air molecules considered were excitation of vibrational and ground to excited electronic states as well as elastic collisions. Oxygen attachment was also included. In the calculations done to date only the ground states were considered to be populated significantly, although no basic difficulty would be encountered in including excited states. Empirical cross-section data for the various interaction channels were obtained from the literature (Refs. 4, 5, 6, 7, 42 and 43). The specific interaction channel was chosen randomly in proportion to the corresponding cross section, and for the channel chosen the electron kinetic energy was reduced appropriately upon collision. A new random direction for the test electron velocity vector was picked after the collision on the assumption of isotropy.

a. Interaction of Electron with Laser Electric Field

The response of the electron to the oscillating electric field of the laser beam was treated classically. By the correspondence principal, this treatment is correct in the limit where the electron kinetic energy gained is large compared to a laser photon energy. The inverse bremsstrahlung absorption of energy by the electron upon scattering from another electron or the scattering of an electron from an ion charge center is correctly described classically in the many photon energy limit for the same reason. It has been shown that when the energy imparted by such a coulomb scattering is small compared to the photon energy, a classical treatment of the scattering also gives the correct answer, where energies of only a fraction of a single photon energy are interpreted as probabilities of there being a one photon energy transfer (Ref. 4). In the intermediate region multiple photon interactions become important and are hard to evaluate. It is assumed that the classical treatment is adequate in this range also.

During a single laser light cycle, the electrons oscillate while the neutral particles remain essentially stationary. Ions can be treated as stationary because of their relatively large mass. The temperature of interest are

low enough so that all particles except electrons can be assumed to have negligible translational velocity at all times. All electron energy distribution curves presented are specified only after removal of the kinetic energy of oscillation due to the electric field, or effectively when the field is turned off, to avoid ambiguity. A collision while the field is on randomizes the directed component of the electron velocity resulting from the oscillating field and thus thermalizes this part of the electron kinetic energy. The velocity of impact of an electron with another particle varies during a laser light cycle, and with it the impact energy and cross section for interaction.

From a classical point of view, the electric vector of the light in a polarized laser beam can be represented by

$$E = E_0 \cos(\omega t) \quad (182)$$

where t is time, and the frequency is given by

$$\omega = 2\pi c/\lambda \quad (183)$$

with c the velocity of light and λ the light wavelength. The peak electric field, E_0 , in volts/cm is related to the average power in the laser beam, P , in watts/cm² by

$$E_0^2 = 240\pi P \quad (184)$$

A free electron in this field has an induced velocity component given by

$$v_E = V_0 \sin(\omega t) \quad (185)$$

where

$$V_0 = \frac{eE_0}{\omega m_0} \quad (186)$$

and e the charge and m_0 the mass of an electron.

Combining equations (183) through (186) gives the numerical formula

$$V_0 = 25.66 \lambda \sqrt{P} \quad (187)$$

where V_0 is in cm/sec, λ in microns, and P in watts/cm².

The actual electron velocity is the vector sum of that due to thermal motion if the laser were off, \vec{v}_0 , and that caused by the field:

$$\vec{v} = \vec{v}_0 + \vec{v}_E \quad (188)$$

Neglecting the motion of all gas particles due to either temperature or laser field, the electron kinetic energy of impact with other gas particles is given simply by

$$W = \frac{1}{2} m_0 v^2 \quad (189)$$

where v is obtained from equation (188).

Using equations (187, 188 and 189), it can be shown that the maximum range of variation in kinetic energy of an electron oscillating in the laser field is

$$\Delta E = 0.6 \sqrt{P \times W} \quad (190)$$

where ΔE is in electron volts, P is in units of 10^9 watts/cm² and W is in ev.

b. Interaction of the Electron with another Particle

In an increment of time Δt , the electron may interact with a gas particle or another electron or not at all. If the time increment is chosen small enough so that during it the laser-induced velocity increment is negligible, then the electron kinetic energy may be taken as constant during this

time increment. For a given electron energy, the cross sections all-particle interaction channels are known. The probability the electron will survive a time, t , without collisions is given by the Poisson probability

$$p(t) = e^{-tv \sum_i \sigma_i n_i} \quad (191)$$

where the cross sections are σ_i for a number/volume, n_i , of interaction targets of type i .

In the increment of time, Δt , the probability of a collision is from equation (191)

$$\Delta p = 1 - e^{-\Delta t v \sum_i \sigma_i n_i} \quad (192)$$

If the time interval is chosen so

$$\Delta t v \sum_i \sigma_i n_i \ll 1 \quad (193)$$

then equation (192) can be approximated as

$$\Delta p \cong \Delta t v \sum_i \sigma_i n_i \quad (194)$$

Equation (194) may be used to choose an interaction channel in the Monte Carlo calculation as follows. A random number, R , is chosen between 0 and 1.

$$0 < R < 1 \quad (195)$$

The quantity

$$q_m = \Delta t v \sum_{i=1}^m \sigma_i n_i \quad (196)$$

is computed for successive values of m and for each value q_m is compared with R . If for any m it is found that

$$q_m > R \quad (197)$$

then the electron is chosen to interact in channel m during Δt . If after summing over all channels the inequality of equation (197) is not satisfied, the electron is chosen to not interact in this particular time interval. For this method to be valid, it is necessary that the time step, Δt , meet condition (193).

The electron-electron scattering cross section must be included in evaluating the condition (193). For this purpose, it will be assumed no interaction occurs beyond the Debye shielding distance given by (Ref. 44)

$$h = \sqrt{\frac{kT}{4\pi m_e e^2}} = K \sqrt{\frac{T}{n_e}} \quad (198)$$

where n_e is the volume density of electrons, and e the electronic charge. For T in deg kelvin and n_e in cm^{-3} , $K = 6.90$ gives h in cm. The cross section for electron-electron interaction is thus

$$\sigma_e = \pi h^2 = \pi K^2 T / n_e \quad (199)$$

It is noteworthy that in the summation of equations (193) and (194) the product $q_i n_i$ for electrons from equation (199) is

$$\sigma_e n_e = \pi K^2 T \quad (200)$$

which is independent of electron density. Since the temperature, T , will not generally correspond to a Maxwellian distribution, in its place $\frac{2}{3}$ times the

average kinetic energy of the electron distribution was used.

If the restriction on-time interval imposed by equation (193) is much more severe than imposed by laser frequency, then it can be more efficient computationally to relax this condition by determining first whether there is any interaction at all by using the condition for there to be one that Δp from equation (194) exceed a random number, R . Only after the existence of interaction is established is a channel for it chosen.

c. Electron-Electron Scattering

In the event of an electron-electron scattering, a target electron must be picked from the distribution for the test electron to scatter from. The second electron energy cannot be simply selected in proportion to its frequency of occurrence in the distribution, because the thermal velocity is not small compared to that of the test electron.

The probability per unit time that the test electron with velocity, \vec{v}_1 , will pass within a Debye length of a target electron is given by

$$\frac{dP}{dt}(\vec{v}_1, \vec{v}_2) = \pi h^2 \int_0^{2\pi} d\theta \int_0^\pi d\varphi \sin\varphi n'(v_2, \theta, \varphi) |\vec{v}_1 - \vec{v}_2| \quad (201)$$

where $n'(v_2, \theta, \varphi)$ is the density of target electrons with velocity \vec{v}_2 and speed v_2 in a spherical coordinate system with polar angle, φ , and azimuth angle, θ . It will be assumed that the target electrons are isotropically distributed in velocity direction, or

$$n'(v_2, \theta, \varphi) = n(v_2)/4\pi \quad (202)$$

Consequently, equation (201) using (202) becomes

$$\frac{dP}{dt}(\vec{v}_1, v_2) = \frac{n(v_2) \pi h^2}{2} \int_0^\pi \sqrt{v_1^2 + v_2^2 - 2v_1 v_2 \cos \phi} \sin \phi d\phi \quad (203)$$

which gives taking into account the absolute value of the velocity difference in equation (201)

$$\frac{dP}{dt}(\vec{v}_1, v_2) = \frac{n(v_2) \pi h^2}{3} \left(3v_A + v_B^2/v_A \right) \quad (204)$$

where

$$v_A = \max(v_1, v_2)$$

$$v_B = \min(v_1, v_2)$$

The quantity $n(v_2)$ in equation (204) may be determined from the distribution function for target electron energies. Thus, for a given test electron velocity the modified distribution function implied by equation (204) may be used to correctly select a target electron speed, v_2 .

The direction of this target electron is assumed isotropically distributed. However, even though it is now determined that an interaction of the test electron will occur with a target of speed, v_2 , the probability the collision will occur depends upon the relative velocity of the two electrons. The velocity of the target electron may be randomly selected by first selecting a random number $0 < R < 1$. The cosine of the angle between the two electron velocities is then given by

$$\mu = \frac{v_1^2 + v_2^2 - \left[(1-R)(v_1+v_2)^3 + R|v_1-v_2|^3 \right]^{2/3}}{v_1 v_2} \quad (205)$$

The vector velocity of the target electron is then

$$\vec{v}_2 = v_2 \left[\left(\mu - \gamma\beta \frac{\vec{v}_1}{v_1} + \beta \hat{R} \right) \right] \quad (206)$$

where \hat{R} is a random unit vector and

$$\gamma \equiv \frac{v_1 \cdot \hat{R}}{v_1} \neq 1$$

and $\beta \equiv \sqrt{\frac{1 - \mu^2}{1 - \gamma^2}}$

The two electrons are now allowed to interact in a center of mass encounter and the new test electron energy and corresponding velocity having a random azimuth angle found and converted into the laboratory frame.

The velocities in the electron-electron center of mass system are

$$\begin{aligned} \vec{w}_1 &= (\vec{v}_1 - \vec{v}_2)/2 = \vec{w} \\ \vec{w}_2 &= -\vec{w} \end{aligned} \quad (207)$$

The angle of scattering in the cm system is found by picking a random number $0 < R < 1$, and finding the impact parameter, x , in terms of the Debye length, h , from

$$\pi x^2 = R\pi h^2 \quad (208)$$

and

$$x = h\sqrt{R}$$

The collision diameter is given by

$$b = e^2 / (m_0 W^2) = \left(\frac{e^2}{mc^2} \right) \left(\frac{c}{W} \right)^2 \quad (209)$$

The scattering angle, θ , is found from

$$\theta = 2 \tan^{-1} \left(\frac{b}{2x} \right) \quad (210)$$

Equation (210) using equation (209) gives

$$\cos \theta = \frac{4h^2 R - b^2}{4h^2 R + b^2} \quad (211)$$

in terms of the random number, R . The azimuth angle is still undetermined and can be picked at random as follows. Let \hat{R} be a randomly picked unit vector. If \hat{w} is a unit vector in the direction of \vec{w} , then the center of mass velocity, \vec{w}' , after scattering is given by

$$\vec{w}' = \left[\frac{\sin \theta \hat{R} + \frac{(\hat{w} \cdot \hat{R}) \hat{w}}{\sqrt{1 - (\hat{w} \cdot \hat{R})^2}} (\cos \theta) - \frac{\sin \theta (\hat{w} \cdot \hat{R}) \hat{w}}{\sqrt{1 - (\hat{w} \cdot \hat{R})^2}} \right] \quad (212)$$

Shifting back to the laboratory system, the velocity of the test electron after scattering is

$$\vec{v}'_1 = \frac{(\vec{v}_1 + \vec{v}_2)}{2} + \vec{w}' \quad (213)$$

From this velocity the electron kinetic energy after the electron-electron scattering even can be found using equation (189).

A computer program, Laser Ionization Rates by Single Electron Monte Carlo (LIRSEM), was written to carry out the calculations described above. It is described in Appendix III. It was used to compute electron energy distribution curves without electron-electron scattering. The results are shown for two laser powers for which calculations were also made by AFWL along with the AFWL results for comparison in figures 23 and 24. Results obtained for a number of other laser powers are shown in figure 25.

It can be seen in the comparison figures that the curves are similar in shape above a few electron volts in energy, but differ considerably at lower energies. There are three plausible reasons for the low-energy differences. One is that the energy bins used in the Monte Carlo (0.2 ev) were too coarse to provide adequate resolution at very low energies. Another is that the Monte Carlo maximum energy was at 20 ev. Any electron exceeding this energy was considered to have caused an ionization to occur. This could artificially lower the high-energy tail of the Monte Carlo curves and at the same time return too many electrons to the minimum energy bin thus distorting the distribution. A third possible reason is that the distributions really are different as a result of the approximations made in the AFWL calculations which are absent in the Monte Carlo.

Monte Carlo calculations were also made including the electron-electron scattering feature of the computer program. However, an error was subsequently found in the program. This resulted from assigning a random direction to the target electron after its speed had been found rather than using equations (205) and (206) to determine its velocity. Consequently, these results are in error, and are not reported here. The program described in Appendix III has not been corrected, but could be relatively easily for this omission. However, another more grave difficulty was also discovered which will take considerably more effort to correct. This difficulty concerns the efficiency of the Monte Carlo method when electron-electron scattering is included.

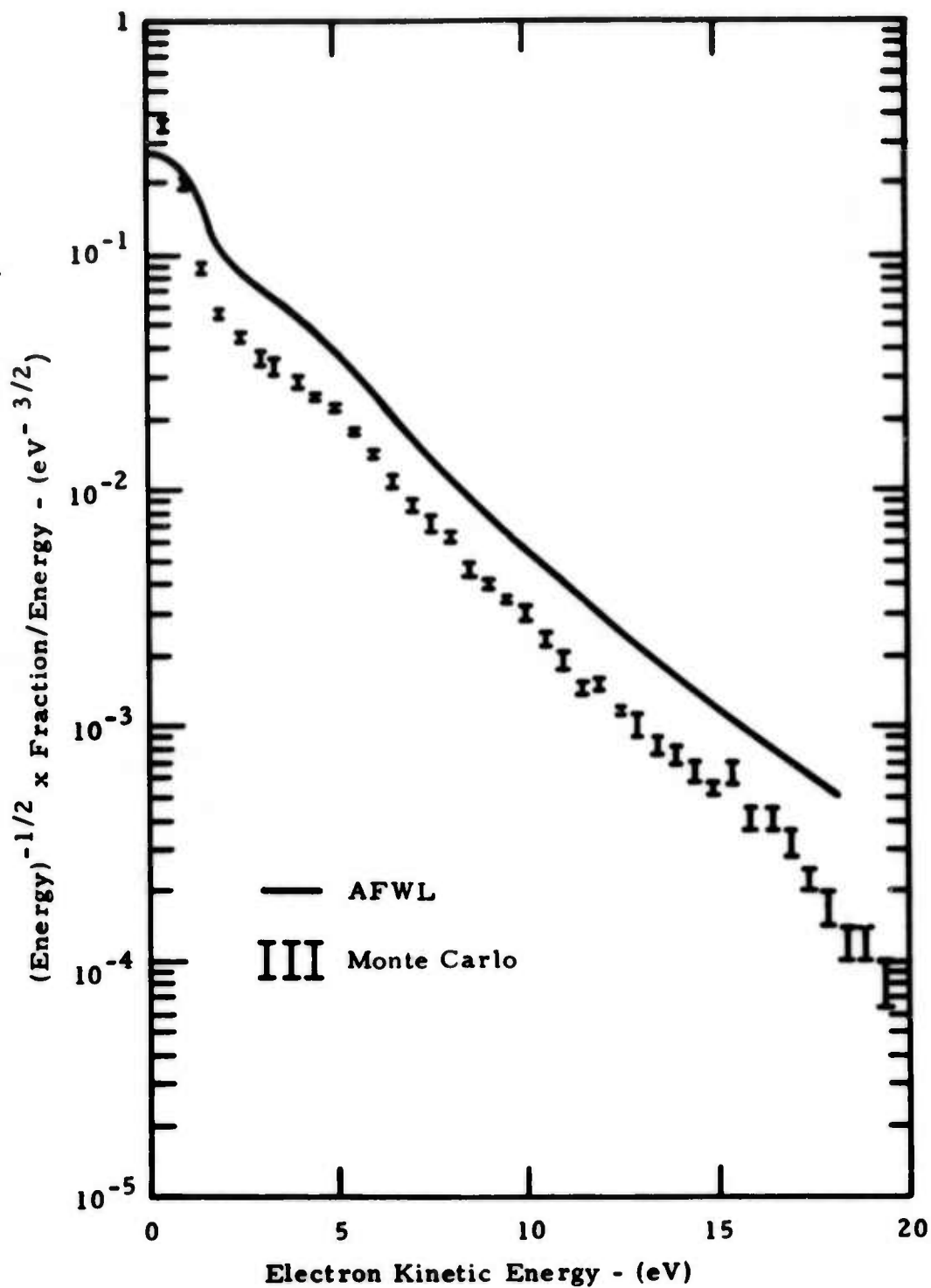


Figure 23. Comparison of electron energy distributions for laser power of 8×10^9 watts/cm²

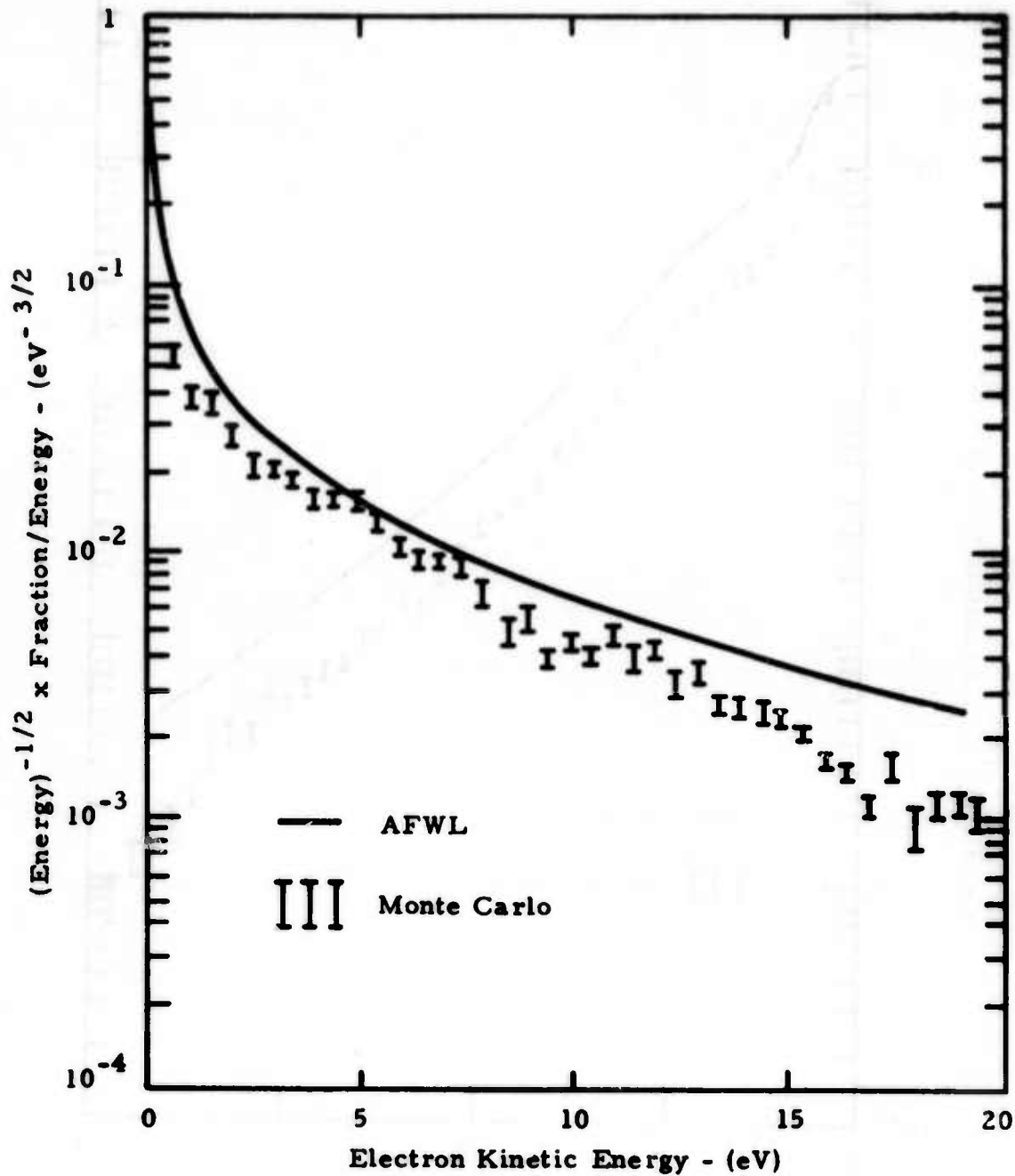


Figure 24. Comparison of electron energy distributions for laser power of 2×10^{11} watts/cm²

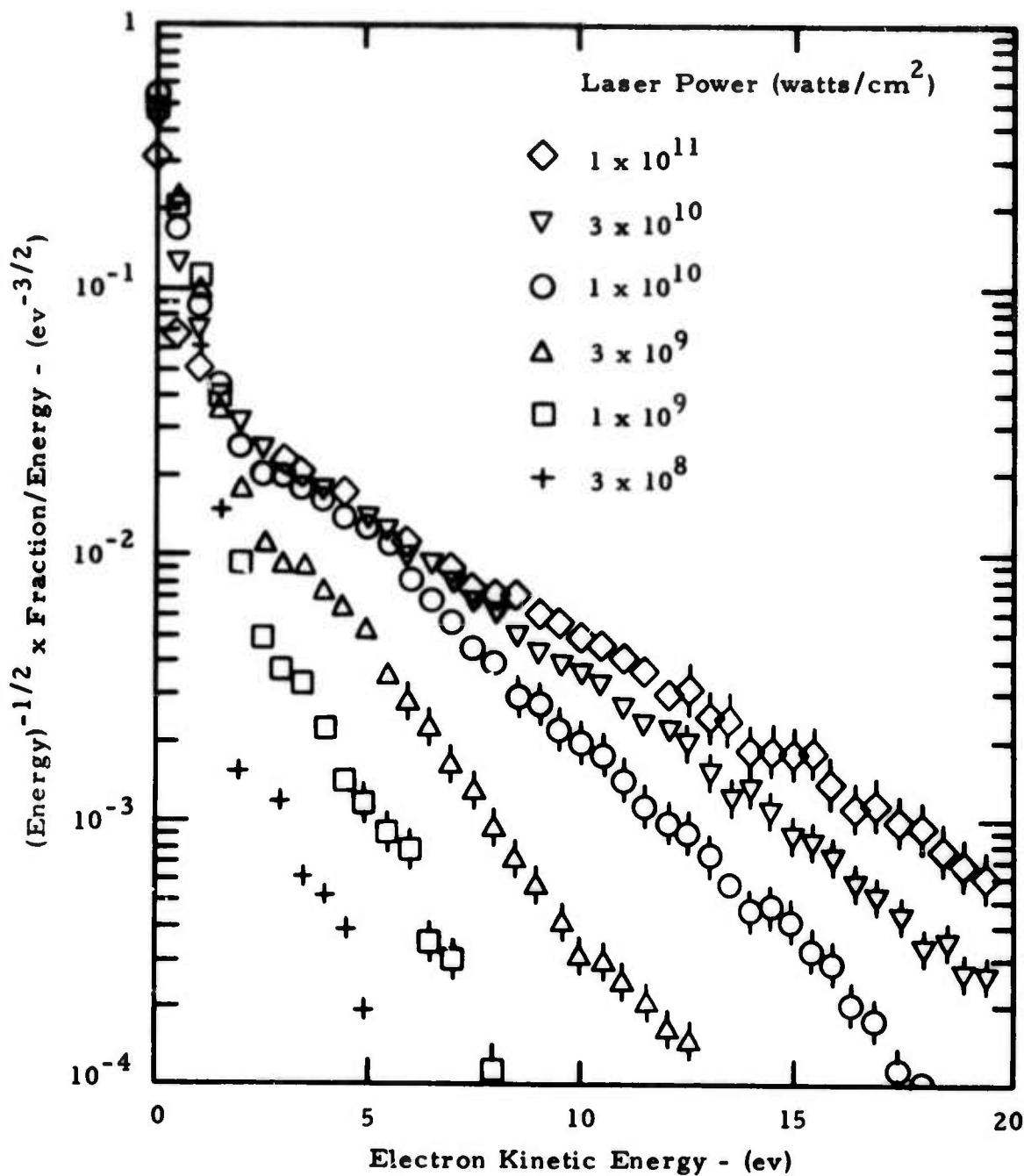


Figure 25. Electron energy distribution functions ($f/E^{1/2}$) from Monte Carlo calculations for various CO₂ laser powers.

The Monte Carlo method employed in LIRSEM is categorized as the "crude" method in a treatise on Monte Carlo methods (Ref. 45). In this method, the statistical uncertainty assigned to the magnitudes of the times spent in each energy bin of the distribution are given by the magnitude and the time spent divided by the square root of the number of entries into the bin when electron-electron scattering is neglected. When electron-electron scattering is included, however, the fact that a target electron was picked by a second random process increases the uncertainty by the square root of the reciprocal of the fraction of the time spent in the bin. In the first instance acceptable accuracy is obtained quite quickly, but in the second only very slowly. Although time did not permit incorporating more efficient methods, a number exist. Either a form of importance sampling using a Maxwellian distribution as a reference function, or one of the sampling or splitting methods would be appropriate (Ref. 45). The rate of attaining a desired accuracy can be increased by orders of magnitude when these better methods are employed which take maximum advantage of all that is known about the answer ahead of time, and which employ Monte Carlo only were absolutely necessary.

With the corrections, improvements, and refinements suggested, it is felt that the Monte Carlo approach to determining electron distribution functions can be made to be a valuable approach. As more empirical cross-section data are introduced into the analysis and as more simplifying assumptions are discarded, the relative value of the Monte Carlo approach increases until for sufficiently complex phenomenon it may become the only feasible approach.

APPENDIX III

MONTE CARLO COMPUTER PROGRAM

A computer program, LIRSEM, was written to carry out the calculations described in Appendix II. A logical flow chart for this program and a listing are included.

The program is dimensioned to allow for 100 energy bins for the electrons. As run, the bins are 0.2 ev wide ranging from 0 to 20 ev energies. Cross-sections are first computed for each interaction channel limited to 30 by present dimensioning. Cross-sections are read into the program as data in the form of energy cross section pairs of points arbitrarily spaced from which mesh values are interpolated. After reading the cross-section data, an initial electron distribution is read in the same format after first reading an arbitrary heading card.

The format for this input data is the following:

Card 1. NCHAN, Number of channels, N, (≤ 30) in columns 1-5 in 115 format.

This is followed by N set of cards consisting of the following:

Card 2. ICHAN, Channel number, J, in 1-5 in 115 format
NJCHAN, No. of pairs of data points in columns 6-10,
115 format
ITYPE(J), Type of cross section according to the code
(in columns 11-15 in 115 format)

- 1 = total cross section
- 2 = ionization cross section
- 3 = vibrational excitation cross section
- 4 = attachment cross section

PARTCL(J), Number density (cm^{-3}) of target particles in this channel in columns 21-30 in E10.4 format

ELOSS(J), Energy loss upon collision (ev) when appropriate for this type of interaction in columns 31-40 in E10.4 format.

Card 3 or more.

Pairs of energy (ev), cross section ($1 \times 10^{-16} \text{cm}^2$) data points in 16F5.2 format.

After reading N sets of cross-section data, an arbitrary heading card in 80A1 format is read followed by one more set of cards in the Card 2 and 3 formats. In this instance, the first word on the first card serves only to indicate the run is to continue if it is nonzero. The next cards in the same form as Card 3 above represent energy (ev), relative distribution height (arbitrary units) data pairs to specify the initial electron distribution. The normalization is discussed below. A run may be terminated by use of a blank card for Card 2.

Following this, control data is read in unformatted input form (Namelist). The variables read in are

WAVE = laser wavelength (cm)
POWER = laser power (watts/cm^2)
ENGZER = initial energy of test electron (ev)
ELECTS = free electron density (cm^{-3}), a constant; program control constants:
NDT = number of time step subdivisions made in the basic laser cycle
NEDIT = the number of basic cycles before an edit is made
NQNIT = the number of basic cycles before run is terminated
NSTART = number of basic cycles assumed to have transpired before input electron distribution occurs. (Serves to normalize this distribution)

NOMOL = ignored if less than or equal to zero. If greater than zero molecular interactions bypassed for pure electron-electron scattering

IWRT = outputs computed cross sections for all channels and bins if greater than zero. If less than one this output bypassed.

If values for these control constants are not specified in the namelist, they are assigned the following values:

NDT = 0

NEDIT = 10,000

NQUIT = 100,000

NSTART = 100

NOMOL = 0

IWRT = 0

Any number of sets of initial electron distributions followed by namelist specifications may be stacked. A blank card terminates the run normally.

In addition to the control constants, a number of interval constants of the program are printed. Also, values of the following variables are printed.

DT = basic time step (sec)

VELZER = maximum velocity induced by laser field (cm/sec)

ANGLE = phase angle (radians) corresponding to one time step

TELECT = average electron temperature (ev)

At each edit time, the electron energy distribution in sec/bin is given as well as the fraction/bin and the number of basic time steps/bin in tabular form.

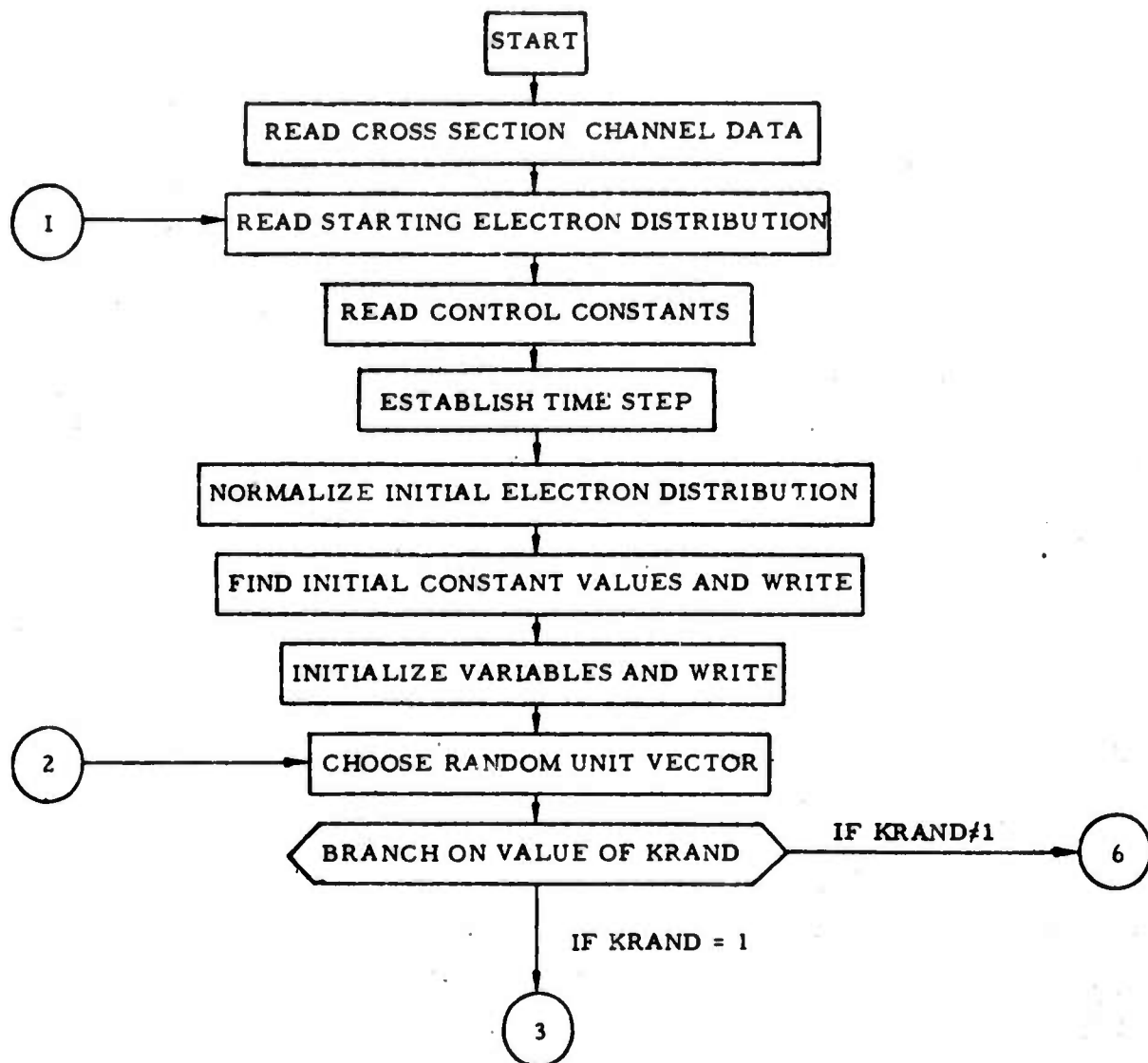
This is followed by a table of values for

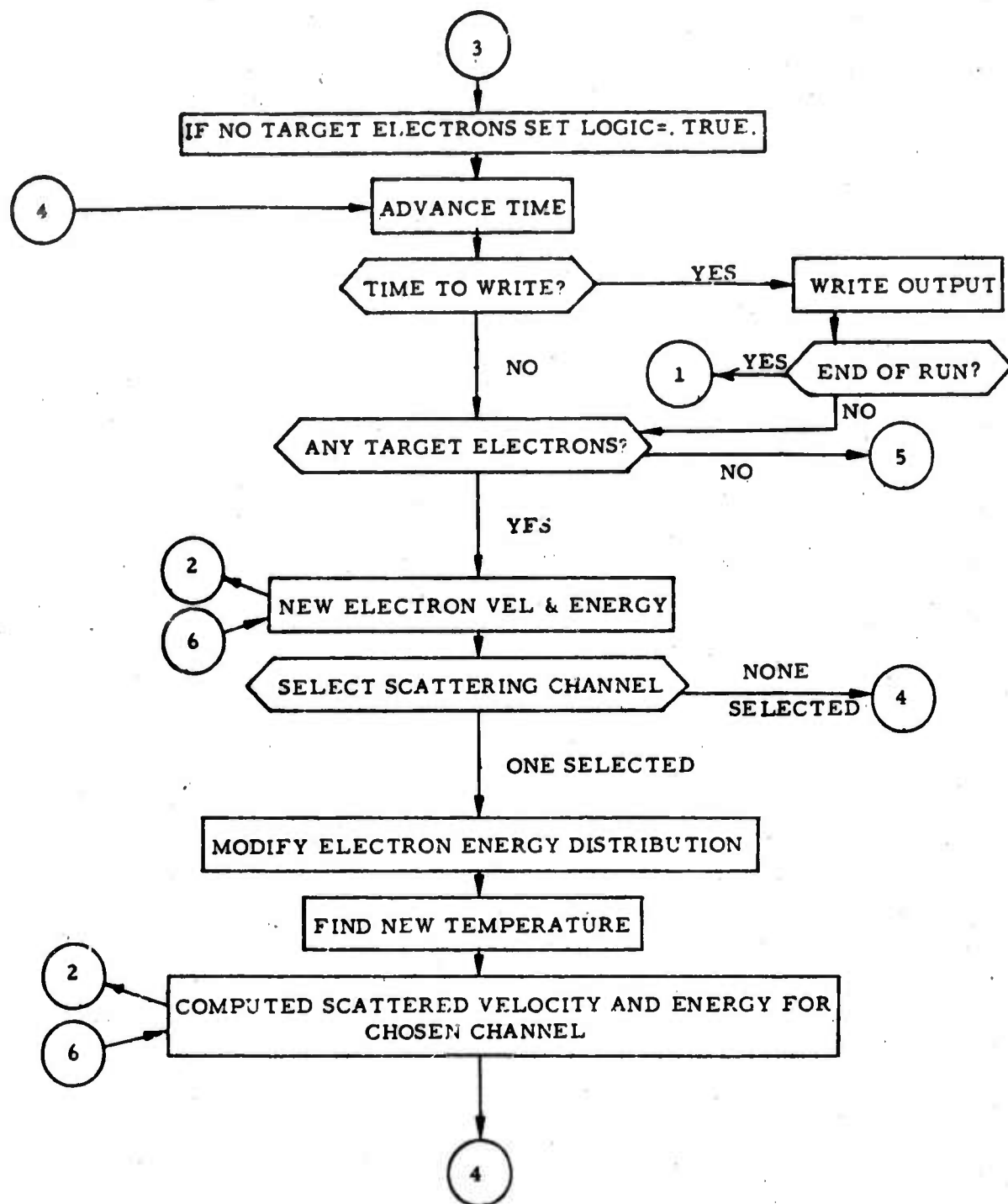
T = time of edit (sec)
 RATION = ionization rate in ionizations per second per cc
 RATERR = statistical uncertainty in RATION
 NION = number of ionization events
 NCYION = cycle number of last ionization
 NCY = total cycles at edit
 NEE = number of electron-electron collisions
 NEM = number of electron-molecule collisions
 NWRITE = cycles to write
 TEV = temperature of electrons (ev)
 EVT = kinetic energy of test electron (ev)
 VT = last electron velocity components (cm/sec)
 with field on
 VZ = last electron velocity components (cm/sec)
 if field were off
 NEL = number of elastic collision
 NELU = number of electron-electron scatterings for
 which the cosine of the scattering angle was less
 than ELNO(= .99999)
 XPBELC = log of probability of an electron scattering in
 one cycle
 PBELC = probability of an electron scattering in one cycle
 LOGIC = value (T, F) of variable to decide if electrons
 JE = number of steps into last laser cycle
 NATCH = number of attachments
 ELNO = cosine of electron-electron scattering angle
 above which scatterings were ignored
 VEZ = electron velocity (cm/sec) after scattering with
 field off
 JE2 = last channel chosen

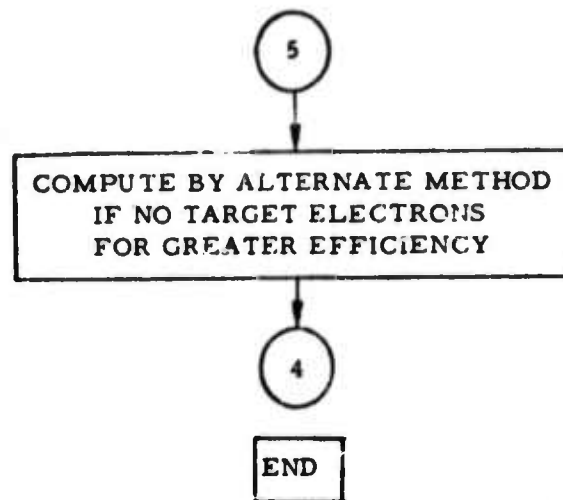
These output values are followed by a plot of the electron energy distribution function at the edit time. The values of the points plotted (in 0.5 ev bins) as well as their uncertainty are listed next to the plot.

The formula employed in the LIRSEM program follow closely those given in Appendix II. One variation was a faster means of advancing time when there are no electron-electron collisions was devised. Essentially it first randomly selects a laser cycle in which there is an event using the cross section averaged over one cycle in this selection. This section of the program is titled "No-Electron Channel Choice."

Logical Flow Chart for
LIRSEM Computer Program







UUUUU

LASER IONIZATION RATES BY SINGLE ELECTRON MONTE-CARLO

SPACE RESERVATION

```

DIMENSION TE(100),SIG(20,100),EIN(25),VAL(25),VE(100),
1  PARTCL(20),ZPTOT(100),PBTOT(100),XPROB(20,100),ELOSS(20),
2  VT(3),VZ(3),VZ2(3),W(3),IX(45),IY(45),IT(80),ITX(80),
3  ITY(80),RI(3),JEC(200),VF(200),H(10)

```

LOGICAL LOGIC

```

NAMELIST /CONTRL/ WAVE,POWER,ENGZER,NDT,NEDIT,NQUIT,
1 NSTART,ELECTS
NAMELIST /CONSTS/CLGT,CPLV,TWOPI,CETOV,PI,CVTOE,EPCON,
1 APROX,CAA,CBB,CELOSS
NAMELIST /OUTPUT/ T,RATION,RATERR,NION,NCYION,NCY,NEE,NEM,NWRITE,
1 TEV,EVT,VT,VZ,NEL,NELU,XPBELC,PBELC,LOGIC,JE
NAMELIST /VALUES/DT,VELZER,ANGLE,TELECT
DATA CLGT/3.E10/CPLV/7.686E7/TWOPI/6.2831852/CETOV/5.9287E7
1 /PI/3.1415926/CVTOE/2.845E-16/EPCON/1.736E6/APROX/,01
2 /CAA/5.526E5/CBB/6.4323E16/CELOSS/.99A9126/CSQANG/1.E-16/
3 ELNO/,999/

```

FORMATS

```

1000 FORMAT(1H1,5X,26HINPUT CARDS LISTED AS READ//)
1010 FORMAT(2I5,2E10.4)
1011 FORMAT(1X,2I5,2E10.4)
1020 FORMAT(16F5.2)
1021 FORMAT(1X,(16F5.2))
1030 FORMAT(80A1)
1040 FORMAT(21X,7HTIME = ,1P1E10.3,7H SECOND //)
1050 FORMAT(1H0,1A6/(1X,1P10E12.3))

```

LIRSEM Listing (Cont)

```

C      READ HISTOGRAM CARDS
C
C      READ(5,1030) ITX,ITY
C
C      READ IN CROSS SECTIONS
C
C      DATA CARD HEADING
C
C      10 WRITE(6,1000)
C
C      CROSS-SECTION POINTS
C
C      READ (5,1010) NCHAN
C      WRITE(6,1011) NCHAN
C      I=0
C      15 I=I+1
C      IF(I.GT.NCHAN) GO TO 100
C      READ (5,1010) ICHAN,NJCHAN,PARTCL(ICCHAN),ELOSS(ICCHAN)
C      WRITE(6,1011) ICHAN,NJCHAN,PARTCL(ICCHAN),ELOSS(ICCHAN)
C      KGO=1
C
C      READ AND INTERPOLATE
C
C      50 READ(5,1020) (EIN(J),VAL(J),J=1,NJCHAN)
C      WRITE(6,1021) (EIN(J),VAL(J),J=1,NJCHAN)
C      DO 99 J=1,100
C      EV=.2*(J-.1)
C      IF(EV-EIN(1)) 90,60,60
C      60 DO 80 K=2,NJCHAN
C      IF(EV-EIN(K)) 70,70,80
C      70 TE(J)=((EIN(K)-EV)*VAL(K-1)+(EV-EIN(K-1))*VAL(K))/
C      ) (EIN(K)-EIN(K-1))
C      GO TO 99
C      80 CONTINUE
C      90 TE(J)=0.
C      99 CONTINUE

```

LIRSEM Listing (Cont)

```

        GO TO (20,120),KGO
    20 CONTINUE
        DO 30 J=1,100
    30 SIG(ICHAN,J)=TE(J)*CSQANG
        GO TO 15

```

```

C
C      READ HISTOGRAM TITLE CARD
C

```

```

    100 READ(5,1030) IT

```

```

C
C      READ IN INITIAL ELECTRON DISTRIBUTION
C

```

```

    110 READ (5,1010) NJCHAN
        IF(NJCHAN.LT.1) STOP NORMAL
        WRITE(6,1011) NJCHAN
        KGO=2
        GO TO 50
    120 CONTINUE

```

```

C
C
C
C
C
C

```

```

        WRITE CONSTANTS
        PRESET VALUES

```

```

        WRITE(6,CONSTS)
        NDT=100
        NEDIT=10000
        NQUIT=100000
        NSTART=100

```

```

C
C      CONTROL CONSTANTS
C

```

```

        READ(5,CONTROL,ERR=130)
        WRITE(6,CONTROL,ERR=130)
        GO TO 135

```

```

    130 STOP CONTROL
    135 IF(NDT.GT.200.OR.NDT.LT.1) STOP CYCLE

```

LIRSEM Listing (Cont)

```

C      BASIC DERIVED CONSTANTS
C
C      TIME STEP
C
C      DT=WAVE/(CLGT*NDT)
C
C      NORMALIZE ELECTRON DISTRIBUTION
C
C      SUM=0.
C      DO 140 I=1,100
C      140 SUM = SUM + TE(I)
C      SUM = NSTART*DT/SUM
C      DO 150 I=1,100
C      150 TE(I)=SUM*TE(I)
C
C      FIELD INDUCED VELOCITY
C
C      VELZER=CPLV*WAVE*SQRT(POWER)
C      ANGLE=TWOPI/FLOAT(NDT)
C      DO 160 I=1,NDT
C      160 VF(I)=VELZER*SIN((I-1)*ANGLE)
C
C      INITIALIZE PROBABILITIES AND TEMPERATURE
C
C      SUM=0.
C      TEV=0.
C      DO 180 J=1,100
C      EV=.2*J-.1
C      VE(J)=CETOV*SQRT(EV)
C      SUM=SUM+TE(J)
C      TEV=TEV+EV*TE(J)
C      XPTOT(J)=0.
C      DO 170 I=1,NCHAN
C      XPROB(I,J)=DT*VE(J)*SIG(I,J)*PARTCL(I)
C      170 XPTOT(J)=XPTOT(J)+XPROB(I,J)

```


LIRSEM Listing (Cont)

```

180 PRTOT(J)=EXP(-XPTOT(J))
TEV=TEV/SUM
TELFCT=TEV

C      WRITE ALL PRECOMPUTED CONSTANTS
C
C      L=6HPARTCL
WRITE(6,1050) L,(PARTCL(I),I=1,20)
L=6HVF
WRITE(6,1050) L,(VF(I),I=1,NDT)
L=6HXPROB
WRITE(6,1050) L,((XPROB(I,J),J=1,100),I=1,NCHAN)
L=6HXPOT
WRITE(6,1050) L,(XPTOT(I),I=1,100)
L=6HPBOT
WRITE(6,1050) L,(PBTOT(I),I=1,100)
L=6HELOSS
WRITE(6,1050) L,(ELOSS(I),I=1,20)

C      SET ELECTRON ENERGY
C
C      EVT=ENGZER
VEZ=CETOV*SQRT(EVT)

C      INITIAL TIME
C
C      T=0.
NCY=0
NEE=0
NEM=0
NEL=0
NELU=0
NCYOLD=0
NION=0
NCYION=0
NWRITE=0

```

LIRSE'M Listing (Cont)

```

C
C      WRITE INITIAL VALUES
C
C      WRITE(6,VALUES)
C
C      CHOOSE ELECTRON VELOCITY
C      RANDOM UNIT VECTOR
C
C      KRND=1
200  RND=URAND(Q)
    R(1)=RND+RND-1.
    WW=SQRT(1.-R(1)**2)
    RND=TWOPI*URAND(Q)
    VV=CCOS(RND)
    R(2)=WW*VV
    VV=SQRT(1.-VV**2)
    IF(RND.GT.PI) VV=-VV
    R(3)=WW*VV
    GO TO (210,440,460,490),KRND
C
C      SET ELECTRON VECTOR
C
210  DO 220 I=1,3
220  VZ(I)=VEZ+R(I)
C
C      ELECTRON PROBABILITIES
C
250  XPBELC=EPCON*DT+VEZ+TEV
    PBELC=EXP(-XPBELC)
    LOGIC = .FALSE.
    IF(ELECTS-1.)260,260,300
260  XPBELC=0.
    PBELC=1.
    LOGIC = .TRUE.
C

```

LIRSEM Listing (Cont)

```

C      BASIC MONTE CARLO CYCLE
C
C      ADVANCE TIME
C
300  IF (NCY.GE.NWRITE) GO TO 600
    IF (LOGIC) GO TO 700
305  NCY=NCY+1
    NSIN=MOD(NCY,NDT)+1
C
C      ADD LASER INDUCED VELOCITY
C
    VT(1)=VZ(1)+VF(NSIN)
    VT(2)=VZ(2)
    VT(3)=VZ(3)
C
C      NEW KINETIC ENERGY
C
    EVT=0.
    DO 310 I=1,3
310  EVT=EVT+VT(I)**2
    EVT=CVTOE+EVT
    JE=MIN0(IFIX(1.+5.*EVT),100)
C
C      SELECT CHANNEL
C
    XTPB=XPRELC+XPTOT(JE)
    ICH=0
    IF (XTPB-APROX) 320,320,340
320  IF (XTPB-URAND(Q)) 300,330,330
330  IF (XPBELC-XTPB*URAND(Q)) J50,350,390
340  IF (PBELC-URAND(Q)) 390,345,345
345  IF (PBTOT(JE)-URAND(Q)) 350,300,300
C
C      NON-ELECTRON CHANNEL
C
350  RND=XPTOT(JE)*URAND(Q)

```

LIRSEM Listing (Cont)

```

XPB=0.
DO 370 I=1,NCHAN
  XPB=XPB+XPROB(I,JE)
  IF(XPB-RND) 370,360,360
360 ICH=I
   GO TO 390
370 CONTINUE
   ICH=NCHAN
C
C      MODIFY DISTRIBUTION
C
390 TE(JE)=TE(JE)+DT*(NCY-NCYOLD)
   NCYOLD=NCY
C
C      NEW TEMPERATURE
C
SUM=0.
TEV=0.
DO 400 I=1,100
  SUM=SUM+TE(I)
  TEV=TEV+TE(I)*I
400 TEV=.2*TEV/SUM-.1
C
C      BRANCH ON CODE NUMBER
C
IF(ICH.LT.1) GO TO 410
IF(ICH.EQ.1) GO TO 530
IF(ICH.NE.2) GO TO 480
GO TO 540
C
C      ELECTRON-ELECTRON SCATTERING CHANNEL
C
C      CHOOSE SECOND ELECTRON
C
410 TSUM=0.
   NEE=NEE+1

```

LIRSEM Listing (Cont)

```

RND=SUM*URAND(Q)
DO 420 JE2=1,100
  TSUM=TSUM+TE(JE2)
  IF (TSUM-RND) 420,430,430
420 CONTINUE

```

C
C
C

RANDOM VELOCITY

```

430 KRND=2
  GO TO 200
440 DO 445 I=1,3
445 VZ2(I)=VE(JE2)*R(I)

```

C
C
C
C

COMPTON SCATTERED ELECTRON VELOCITY
CENTER OF MASS VELOCITY

```

SUM=0.
DO 450 I=1,3
  W(I)=.5*(VZ(I)-VZ2(I))
450 SUM=SUM+W(I)**2
  WLGTH=SQRT(SUM)

```

C
C
C

SCATTERING ANGLE SIN AND COS

```

AA=CAA*URAND(Q)*TEV/ELECTS
BB=CBB/SUM**2
UC=(AA-BB)/(AA+BB)
IF (UC-ELNO) 455,455,300
455 US=SQRT(1.-UC**2)
  NELU=NELU+1
  UW=US/WLGTH

```

C
C
C

RANDOM UNIT VECTOR

```

KRND=3
GO TO 200

```

LIRSEM Listing (Cont)

```

C
C
C      NEW CM AND LAB VELOCITY
C
C      460 SUM=0.
C      DO 470 I=1,3
C      W(I)=WLGTH*US*R(I)+(UC-UW*R(I)*W(I))*W(I)
C      470 VZ(I)=.5*(VZ(I)+VZ2(I))*W(I)
C      VEZ=SQRT(VZ(1)**2+VZ(2)**2+VZ(3)**2)
C      GO TO 250
C
C      NON-ELECTRON SCATTERING CHANNEL
C
C      LOSS AND NEW VELOCITY
C
C      480 EVT=EVT-ELOSS(ICH)
C      485 EVT=AMAX0(0.,EVT)
C      VEZ=CETOV*SQRT(EVT)
C      KRND=4
C      GO TO 200
C      490 DO 500 I=1,3
C      VT(I)=VEZ*R(I)
C      500 VZ(I)=VT(I)
C      VZ(1)=VZ(1)-VF(NSIN)
C
C      COUNT NON-ELECTRON COLLISIONS
C
C      NEM=NEM+1
C      GO TO 250
C
C      ELASTIC SCATTERING CHANNEL
C
C      530 EVT=CELOSS*EVT
C      NEL=NEL+1
C      GO TO 485
C
C      IONIZATION CHANNEL
C

```


LIRSEM Listing (Cont)

```

C      540 NION=NION+1
      NCYION=NCY
      EVT=AMAX1(.5*(EVT-ELOSS(ICH)),0.)
      GO TO 485

C      WRITE OUTPUT HISTOGRAM
C
C      600 NX=39
      GO TO 800
C      601 CONTINUE
      T=NCY*DT
      DO 610 I=1,NX
      IX(I)=5*I-1
      J=2.5*I+1.E-6
      IF (MOD(J,2).EQ.1) GO TO 605
      IY(I)=(TE(J-1)+TE(J)+.5*TE(J+1))/DT+.5
      GO TO 610
C      605 IY(I)=(.5*TE(J-2)+TE(J-1)+TE(J))/DT+.5
      610 CONTINUE
      CALL HISTGM(IT,ITX,ITY,IX,IY,NX)
      WRITE(6,1040) T
      RATION=FLOAT(NION)/FLOAT(NCYION)/DT
      RATERR=SQRT(FLOAT(NION)/FLOAT(NCYION)/DT
      WRITE(6,OUTPUT)
      NWRITE=NWRITE+NEDIT
      IF (NWRITE.GT.NQUIT) GO TO 100
      GO TO 305

C      NO-ELECTRON CHANNEL CHOICE
C
C      700 SUM=0.
      DO 710 I=1,NDT
      EVC=CVTOE*((VZ(1)+VF(I))*2+VZ(2))*2+VZ(3))*2)
      JEC(I)=MIN0(IFIX(1+.5*EVT),100)
      J=JEC(I)

```

LIRSEM Listing (Cont)

```

710 SUM=SUM+XPTOT(J)
   RND=ALOG(1./URAND(Q))
   NCY=NCY+FIX(RND/SUM)
   RND=AMOD(RND,SUM)
   SUM=0.
   DO 720 I=1,NDT
   NCY=NCY+1
   JE=JEC(I)
   SUM=SUM+XPTOT(JE)
   IF (SUM-RND) 720,350,350
720 CONTINUE
   GO TO 350

C      OUTPUT TABLES
C
C      800 WRITE(6,2000)IT,T
2000 FORMAT(1H1,80A1//1X,13HTIME (SEC) = ,1E10.4/)
   KH=1
   GO TO 835
810 WRITE(6,2010)
2010 FORMAT(43X,38HELECTRON ENERGY DISTRIBUTION (SEC/EV)/)
   WRITE(6,2020) (H(I),I=1,10)
2020 FORMAT(1X,10HENERGY(EV),10F10.1/)
   DO 830 I=0,9
   EG=2*I
   DO 820 J=1,10
820 H(J)=5.*TE(10*I+J)
830 WRITE(6,2030) EG,(H(J),J=1,10)
2030 FORMAT(1X,1F9.1,1X,10E10.3)
835 KH=2
   H(1)=.1
   DO 840 I=2,10
840 H(I)=H(I-1)*.2
   GO TO (H10,845),KH
845 WRITE(6,2040)
2040 FORMAT(//,35X,

```

LIRSEM Listing (Cont)

```
1 53HNORMALIZED ELECTRON ENERGY DISTRIBUTION (FRACTION/EV) /)
WRITE(6,2020) (H(I),I=1,10)
SUM=0.
DO 850 I=1,100
850 SUM=SUM+TE(I)
DO 870 I=0,9
EG=2*I
DO 860 J=1,10
860 H(J)=.5*TE(10*I+J)/SUM
870 WRITE(6,2030)EG,(H(J),J=1,10)
WRITE(6,OUTPUT)
GO TO 601
END
```

REFERENCES

1. Smith, D. C., "Gas-Breakdown Dependence on Beam Size and Pulse Duration with 10.6 μ Wavelength Radiation," Appl. Phys. Let. **19**, 405 (1971).
2. Hull, R. J., Marquet, L. C., and Lencioni, D. E., Optics Research, Lincoln Laboratory, ESD-TR-2 (1971), Lexington, Mass.
3. Zeldovich, Y. B., and Raizer, Y. P., "Cascade Ionization of a Gas by a Light Pulse," Soviet Phys. JETP **20**, 772 (1965).
4. Chanin, L. M., Phelps, A. V., Biondi, M. A., "Measurements of the Attachment of Low Energy Electrons to Oxygen Molecules," Phys. Rev., **128**, 219, 1962.
5. Schulz, G. J., "Vibrational Excitation of N_2 , CO, and H_2 by Electron Impact," Phys. Rev., **135**, A988, 1964.
6. Engelhardt, A. G., Phelps, A. V., Risk, C. G., "Determination of Momentum Transfer and Inelastic Collision Cross Sections for Electrons in Nitrogen Using Transport Coefficients," Phys. Rev., **135**, A1566, 1964.
7. Hake, R. D., Phelps, A. V., "Momentum-Transfer and Inelastic-Collision Cross Sections for Electrons in O_2 , CO, and CO_2 ," Phys. Rev., **158**, 70, 1967.
8. Borst, W., "Excitation of Several Important Metastable States of N_2 by Electron Impact," Phys. Rev., **A5**, No. 2 p. 648 (Feb. 1972).
9. Ajello, J., "Emission Cross Sections of N_2 in the Vacuum Ultraviolet by Electron Impact," Jour. Chem. Phys., **53**, No. 3, p. 1156 (Aug. 1970).

References (Cont.)

10. Goldstein, H., Classical Mechanics, p. 84, Addison-Wesley Press, Inc., Cambridge, Mass. (1951).
11. Kroll, N., and Watson, K., "Theoretical Study of Ionization of Air by Intense Laser Pulses," Phys. Rev., A5, No. 4, 1883 (April 1972).
12. Chung, S., and Lin, J., "Excitation of the Electronic States of the Nitrogen Molecule by Electron Impact," Phys. Rev., A6, No. 3, 988 (Sept. 1971).
13. Golden, D., "Low Energy Resonances in e^- -N₂ Total Scattering Cross Sections: The Temporary Formation of N₂⁻," Phys. Rev. Lett., 17, No. 16, 847 (17 Oct. 1966).
14. Baraff, G., and Buchsbaum, S., "Anisotropic Electron Distribution and the dc and Microwave Avalanche Breakdown in Hydrogen," Phys. Rev. 130, 1007 (1 May 1963).
15. Abramowitz, M., Stegun, G. A., Handbook of Mathematical Functions, p. 376 (1965) Dover Publications, Inc., N. Y.
16. Canavan, G. H., Proctor, W. A., Nielsen, P. E., and Rockwood, S. D., "CO₂ Laser Air Breakdown Calculations," IEEE J. Quant. Electronics QE8, 564 (1972).
17. Richtmyer, R. D., and Morton, K. W., Difference Methods for Initial-Value Problems, Interscience Publishers, New York (1967), 2nd ed.
18. Chapman, S., and Cowling, T., The Mathematical Theory of Non-Uniform Gases, Cambridge University Press, Chapt. 10 (1958).
19. Jung, C. E., Air Chemistry and Radioactivity, Academic Press, New York (1963).

References (Cont.)

20. American Institute of Physics Handbook, McGraw-Hill, New York (1963), 2nd ed.
21. Wolfe, W., Handbook of Military Infrared Technology, Office of Naval Research, Department of the Navy, Washington, D. C. (1965).
22. Gryvnak, D. A., and Burch, P. E., "Optical and Infrared Properties of Al_2O_3 at Elevated Temperatures," J. Opt. Soc. Amer. 55, 625 (1965).
23. Chang, D. B., Drummond, J. E. and Hall, R. B., "High-Power Laser Radiation Interaction with Quartz," J. Appl. Phys. 41, 4851 (1970).
24. Basov, N. G., et al. "Reduction of Reflection Coefficient for Intense Laser Radiation on Solid Surfaces," Sov. Phys. -Tech. Phys. 13, 1581 (1969).
25. McCarthy, D. E., "The Reflection and Transmission of Infrared Materials: I, Spectra from 2-50 Microns," Applied Optics 2, 591 (1963).
26. Hoss, G. and Salzberg, C. D., "Optical Properties of Silicon Monoxide in the Wavelength Region from 0.24 to 14.0 Microns," J. Opt. Soc. Amer. 44, 181 (1954).
27. Calingaert, Heron and Stair, Trans. Soc. Auto. Eng. 39, 448 (1936) as reported in American Institute of Physics Handbook, 2nd ed. (1963) p. (6-66).
28. Ubbelohde, A. R. and Lewis, F. A., Graphite and Its Crystal Components, Oxford Press, 1960, Clarendon Press.
29. Harris, Louis, The Optical Properties of Metal Blocks and Carbon Blocks, MIT, Cambridge, Mass. (December, 1967), p. 91.

References (Cont.)

30. Nielsen, P. E. and Canavan, G. H., Private Communications, Air Force Weapons Laboratory, LRD-71-1 (1971) Kirtland AFB, N. M. pg. 273.
31. Brodie, R. N. and Hormuth, J. E., The PUFF 66 and P PUFF 66 Computer Programs, AFWF-TR-66-48, Air Force Weapons Laboratory, Kirtland AFB, New Mexico, May 1966. (Private Communications)
32. Kohn, B. J., Compilation of Hugoniot Equations of State, AFWL-TR-69-38, Air Force Weapons Laboratory, Kirtland AFB, New Mexico, April 1969.
33. Zavitsanos, P. D. "Mass Spectrometric Analysis of Carbon Species Generated by Laser Evaporation," Carbon 6, 731 (1968).
34. Gilmore, F. R. Equilibrium Composition and Thermodynamic Properties of Air to 24000°K, Rand Corp., Santa Monica, Calif., RM1543, Aug. 1955. (Unpublished, Private Communication)
35. Zel'dovich, Y. B. and Raizer, Y. P., Physics of Shock Waves and High Temperature Hydrodynamic Phenomena, Acad. Press, New York (1966).
36. Vedeneyev, V. I. et al., Band Energies Ionization Potentials and Electron Affinities, St. Martin's Press, New York (1966).
37. Sears, F. W. An Introduction to Thermodynamics, The Kinetic Theory of Gases, and Statistical Mechanics, Addison-Wesley Publishing, Reading, Mass. (1953), 2nd ed.
38. Peierls, R. E., Quantum Theory of Solids 1st ed., Oxford at the Clarendon Press, p. 97 (1955).
39. Ready, John F., Effects of High-Power Laser Radiation, Acad. Press, N. Y. p. 207 (1971).

References (Cont.)

40. Personal communication with K. Brueckner, KMS Industries, Ann Arbor, Mich.
41. Tolman, R. C. The Principles of Statistical Mechanics, Oxford University Press (1938).
42. Rapp, D., Englander-Golden, P., "Total Cross Sections for Ionization and Attachment in Gases by Electron Impact. I. Positive Ionization," Jour. Chem. Phys., **43**, 1464, 1965.
43. Rapp, D., Briglia, D. D., "Total Cross Sections for Ionization and Attachment in Gases by Electron Impact. II. Negative-Ion Formation," Jour. Chem. Phys., **43**, 1480, 1965.
44. Spitzer, L. Physics of Fully Ionized Gases, Interscience, N. Y. (1967).
45. Hammersley, J. M., Handscomb, D. C., Monte Carlo Methods, John Wiley & Sons, N. Y. (1964).